CREATING THE BLIND PEPPER'S GHOST: ANALYZING SOUND SPECTRA USING FOURIER TRANSFORMS TO PREDICT DIMENSIONAL VARIATION FOR IMAGE RECONSTRUCTION

By
Kylie Shellington

A SENIOR RESEARCH PAPER PRESENTED TO THE DEPARTMENT OF MATHEMATICS AND COMPUTER SCIENCE OF STETSON UNIVERSITY IN PARTIAL FULFILLMENT OF THE REQUIREMENTS FOR THE DEGREE OF BACHELOR OF SCIENCE

STETSON UNIVERSITY
2015

ACKNOWLEDGMENTS

I would like to extend my sincerest gratitude to my advisor, Dr. Miles, for guiding me through the senior research process. He always greets me with encouraging words and a deep understanding of the concepts I struggle to wrap my head around. Thank you for always showing such interest in your students' interests outside the classroom, and thank you for being so approachable.

Secondly, I would like to thank Dr. Vogel for asking me to stop by his office during the first semester of my freshman year. I was terrified to go, but he only wanted to convince me to major in mathematics. Knowing that the faculty wanted me to join the department was a definitive moment of my college career at Stetson.

Thank you to Dr. Plante for always having faith in my abilities from the very beginning. His confidence became my confidence.

An enormous thank you goes out to the rest of the professors of the Math and Computer Science Department. It is because of you that I have learned to love learning.

I would also like to thank my ever-optimistic friend, pseudo-sister, and roommate, Sammi Smith, for talking me off the ledge when I needed it most. Her wisdom, experience, and encouragement were invaluable to me this semester.

To my fellow senior math majors, I am grateful for your support and laughter over the past few years. Thank you.

Finally, thank you to my parents. I would not be where I am without them. Thanks for sticking with me through the ups and downs. They must like me or something.

TABLE OF CONTENTS

LIST OF FIGURES

FIGURE

ABSTRACT

CREATING THE BLIND PEPPER'S GHOST:
ANALYZING SOUND SPECTRA USING FOURIER TRANSFORMS TO PREDICT DIMENSIONAL VARIATION FOR IMAGE RECONSTRUCTION

By

Kylie Shellington
May 2015

Advisor: Dr. William Miles
Department: Mathematics and Computer Science

Disney's Haunted Mansion attraction serves as the home to the largest implementation of the Pepper's Ghost illusion ever constructed. This optical illusion is created with a flat pane of glass that acts as a mirror when an object is lit properly. In the search to find the mathematics behind this effect, we propose the creation of a new illusion known as the Blind Pepper's Ghost. Inspired by the configuration of the original Pepper's Ghost effect, we replace the light waves of the old illusion with sound waves in order to create an image of an object. In this study, we will use partial differential equations to find the solution of the one-dimensional wave equation over a semi-infinite boundary to model the sound waves of the Blind Pepper's Ghost effect. Implementing an experimental configuration of the effect, we develop two different models to predict dimensional variation between objects. These models provide the framework for future configurations that allow us to predict the thickness of an object on multiple planes. By drawing cross-sections to the appropriate predicted dimensions, we can use the Blind Pepper's Ghost to reconstruct a three-dimensional image of the physical object.

CHAPTER 1
INTRODUCTION

1.1. OBJECTIVE

Since the opening of the first park in 1959, Walt Disney theme parks around the world have been known as the ultimate places of magic and fantasy. Despite the fact that Disney wants all guests to believe the magic is real, a team of Imagineers exists to create, design, and build the illusion of magic into the parks. Known for configuring ingenious visual tricks, Disney Imagineers are responsible for developing some of the most groundbreaking special effects in the theme park industry. With intent to study the inner workings of the special effects Disney executes so well, we want to focus our attention on one of the most visually-reliant attractions Disney Imagineers have ever created: the Haunted Mansion. Full of sight gags and eerie ghostly illusions, the Haunted Mansion is home to one of the largest executions of the Pepper's Ghost illusion, a theatrical optical effect, ever built. Our goal is to delve into the mathematics of this famous illusion. Inspired by the configuration of the massive Pepper's Ghost effect so successfully implemented in the Haunted Mansion, we create a new optical illusion using sound waves modeled by the one-dimensional wave equation. We then implement an experimental configuration of the new illusion which allows us to model sound spectra with Fourier transforms and provides a framework for image reconstruction.

1.2. DESCRIPTION OF THE PEPPER'S GHOST ILLUSION

The optical illusion known as Pepper's Ghost was developed in 1862 by John Henry Pepper, a chemistry professor at London Polytechnic Institute [3]. Created for the London stage, Pepper's Ghost was first used in Charles Dickens's play, *The Haunted Man* [9]. The effect is created by placing a large sheet of glass tilted at a forty-five degree angle away from the stage between the audience and the actors. A level beneath the stage, an off-stage actor is lit and reflected by the glass, thus becoming visible to the audience [14]. The use of carefully controlled lighting will illuminate the off-stage actor's reflection in the glass, allowing the audience to see the juxtaposition of the on-stage actor and the off-stage actor's

reflected image. Thus, the two sets of actors will appear to interact onstage. While the audience is only seeing a reflection on a flat panel of glass, "the reflected 'ghostly figure' appears to be on stage, the image landing at exactly the same distance behind the glass as the illuminated actor is from the front of the glass" [17]. This depth makes it seem as if the reflected image can interact with its surroundings onstage. A Pepper's Ghost configuration can be seen in the figure below.

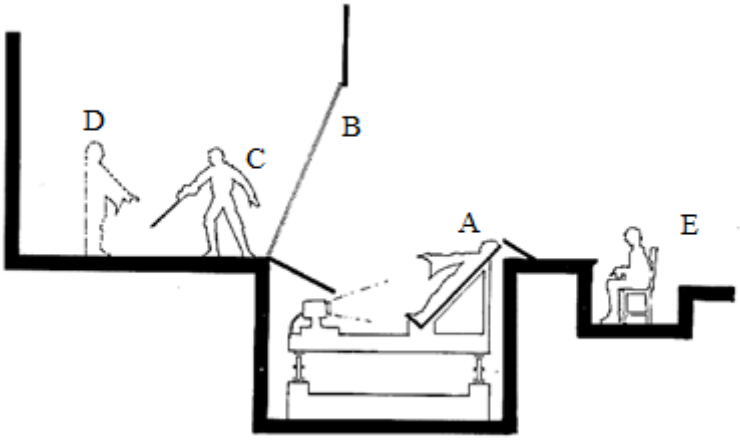

Figure 1: A Classic Pepper's Ghost Configuration. (A) is the off-stage actor whose reflection will become the ghost. The reflective panel of glass is the feature (B). (C) is an on-stage actor visible to the audience, (E). (D) is the image reflection of the off-stage actor as it appears to the audience. Notice the off-stage actor is placed at an angle to match the angle of the glass, prohibiting actor movement. Image courtesy of Jim Steinmeyer's *The Science Behind the Ghost* [22].

Pepper's Ghost persisted as a common theatrical illusion in the 1800s but quickly fell out of popularity as the large pane of glass was difficult to slide into position and acted as a sound barrier between performers and audience [9]. Despite the drawbacks the effect suffered in the theatre, "Pepper's Ghost has found a major afterlife in the great theme parks: the various Disneylands and Disney Worlds around the globe all have some version of a Haunted Mansion in which this is the most striking effect" [13]. In one of the largest versions of Pepper's Ghost ever built, the Haunted Mansion contains a massive scene in which guests witness this clever usage of lighting and glass.

Built in 1963, the Haunted Mansion's Pepper's Ghost configuration was developed by Walt Disney Imagineer, Yale Gracey. Gracey housed the attraction's famous effect in what is known as the Grand Ballroom scene, a ride-through display in which guests experience Pepper's Ghost on a large scale

[24]. The effect is accomplished in Disney parks around the world with a slightly different approach than the original layout utilized by Pepper. Guests ride parallel to a scene on the second story of a grand ballroom in the midst of a "swinging wake" [1]. The scene consists of ghostly images of Audio Animatronics (Disney's unique three-dimensional animated robotic figures) dancing, swinging from chandeliers, and enjoying the atmosphere of a festive party [21]. To the observer, it appears as though the ghosts fade in and out, disappearing of their own accord. This illusion is achieved with massive, undetectable twelve by twenty-one foot panels of glass inserted between the observer and the ballroom. The physical Audio Animatronics are not seen by the guests, for the figures are directly beneath and directly above the track on which the passengers are riding [11]. These figures are housed in a dark room that mirrors the same dimensions of the ballroom; there is no official term used to refer to this separate room, so for the purpose of discerning between each space, we will call it the black box room. When the figures are lit within the black box room beneath the track, their semi-transparent reflections are visible on the sheet of glass in front of the observer [22]. While the observer is seeing the image projected upon a flat plane, the ghosts appear to be at different depths within the ballroom. The image shown in Figure 2 in is a diagram of the Pepper's Ghost illusion within the Haunted Mansion.

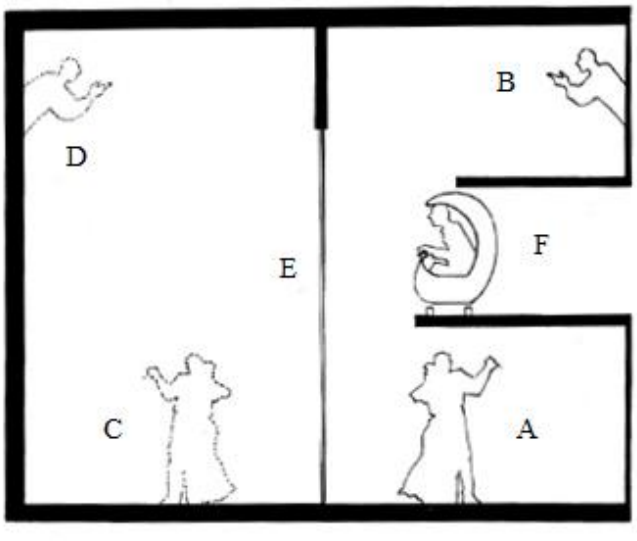

Figure 2: The Pepper's Ghost Configuration within the Haunted Mansion. (A) and (B) are the unseen Audio Animatronics in the black box rooms beneath and above the track on which the observer is riding (F). The

reflections of the figures (C) and (D) appear at different depths to an observer. (E) is the panel of glass between the observer and the ballroom. Image courtesy of Jim Steinmeyer's *The Science Behind the Ghost* [22].

CHAPTER 2
BACKGROUND RESEARCH

2.1. OPTICS OF REFLECTION

In order to create a model of the Pepper's Ghost illusion, we must first understand why such an effect executes so successfully. Because this illusion is reliant on lighting and reflection, a basic understanding of the optical properties of light is beneficial to this study. According to K.K. Sharma's *Optics: Principles and Applications*, it is known that "image formation by optical instruments is critically dependent on the wave nature of light" [19]. Hence, we will not consider the particle behavior of light in the Pepper's Ghost system. Instead, we will examine the interaction of light waves with a reflective interface, in our case, a flat panel of transparent glass. Due to the transparency and reflective properties of the glass, we can consider the panel to be both a lens and a mirror. With the sheet of glass acting as an interface in this optical system, we can use Snell's Law to trace the paths of the light rays in the system. Snell's Law describes the relationship between a light ray's refractive indices and angles of incidence as it passes through an interface separating two different media as shown by the equation below:

$$n_1 \sin\theta_1 = n_2 \sin\theta_2.$$

The index of refraction is the measure of how severely a light ray bends when passing into a different medium. This can be calculated as $n = \frac{c}{v}$ where c is the speed of light within a vacuum and v is the speed of light in a particular medium. The angle of incidence, denoted as θ, is defined as the angle between a light ray and the normal, a line perpendicular to an interface [19].

We can see by Figure 3 below, that a plane mirror will reverse a light ray's path of propagation. The virtual image formed by a plane mirror will appear to be on the side of the mirror opposite the observer. This property explains why the reflections of the objects in the Pepper's Ghost illusion appear within the ballroom on the opposite side of the glass in reference to the observer. As the distance from the

figure to the mirror is equal to the distance from the image to the mirror, our eyes perceive the images to be at varying depths within the ballroom due to the different distances at which the objects are placed within the black box room [12].

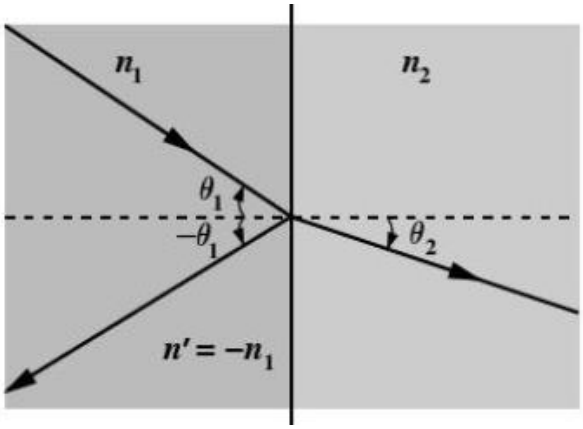

Figure 3: The Reflection and Refraction of Light Rays at an Interface. The ray of incidence comes in at an angle θ_1 with a refraction index n_1. When refracted at the interface, the ray is bent at an angle θ_2 with a refraction index n_2. When reflected, the ray is reflected at an angle $-\theta_1$ with a refraction index $-n_1$ [19].

Since the Pepper's Ghost effect hinges on reflection in a mirror-like interface, we will examine the physics of reflection in a plane mirror to understand why Pepper's Ghost works. By the figure above, notice that the index of refraction n_1 of an incoming light ray is equal to the negative refractive index $-n_1$when the ray interacts with a plane mirror. Applying Snell's Law, we can substitute $-n_1$for n_2 to get

$$n_1 \sin\theta_1 = -n_1 \sin\theta_2$$

$$\Rightarrow -\theta_1 = \theta_2.$$

Thus, we know the angle of incidence of a light ray is equal to the angle of reflection when a ray interacts with a plane mirror. We therefore conclude "reflection at a plane […] interface may be mathematically treated as refraction from a medium of refractive index n to a medium of refractive index –n" [19]. Essentially, reflection is just a form of severe refraction.

We initially had hopes of constructing a model of the Pepper's Ghost illusion using the properties of light reflection. Understanding the foundations of the optics in mirrors provided us with preliminary mathematical research of reflection matrices.

2.2. REFLECTION MATRICES

Though, at the time, unsure of our direction of research, we felt building a repertoire of foundational mathematics was important to this study. In early attempts at modeling the reflective surface of glass featured in the Pepper's Ghost optical system, we focused our attention on studying the mathematical characteristics of reflection matrices. If we consider the y-axis of a coordinate plane to be the panel of glass, then the reflection of a point about this axis would involve a simple multiplication by the reflection matrix $\begin{pmatrix} -1 & 0 \\ 0 & 1 \end{pmatrix}$ [13]. A basic demonstration of this can be found in the Mathematica code in the appendix.

Because a simple reflection about the y-axis does not yield mathematically interesting results, we felt it would be beneficial to learn the techniques of reflecting a figure about any arbitrary line. Assume we want to reflect a figure about a line of the form $ax + by + c = 0$. There is a series of five matrix transformations we must perform in order to achieve a reflection matrix. First, we must translate the arbitrary line to pass through the origin with the matrix

$$\begin{pmatrix} 1 & 0 & 0 \\ 0 & 1 & -\frac{c}{b} \\ 0 & 0 & 1 \end{pmatrix}. \tag{1}$$

This matrix will shift the matrix up or down by a height of $\frac{c}{b}$. As a technicality, we notice $b \neq 0$, however, we will later remove this condition. We will notice that the line we are reflecting about creates an angle θ with the x-axis. Now the line must be rotated by $-\theta$, thus aligning with the x-axis. This rotation can be achieved with the following matrix:

$$\begin{pmatrix} \cos\theta & -\sin\theta & 0 \\ \sin\theta & \cos\theta & 0 \\ 0 & 0 & 1 \end{pmatrix}. \tag{2}$$

Now that the line has been transformed into the x-axis, we can reflect our figure about this axis using the well-known reflection matrix:

$$\begin{pmatrix} 1 & 0 & 0 \\ 0 & -1 & 0 \\ 0 & 0 & 1 \end{pmatrix}. \tag{3}$$

After the object has been reflected, we shall use the matrix

$$\begin{pmatrix} \cos\theta & \sin\theta & 0 \\ -\sin\theta & \cos\theta & 0 \\ 0 & 0 & 1 \end{pmatrix} \tag{4}$$

to rotate by θ, returning the line to its original orientation. Finally, the matrix

$$\begin{pmatrix} 1 & 0 & 0 \\ 0 & 1 & \frac{c}{b} \\ 0 & 0 & 1 \end{pmatrix} \tag{5}$$

shifts the line back to its original position where $(0, -\frac{c}{b})$ is the y-intercept. After obtaining the five necessary matrices to achieve a reflection about an arbitrary line, we can multiply matrices (1), (2), (3), (4), and (5) together to obtain the final reflection matrix [13]:

$$\begin{pmatrix} \cos^2\theta - \sin^2\theta & 2\sin\theta\cos\theta & \frac{2c}{b}\sin\theta\cos\theta \\ 2\sin\theta\cos\theta & \sin^2\theta - \cos^2\theta & -\frac{2c}{b}\cos^2\theta \\ 0 & 0 & 1 \end{pmatrix}. \tag{6}$$

To obtain a more practical reflection matrix, we will put matrix (6) in terms of $a, b,$ and c. Notice $\tan\theta = -\frac{a}{b}$. Using the common trigonometric identities

$$\sin^2\theta + \cos^2\theta = 1 \text{ and}$$

$$\sec^2\theta - \tan^2\theta = 1,$$

we know that

$$\cos^2\theta = \frac{1}{1+\tan^2\theta} = \frac{b^2}{a^2+b^2}, \tag{7}$$

$$\sin^2\theta = 1 - \cos^2\theta = \frac{a^2}{a^2+b^2}, \text{ and} \tag{8}$$

$$\sin\theta\cos\theta = \tan\theta\cos^2\theta = -\frac{ab}{a^2+b^2}. \tag{9}$$

The results from (7), (8), and (9) can be substituted into matrix (6) to obtain the simplified reflection matrix

$$\begin{pmatrix} \frac{b^2-a^2}{a^2+b^2} & -\frac{2ab}{a^2+b^2} & -\frac{2ac}{a^2+b^2} \\ -\frac{2ab}{a^2+b^2} & \frac{a^2-b^2}{a^2+b^2} & -\frac{2bc}{a^2+b^2} \\ 0 & 0 & 1 \end{pmatrix}. \tag{10}$$

Now that we have determined the final reflection matrix, notice that we can allow $b = 0$ as there are no longer any restrictions for the presence of b in the denominator [13]. To reflect a figure about an arbitrary line, we can put the ordered pairs of each vertex of the figure into matrix form and multiply this matrix by (10). Additional work with this reflection matrix is featured in the Mathematica code in the appendix.

This work with reflection matrices laid the foundation for a few possible directions of research involving the components of the Pepper's Ghost configuration.

CHAPTER 3
ATTEMPTED RESEARCH

Upon fully understanding the Pepper's Ghost illusion and the details of the reflection behind it, we were met with the question of: What kind of sophisticated mathematics can we uncover in this effect? Unfortunately, many of our motivated paths of research failed to yield any mathematically interesting results. We began exploring two possible routes of research. We first discussed how we could potentially alter the Pepper's Ghost illusion by modifying some of the components of the physical set up of the effect. Secondly, we discussed methods of imposing changes that would potentially ruin the visuals of the effect for observers.

While we had some unsuccessful attempts at finding interesting mathematics behind the Pepper's Ghost effect, we began exploring the possibilities of complicating a rather simple illusion.

3.1. ALTERING THE GLASS

The invisible sheet of glass featured in the Pepper's Ghost illusion is easily the most fascinating component of the optical system. Much thought went into the mathematical potential of altering some

aspect of the glass. We discussed tampering with the transparency of the glass, which acts as both a mirror and a transparent lens, to see how it would affect a reflected image through the use of refractive and reflective indices in a matrix. We also considered building a matrix to reflect a partial image based on the transparency of the glass. However, it was determined that this approach would only leave us with some blurry images, matrix multiplication, and an uninteresting model of Pepper's Ghost.

Though the illusion commonly uses a flat sheet of glass, we also discussed how creating curvature in the surface could distort the reflected image. Once again, a stretched, flipped, or transformed image could only be modeled with basic matrix transformations and optical ray diagrams.

Since the alteration of existing components of Pepper's Ghost seemed to be a dead end, we instead considered how the addition of another component could potentially disturb the flawless execution of the illusion within the Haunted Mansion.

3.2 RUINING THE EFFECT

The Pepper's Ghost set up in the Haunted Mansion is heavily reliant on the dimensions of the ballroom matching the dimensions and distances of the figures within the black box room. We discussed potentially changing the dimensions of the ballroom to see if our eyes would perceive the images differently in their new positions relative to the room. For example, moving the back wall of the ballroom closer to the pane of glass would potentially confuse the vision of the observer. Imagine a scenario in which a figure was placed in the back of the black box room, as far as possible from the glass panel. Moving the back wall of the ballroom closer to the glass would seem to render that figure, in a sense, out of range for reflection. However, when lit properly, that figure would still be reflected onto the glass. We wanted to consider how this figure would appear to the observer in reference to the ballroom. If the wall was transparent, the figure should appear behind it. However, since the wall is opaque, where would the observer's eyes place this figure in the ballroom? While these seemed to be interesting questions to explore, our mathematical analysis would only include the geometry of lighting and sight lines.

Another way we potentially wanted to ruin the effect was through adding different light sources along the back wall of the ballroom. The objects are lit from behind in the black box room, but placing more lighting along the back wall of the ballroom could potentially ruin the depth our eyes are perceiving the on the images. We also predicted that brightening the lighting of the ballroom would make the reflected images fainter. Recognizing that this method of ruining the illusion would not lead to useful results, we moved in yet another direction.

The most promising attempt at ruining the Pepper's Ghost illusion involved the addition of another reflective surface to the optical system. By adding a mirror to the back wall, we hypothesized our results would include multiple reflections back and forth between the glass and the additional surface. This system would have most likely yielded an infinite mirror effect in which two parallel reflective surfaces would bounce an infinite amount of reflected images between the two surfaces. With such reflections, we believed we would be able to construct sequences of matrices to model the effect. Once again, before delving into the math, we found nothing exciting or unique about this optical system.

Though these approaches did not produce any mathematically complicated results, the ideas featured in this chapter inspired our line of thinking to veer toward the question: How can we alter or complicate the Pepper's Ghost illusion? Once it became apparent that the original Pepper's Ghost illusion really was as simple as a flat pane of glass and a light source reflecting the image of an object, we decided to move in another direction.

CHAPTER 4
BLIND PEPPER'S GHOST

4.1. CREATING A NEW ILLUSION WITH SOUND

After determining that alteration of the existing configuration would not yield an innovative analysis, it became clear we had to rethink our approach. Instead of changing such a well-known effect, we propose the idea of creating a new illusion inspired by Pepper's Ghost. In this new illusion, we want to eliminate the need for light waves and use another type of wave to project toward an object. Using the

idea of creating an effect based on 'visible sound,' we can replace the light waves of the original effect with sound waves. Thus, we are creating the Blind Pepper's Ghost.

Instead of featuring a reflective panel of glass, a physical interpretation of the new illusion will use a wall made of a material receptive to sound, such as a wall of microphones. Placing a source of sound behind an object, we will study how the sound waves interact with the object. We want to analyze the differences in frequency of the sound waves as they hit the wall to detect the presence of an object. Using the data we receive based on the damping of the sound waves, we want to draw an image of the object on the wall. Figure 4 below demonstrates a simple configuration of the Blind Pepper's Ghost illusion.

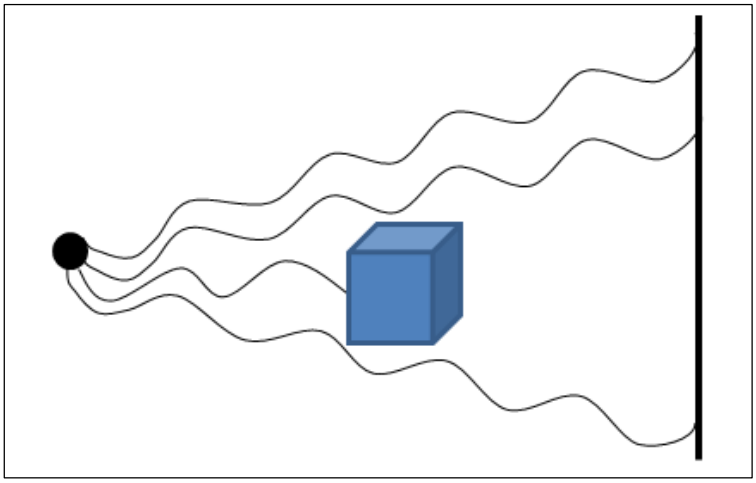

Figure 4: Blind Pepper's Ghost Configuration. An object, the blue box, is placed between a source of sound, the dark circle, and a wall. Sound waves emanating from the sound source then interact with the object.

4.2. THE WAVE EQUATION

In order to model the sound waves utilized in the Blind Pepper's Ghost effect, we must first understand the one-dimensional wave equation. The goal of this chapter is to develop mathematics to model a sound wave over a semi-infinite interval. We will find a solution to the one-dimensional wave equation and establish boundary conditions that model a wave with one fixed end, leaving the rest of the wave unbounded. We begin by solving the wave equation with fixed boundaries by a Fourier sine series in section 4.2.1. Using our findings from 4.2.1, we will solve the wave equation to obtain d'Alembert's

solution, a useful tool for determining solutions over an infinite boundary. Finally, we will modify our boundary problem to include a semi-infinite interval and use d'Alembert's solution to obtain the proper wave model we plan to use in the Blind Pepper's Ghost effect.

4.2.1. SOLVING THE WAVE EQUATION OVER A FINITE BOUNDARY

In order to model the sound waves passing through an object, it is important to understand the mathematics behind the one-dimensional wave equation. Finding a solution to describe the oscillating nature of the wave equation will require some rigorous work with partial differential equations. Note, the waves we will consider are horizontally stretched.

Using Newton's second law of motion, $F = ma$, the one-dimensional wave equation is derived from tension forces acting on both ends of the wave (gravity is neglected). Our solution, $u(x,t)$, will describe the vertical displacement of the wave from equilibrium at a time t with a horizontal spatial component x. Furthermore, the velocity of the propagation of the wave is denoted by c. The one-dimensional wave equation is as follows:

$$\frac{\partial^2 u}{\partial t^2} = c^2 \frac{\partial^2 u}{\partial x^2} \tag{11}$$

The first boundaries we will consider will be over a finite interval in which the both ends of the wave are fixed at equilibrium. Though it is not really possible to bound two ends of a sound wave, this is just a hypothetical case we will use to help us find an initial solution. Therefore the boundary conditions are

$$u(0,t) = 0, \tag{12}$$

$$u(L,t) = 0, \tag{13}$$

and the initial conditions are

$$u(x,0) = f(x), \tag{14}$$

$$\frac{\partial u}{\partial t}(x,0) = g(x). \tag{15}$$

Initial condition (14) assumes the initial displacement of the wave is $f(x)$, and initial condition (15) describes how quickly displacement is changing at an initial time zero with the function $g(x)$. Because the wave equation is both linear and homogenous, we can use separation of variables to solve and then apply the boundary conditions and initial conditions. In order to use this separation technique, it is important to recognize that we are looking for solutions of the form $u(x,t) = \varphi(x)h(t)$ [10]. This form is known as a product solution. Note:

$$\begin{aligned} \frac{\partial u}{\partial x} &= h(t)\frac{d\varphi}{dx}, \\ \frac{\partial^2 u}{\partial x^2} &= h(t)\frac{d^2\varphi}{dx^2} \text{ and} \\ \frac{\partial u}{\partial t} &= \varphi(x)\frac{dh}{dt}, \\ \frac{\partial^2 u}{\partial t^2} &= \varphi(x)\frac{d^2h}{dt^2}. \end{aligned} \tag{16}$$

Plugging the derivatives (16) into the wave equation (11), we obtain

$$\varphi(t)\frac{d^2h}{dt^2} = c^2\, h(t)\frac{d^2\varphi}{dx^2}.$$

Hence, we have reduced (11) to only include ordinary differential equations. Next, we separate the variables h and φ:

$$\frac{1}{c^2h}\,\frac{d^2h}{dt^2} = \frac{1}{\varphi}\,\frac{d^2\varphi}{dx^2} = -\lambda \tag{17}$$

where λ is a separation constant. This separation constant is introduced because we notice that the left hand side and right hand side of the equation above is constant when varying either x or t. We have made λ negative for convenience in the coming steps. Now equation (17) can be split into the following ordinary differential equations:

$$\frac{d^2h}{dt^2} = -\lambda c^2 h, \tag{18}$$

$$\frac{d^2\varphi}{dx^2} = -\lambda\varphi. \tag{19}$$

Using the boundary conditions (12) and (13), we can now determine the value of λ. We know

$$u(0,t) = \varphi(0)h(t) = 0, \tag{20}$$

$$u(L,t) = \varphi(L)h(t) = 0. \tag{21}$$

Focusing on (20), we recognize either $\varphi(0) = 0$ or $h(t) = 0$ for every t. If $h(t) = 0$, then the trivial solution $u(x,t) = 0$ arises. Since we want to find a nontrivial solution, let $\varphi(0) = 0$. A similar argument can be applied to (21), implying

$$\varphi(0) = \varphi(L) = 0. \tag{22}$$

A boundary problem is formed by (19) and (22). Now we must find the solutions to the ordinary differential equations (18) and (19). There are three cases we will analyze when solving for λ: $\lambda > 0$, $\lambda = 0$, and $\lambda < 0$ [10]. We will begin by first considering equation (19)

If $\lambda = 0$, then $\varphi(x) = c_1 + c_2 x$. However, as we are looking for the solution to (19), we notice that the second derivative of $\varphi(x) = c_1 + c_2 x$ will be zero. We would obtain the trivial solution $\frac{d^2\varphi}{dx^2} = 0$. Thus, we can disregard the case $\lambda = 0$.

We now consider the cases $\lambda > 0$ and $\lambda < 0$. First, notice that (19) becomes

$$\frac{d^2\varphi}{dx^2} + \lambda\varphi = 0 \tag{23}$$

Using methods for solving homogenous linear ordinary differential equations with constant coefficients, we assume e^{ax} is a solution to equation (23). Plugging the second derivative of e^{ax} into (23), we obtain

$$a^2 e^{ax} + \lambda e^{ax} = 0$$

$$\Rightarrow\ a^2 + \lambda = 0$$

$$\Rightarrow a = \pm\sqrt{-\lambda}.$$

If we let $\lambda < 0$, the square root of λ becomes real. Thus, we obtain

$$\varphi(x) = c_1 e^{x\sqrt{-\lambda}} + c_2 e^{-x\sqrt{-\lambda}}$$

Now we must apply the initial conditions (22) to get the system

$$\begin{cases} c_1 + c_2 = 0 \\ c_1 e^{L\sqrt{-\lambda}} + c_2 e^{-L\sqrt{-\lambda}} = 0. \end{cases}$$

Placing the coefficients of the system into a Wronskian, we get

$$\begin{vmatrix} 1 & 1 \\ e^{L\sqrt{-\lambda}} & e^{-L\sqrt{-\lambda}} \end{vmatrix} = e^{-L\sqrt{-\lambda}} - e^{L\sqrt{-\lambda}}.$$

If we can prove that the result of this Wronskian can be equal to zero, then we have shown that this solution $\varphi(x)$ is not linearly independent, and we cannot form a general solution when $\lambda < 0$ [18].

Let $y = L\sqrt{-\lambda}$. Then we allow

$$e^{-y} - e^{y} = 0$$

$$\Rightarrow 1 = \frac{e^{y}}{e^{-y}}$$

$$\Rightarrow 1 = e^{2y}$$

$$\Rightarrow y = 0.$$

Therefore, we have shown that $\varphi(x)$ does not have any negative eigenvalues [10].

Now if we let $\lambda > 0$, then the square root of λ is not real. Thus, we choose λ to be negative.

$$\varphi(x) = c_1 e^{xi\sqrt{\lambda}} + c_2 e^{-xi\sqrt{\lambda}}.$$

Using Euler's Formula, $e^{i\theta} = \cos\theta + i\sin\theta$, we obtain the following solution [18]:

$$\varphi(x) = c_1 \cos\left(x\sqrt{\lambda}\right) + c_2 \sin(x\sqrt{\lambda}). \tag{24}$$

Applying the boundary conditions (22), we get $\varphi(0) = 0 = c_1$ and $\varphi(L) = 0 = c_2 \sin(L\sqrt{\lambda})$. Now we can solve for λ:

$$0 = c_2 \sin\left(L\sqrt{\lambda}\right).$$

Because $0 = \sin(0) = \sin(\pi)$, then

$$L\sqrt{\lambda} = n\pi \text{ for all } n \in \mathbb{N}.$$

Hence,

$$\lambda = \left(\frac{n\pi}{L}\right)^2 \text{ for all } n \in \mathbb{N} \tag{25}$$

and the eigenfunctions are $\sin(\frac{n\pi x}{L})$. Note that these eigenfunctions are spatially dependent.

A similar consideration of three cases of λ can be used to determine that the solution to the time dependent equation (18) is

$$h(t) = c_1 \cos\left(ct\sqrt{\lambda}\right) + c_2 \sin\left(ct\sqrt{\lambda}\right). \tag{26}$$

Because we know the value of λ, we know (26) becomes

$$h(t) = c_1 \cos\left(\frac{n\pi ct}{L}\right) + c_2 \sin\left(\frac{n\pi ct}{L}\right) \tag{27}$$

where $h(t)$ is the solution to (18). Recall we are searching for a solution of the form $u(x,t) = \varphi(x)h(t)$. Multiplying the spatial eigenfunction by the time component (27) yields two product solutions:

$$u_n(x,t) = A_n \cos\left(\frac{n\pi ct}{L}\right) \sin\left(\frac{n\pi x}{L}\right),$$

$$u_n(x,t) = B_n \sin\left(\frac{n\pi ct}{L}\right) \sin\left(\frac{n\pi x}{L}\right)$$

where A_n and B_n are Fourier coefficients that are soon to be determined [10].

Because we notice that n can be any element of the natural numbers, we have an infinite number of linearly independent solutions with distinct eigenvalues. Thus, using the principle of superposition, we find that

$$u(x,t) = \sum_{n=1}^{\infty} \left(A_n \cos\left(\frac{n\pi ct}{L}\right) \sin\left(\frac{n\pi x}{L}\right) + B_n \sin\left(\frac{n\pi ct}{L}\right) \sin\left(\frac{n\pi x}{L}\right)\right) \text{ and} \tag{28}$$

$$\frac{\partial u}{\partial t} = \sum_{n=1}^{\infty} \left(A_n \left(\frac{-n\pi c}{L}\right) \sin\left(\frac{n\pi ct}{L}\right) \sin\left(\frac{n\pi x}{L}\right) + B_n \left(\frac{n\pi c}{L}\right) \cos\left(\frac{n\pi ct}{L}\right) \sin\left(\frac{n\pi x}{L}\right)\right).$$

Recalling initial conditions (14) and (15), the following can be established:

$$f(x) = u(x,0) = \sum_{n=1}^{\infty} \left(A_n \sin\left(\frac{n\pi x}{L}\right)\right), \tag{29}$$

$$g(x) = \frac{\partial u}{\partial t}(x,0) = \sum_{n=1}^{\infty} \left(B_n \left(\frac{n\pi c}{L}\right) \sin\left(\frac{n\pi x}{L}\right)\right). \tag{30}$$

From (29) and (30), we can see that $f(x)$and $g(x)$ are both Fourier sine series on $-L \leq x \leq L$. As mentioned previously, we can now solve for the coefficients A_n and B_n. First consider equation (29). Multiplying both sides of the equation by $\sin\left(\frac{mx\pi}{L}\right)$ where m is any natural number 1,2,3…, we get

$$f(x) \sin\left(\frac{mx\pi}{L}\right) = \sum_{n=1}^{\infty} A_n \sin\left(\frac{nx\pi}{L}\right) \sin\left(\frac{mx\pi}{L}\right).$$

By integrating both sides, the equation above becomes

$$\int_{-L}^{L} f(x) \sin\left(\frac{mx\pi}{L}\right) dx = \int_{-L}^{L} \sum_{n=1}^{\infty} A_n \sin\left(\frac{nx\pi}{L}\right) \sin\left(\frac{mx\pi}{L}\right)\, dx\,.$$

Notice that the series and the integral are interchangeable on the right hand side of the equation, and A_n can be pulled outside of the integral [10]. Because we are looking for solutions to the wave equation, a second order partial differential equation, we know that our solution u will be twice differentiable. Due to this fact, we can assume that the function we are integrating is uniformly convergent on the closed interval $[-L, L]$. Since the terms of the series are uniformly convergent and continuous we can switch the series and the integral as shown below [25]:

$$\int_{-L}^{L} f(x) \sin\left(\frac{mx\pi}{L}\right)\, dx = \sum_{n=1}^{\infty} A_n \int_{-L}^{L} \sin\left(\frac{nx\pi}{L}\right) \sin\left(\frac{mx\pi}{L}\right)\, dx. \tag{31}$$

In continuation, we are now left to solve the integral

$$\int_{-L}^{L} \sin\left(\frac{nx\pi}{L}\right) \sin\left(\frac{mx\pi}{L}\right)\, dx. \tag{32}$$

There are two cases we must consider in order to solve: $n = m$ and $n \neq m$. First consider the case $n = m$ in which

$$\int_{-L}^{L} \sin^2\left(\frac{nx\pi}{L}\right)\, dx$$

$$\Rightarrow \int_{-L}^{L} \frac{1-\cos\left(\frac{2nx\pi}{L}\right)}{2}\, dx. \tag{33}$$

Substituting $u = \frac{2nx\pi}{L}$ and $du = \frac{2n\pi}{L}dx$ into integral (33), we obtain the simplified integral

$$\frac{L}{4n\pi}\int 1-\cos(u)\ du.$$

Integrating and reverting back to the original terms, the solution becomes

$$\frac{L}{4n\pi}\left[x-\sin\left(\frac{2n\pi x}{L}\right)\right]\Big|_{-L}^{L} = L-\left(\frac{L\sin(2n\pi)}{2n\pi}\right) = L.$$

Because n is a natural number, note that $\sin(n\pi) = 0$ for any n. Thus, when $n = m$, the solution to integral (32) is L.

Now consider the case $n \neq m$. The integral (32) becomes

$$\frac{1}{2}\int_{-L}^{L} \cos\left(\frac{(n-m)\pi}{L}x\right) - \cos\left(\frac{(n+m)\pi}{L}x\right) dx \tag{34}$$

using trigonometric identities.

By splitting (34) into two integrals and using u-substitution, we get

$$\frac{L}{2(n\pi-m\pi)}\sin\left(\frac{(n-m)\pi x}{L}\right) - \frac{L}{2(n\pi+m\pi)}\sin\left(\frac{(n+m)\pi x}{L}\right)\Big|_{-L}^{L}$$

$$= \frac{L}{(n\pi-m\pi)}\sin\big((n-m)\pi\big) - \frac{L}{(n\pi+m\pi)}\sin\big((n+m)\pi\big) = 0.$$

Once again, $\sin(k\pi) = 0$ for any natural number k. Therefore, $\sin\big((n-m)\pi\big)$ and $\sin\big((n+m)\pi\big)$ will always be equal to zero. We conclude integral (32) is zero when $n \neq m$.

We denote these solutions as

$$\int_{-L}^{L} \sin\left(\frac{nx\pi}{L}\right)\sin\left(\frac{mx\pi}{L}\right) dx = \begin{cases} L & \text{if } n = m, \\ 0 & \text{if } n \neq m. \end{cases} \tag{35}$$

Recalling equation (31), we must now determine the infinite sum of (35) above. Recognize there only exists one instance in which $n = m$ but there are an infinite amount of cases when $n \neq m$. Hence,

$$\int_{-L}^{L} f(x)\sin\left(\frac{mx\pi}{L}\right)\,dx = \sum_{n=1}^{\infty} A_n \int_{-L}^{L} \sin\left(\frac{nx\pi}{L}\right)\sin\left(\frac{mx\pi}{L}\right)\,dx$$

$$= A_n(L + 0 + 0 + 0 + \cdots) = A_n L.$$

As we are integrating an even function, we can see that

$$2\int_{0}^{L} f(x)\sin\left(\frac{mx\pi}{L}\right)\,dx = A_n L\,. \tag{36}$$

Because the series behaves as if $n = m$, we will disregard the m in equation (36) and replace it with n. With a similar derivation, we can also solve for B_n using equation (30). Therefore, the Fourier coefficients are

$$A_n = \frac{2}{L}\int_{0}^{L} f(x)\sin\left(\frac{n\pi x}{L}\right)\,dx, \tag{37}$$

$$B_n = \frac{2}{n\pi c}\int_{0}^{L} g(x)\sin\left(\frac{n\pi x}{L}\right)\,dx. \tag{38}$$

Upon solving the wave equation (11) using separation of variables, we have concluded the solution is (28) where the coefficients A_n and B_n are (37) and (38), respectively. The solution $u(x,t)$ represents the wave's displacement from equilibrium [10]. While this solution is useful for a wave with fixed endpoints where there is no displacement from equilibrium at $x = 0$ and $x = L$, we wish to change the boundary conditions of the wave, allowing one end of the wave to be unbounded.

4.2.2 GENERALIZING THE SOLUTION OF THE WAVE EQUATION

Before finding the solution over a semi-infinite boundary, we must first show the wave equation solution can be generalized into d'Alembert's formula: $u(x,t) = F(x - ct) + G(x + ct)$ where F and G are arbitrary functions [10]. Then, we will solve the boundary problem over an infinite domain and modify this problem to include a semi-infinite domain with only one fixed endpoint on the wave. Understanding the characteristics of a semi-infinite wave will allow us to model the sound waves in the blind Pepper's Ghost effect.

Consider that the wave equation can be written as

$$\frac{\partial^2 u}{\partial t^2} - c^2 \frac{\partial^2 u}{\partial x^2} = 0 \tag{39}$$

$$\Rightarrow \frac{\partial}{\partial t}\left(\frac{\partial u}{\partial t}\right) - c\frac{\partial}{\partial x}\left(c\frac{\partial u}{\partial x}\right) = 0. \tag{40}$$

There are two ways in which equation (40) can be factored:

$$\left(\frac{\partial}{\partial t} + c\,\frac{\partial}{\partial x}\right)\left(\frac{\partial u}{\partial t} - c\,\frac{\partial u}{\partial x}\right) = 0 \text{ and} \tag{41}$$

$$\left(\frac{\partial}{\partial t} - c\,\frac{\partial}{\partial x}\right)\left(\frac{\partial u}{\partial t} + c\,\frac{\partial u}{\partial x}\right) = 0. \tag{42}$$

If we let

$$w = \left(\frac{\partial u}{\partial t} - c\,\frac{\partial u}{\partial x}\right), \tag{43}$$

$$v = \left(\frac{\partial u}{\partial t} + c\,\frac{\partial u}{\partial x}\right), \tag{44}$$

then (39) can be reduced into two first-order wave equations. Substituting w and v into (41) and (42), respectively, yields

$$\frac{\partial w}{\partial t} + c\frac{\partial w}{\partial x} = 0, \tag{45}$$

$$\frac{\partial v}{\partial t} - c\frac{\partial v}{\partial x} = 0. \tag{46}$$

We can find general solutions for each of these equations, focusing first on (45). By taking the derivative of $w(x(t), t)$, we analyze the rate of change "as measured by a moving observer $x = x(t)$" [10]. Thus, by the chain rule, the derivative is

$$\frac{d}{dt}\, w(x(t), t) = \frac{dx}{dt}\,\frac{\partial w}{\partial x} + \frac{\partial w}{\partial t}. \tag{47}$$

We interpret $\frac{\partial w}{\partial t}$ to be the change in w at a particular fixed position, $\frac{dx}{dt}$ is the rate of change of a moving observer, and $\frac{\partial w}{\partial x}$ is the rate of change of w with respect to a moving observer. Thus, comparing (47) to (45), we can interpret that if

$$\frac{dx}{dt} = c, \tag{48}$$

then

$$0 = c\frac{\partial x}{\partial t} + \frac{\partial w}{\partial t} = \frac{d}{dt}\, w(x(t), t)$$

$$\Rightarrow \frac{dw}{dt} = 0. \tag{49}$$

This means that if an observer is moving at a velocity c, then w is constant [10]. When this special case occurs, (45) can be reduced into two ordinary differential equations: (48) and (49).

Consider that the integration of (48) results in

$$x = ct + x_0 \tag{50}$$

where x_0 is the integration constant.

To find a general solution of w, we will begin by noting that if $t = 0$, then $w(x, 0) = P(x)$ where $P(x)$ is an arbitrary function. Then, it is possible to determine w at the point (x, t). Along the characteristic line, a line along which the characteristic of the wave is constant, we notice w is constant. Therefore we know that when $t = 0$, then $x = x_0$. This yields

$$w(x, t) = w(x_0, 0) = P(x_0).$$

Recognizing that $x_0 = x - ct$ by equation (50), then we can conclude

$$w(x, t) = P(x - ct).$$

This is known as the general solution to (45) [10]. A similar derivation will yield the general solution of (46) shown below:

$$v(x, t) = Q(x + ct).$$

Thus far, we know

$$w(x,t) = \left(\frac{\partial u}{\partial t} - c\,\frac{\partial u}{\partial x}\right) = P(x-ct) \text{ and}$$

$$v(x,t) = \left(\frac{\partial u}{\partial t} + c\,\frac{\partial u}{\partial x}\right) = Q(x+ct)$$

by equations (43) and (44). Adding w and v yields the equation

$$\frac{\partial u}{\partial t} = \frac{1}{2}[P(x-ct) + Q(x+ct)].$$

Thus, integrating to find u, we obtain the following general solution to the wave equation:

$$u(x,t) = F(x-ct) + G(x+ct). \tag{51}$$

Notice $F = \int \frac{1}{2}P(x-ct)\,dt$ and $G = \int \frac{1}{2}Q(x+ct)\,dt$ where F and G are arbitrary functions. This solution is interpreted as the sum of a wave $F(x-ct)$ moving right at a velocity c and a wave $G(x+ct)$ moving left at a velocity $-c$ [10].

Equation (51) was obtained in 1947 by French mathematician Jean le Rond d'Alembert. Known as d'Alembert's formula for the wave equation, we will use (51) to further solve the wave equation over different boundaries.

4.2.3 D'ALEMBERT'S SOLUTION OVER AN INFINITE BOUNDARY

Next, we will solve for F and G to find d'Alembert's solution to the one-dimensional wave equation over an infinite boundary. It is important to understand the solution over an infinite boundary in order to obtain the solution to the wave equation over a semi-infinite boundary.

The initial conditions over the infinite boundary are

$$u(x,0) = f(x) \qquad -\infty < x < \infty, \tag{52}$$

$$\frac{\partial u}{\partial t}(x,0) = g(x) \qquad -\infty < x < \infty. \tag{53}$$

Using equation (51), the initial condition (52) implies

$$f(x) = F(x) + G(x). \tag{54}$$

Note, the partial derivative of u with respect to t is

$$\frac{\partial u}{\partial t} = -c\,F'(x-ct) + c\,G'(x+ct).$$

Applying initial condition (53) by letting $t = 0$, this becomes

$$\frac{\partial u}{\partial t} = -c\frac{dF}{dx} + c\frac{dG}{dx}.$$

Thus, we get

$$\frac{g(x)}{c} = -\frac{dF}{dx} + \frac{dG}{dx}. \tag{55}$$

Taking the derivative of (54) with respect to x yields

$$\frac{df}{dx} = \frac{dF}{dx} + \frac{dG}{dx}. \tag{56}$$

We can create a system of equations with (55) and (56). By eliminating $\frac{dF}{dx}$, we get

$$\frac{dG}{dx} = \frac{1}{2}\left(\frac{df}{dx} + \frac{g(x)}{c}\right). \tag{57}$$

Now we can integrate to find G as shown below:

$$G(x) = \frac{1}{2}f(x) + \frac{1}{2c}\int_0^x g(\bar{x})\,d\bar{x}\,.$$

Additionally, we can solve for $F(x)$. Recall equation (54) can be rearranged to get $F(x) = f(x) - G(x)$.

Substituting (57) into this equation yields

$$F(x) = \frac{1}{2}f(x) - \frac{1}{2c}\int_0^x g(\bar{x})\,d\bar{x}\,.$$

Now we can substitute $F(x)$ and $G(x)$ into (51) to get

$$u(x,t) = \frac{f(x-ct)}{2} + \frac{f(x+ct)}{2} + \frac{1}{2c}\left[\int_0^{x+ct} g(\bar{x})d\bar{x} - \int_0^{x-ct} g(\bar{x})\,d\bar{x}\right]$$

$$\Rightarrow\ u(x,t) = \frac{f(x-ct)}{2} + \frac{f(x+ct)}{2} + \frac{1}{2c}\left[\int_{x-ct}^{x+ct} g(\bar{x})d\bar{x}\right]. \tag{58}$$

Equation (58) is known as d'Alembert's solution [10]. Instead of using the rather complicated Fourier sine series solution to the one-dimensional wave equation obtained in section 4.2.1 to model a sound wave, we will use d'Alembert's far more elegant solution.

4.2.4. WAVE EQUATION SOLUTION OVER A SEMI-INFINITE BOUNDARY

The next step is to fix one end of the wave and unbound the other end to find a solution over a semi-infinite boundary.

To recap our findings so far, recall the wave equation:

$$\frac{\partial^2 u}{\partial t^2} = c^2 \frac{\partial^2 u}{\partial x^2}.$$

The boundary condition is

$$u(0,t) = 0,$$

and the initial conditions are

$$u(x,0) = f(x) \text{ and}$$
$$\frac{\partial u}{\partial t}(x,0) = g(x).$$

Also recall d'Alembert's solution is

$$u(x,t) = F(x-ct) + G(x+ct).$$

where the initial conditions are satisfied if

$$F(x) = \frac{1}{2}f(x) - \frac{1}{2c}\int_0^x g(\bar{x})\, d\bar{x} \quad \text{where } x > 0, \tag{59}$$

$$G(x) = \frac{1}{2}f(x) + \frac{1}{2c}\int_0^x g(\bar{x})\, d\bar{x} \quad \text{where } x > 0. \tag{60}$$

The functions F and G do not allow x to be infinite. Hence, these functions are only valid over a semi-infinite boundary where $x > 0$. Now when considering the d'Alembert formula (51), we must ensure the arguments of F and G remain positive. Considering G, we notice that $x + ct$ will always be positive because $x > 0$ and $t > 0$. However, the arguments of F are more complicated. We will consider

the cases in which $x - ct > 0$. For $x > ct$, the function F requires x and t to be positive. In the case of $x < ct$, x and t must be negative to get a positive argument for the function $F(-x + ct)$.

Therefore, when $x > ct$, all of the arguments are positive, and we determine that the solution to the wave equation over a semi-infinite boundary is the same as the solution over an infinite boundary:

$$u(x,t) = \frac{f(x-ct) + f(x+ct)}{2} + \frac{1}{2c}\left[\int_{x-ct}^{x+ct} g(\bar{x})d\bar{x}\right], \qquad x > ct. \tag{61}$$

However, this solution cannot be utilized when $x < ct$. As stated above, the function G is always valid due to the positivity of x and t. We will have to apply the boundary condition (12) to F to obtain a solution for negative arguments. If $u(0,t) = 0$, then $0 = F(-ct) + G(ct)$ according to the d'Alembert solution to the wave equation. Since $t < 0$, notice that $F(-ct)$ becomes $F(ct)$and $G(ct)$ becomes $G(-ct)$ in this case. For an arbitrary value z, this implies

$$F(z) = -G(-z). \tag{62}$$

Using the results of (62), we have determined that the wave equation solution is

$$u(x,t) = G(x+ct) - G(-x+ct)$$

when $x - ct < 0$. Thus,

$$u(x,t) = \frac{f(x+ct) - f(-x+ct)}{2} + \frac{1}{2c}\left[\int_{x-ct}^{x+ct} g(\bar{x})d\bar{x}\right], \qquad x < ct. \tag{63}$$

In summation, we have determined two possible solutions for the wave equation over a semi-infinite boundary. We have determined when $x > ct$ solution (61) should be used, and when $x < ct$, solution (63) should be utilized [10]. However, since we intend to use the wave equation to model a real world scenario capable of being physically constructed, we will disregard the case of $x < ct$ due to the negativity of the time and space arguments. Therefore, the solution we will be utilizing in the model of the blind Pepper's Ghost illusion will be equation (61).

4.3. POSSIBLE USES FOR THE WAVE EQUATION

Understanding the solution of the wave equation now allows us to begin working with the Blind Pepper's Ghost illusion. We can use MATLAB to draw sound waves using the Fourier solution for a finite boundary to gain a better understanding of the behavior of a simulated wave. The code demonstrating the displacement of a wave at a particular time can be found in the appendix.

4.3.1. FINDING THE ARBITRARY FUNCTIONS

Modeling such waves would require us to find the functions $f(x)$ and $g(x)$ of equation (61) so they are no longer arbitrary. We have determined that certain types of sound waves will take on different forms, so $f(x)$ and $g(x)$ will be dependent on the type of sound source featured in the new effect. The basics of creating this system in MATLAB will include using this idea of sonar to simply detect a barrier placed between the sound source and the wall before proceeding to draw more complicated objects.

4.3.2. DETECTING BARRIERS USING DAMPED AMPLITUDE

Once we are able to successfully detect the presence of a basic obstacle interfering with the waves, we will want to study how the waves will interact with an actual object we want to project onto the wall. Using the solution to the wave equation over a semi-infinite boundary, we could attempt to pass a series of sound waves at this object. Allowing the waves to propagate through the object to the wall, we could analyze the amplitudes of the waves at their point of impact with the wall. Recall that the wave equation solution yields a wave's displacement from equilibrium. With this information, we consider the maximum displacement to be the amplitude of the wave. We anticipate damping to occur if a wave passes through an object, so we should be able to draw the outline of an object based on the locations on the wall where amplitude has been changed. We will assume if the amplitude has not changed, then the wave did not encounter an object.

CHAPTER 5
FURTHER DEVELOPING THE BLIND PEPPER'S GHOST

5.1 ENHANCING THE BLIND PEPPER'S GHOST MODEL WITH MULTI-DIRECTIONAL WAVES

Thus far, we have solved the one-dimensional wave equation over a semi-infinite boundary. With this solution, we can model the mathematics of a new version of the Pepper's Ghost illusion using sound waves. Using the amplitude of the sound waves, we want to detect the presence of a barrier. Once this is accomplished, we could draw the simple outline of an object based on an analysis of the existence of varying amplitudes in the sound waves as they make contact with the back wall.

We would also like to enhance the Blind Pepper's Ghost illusion one step further. In the proposed configuration for the Blind Pepper's Ghost effect, we allow waves to propagate through an object in a single direction. This modeling technique only yields the two-dimensional outline of an object to be drawn. A far cry from the impressive, three-dimensional appearance of reflected figures in the original Pepper's Ghost illusion, we can achieve an effect that can imitate the original more closely. Instead of sending waves through a figure in one direction, we want to project waves at an object in multiple directions. Each direction should draw the outline of the figure from a different angle. When combining each outline into one image, we can produce a more detailed dimensional picture. This method would force us to find a way to project this image to another location, as there will have to be a different wall facing each set of sound waves. The physical set up would consist of at least two sets of sound sources. In the simplest version of this set up, we can consider the two sets of sound sources to be separated by ninety degrees. In this situation, when waves are emitted, they will be perpendicular. Instead of using one wall to measure the amplitude of the waves, we must now include two walls: one placed between each set of sound sources and the object.

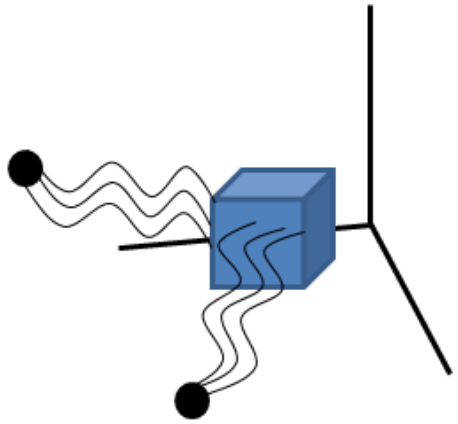

Figure 7: A Multi-Directional Wave Blind Pepper's Ghost Configuration.

The more sound sources we place at different angles, the more outlines we will acquire.

5.2 CHOOSING A PATH FOR MODELING

After further developing the concept of the Blind Pepper's Ghost model, it became clear that there were two possible directions in which to continue our research.

By studying sound wave interactions within different mediums, we could proceed to add damping terms to the one-dimensional wave equation and analyze the difference in wave amplitudes as they encounter an object. With this approach, we anticipate to encounter some insurmountable problems given our available resources. As a sound wave passes from one medium to another, it may exhibit a specific boundary behavior, a wave's reaction at the interface of a new medium. These boundary behaviors are either reflected pulses or transmitted pulses [5]. With the promise of unpredictable wave reflection, we expect to encounter interfering sound waves at the boundaries of new media, making it difficult to analyze amplitude. Thus, we settle upon the conclusion that studying the amplitudes of individual sound waves may not yield any conclusive results.

The second direction of research leads us to study the image reconstruction aspect of the Blind Pepper's Ghost model with multi-directional waves. Instead of using the wave equation to determine the presence of an object, we could assume the proposed model functions properly to produce image

projections from multiple angles. We now want to know how to recreate a three-dimensional image of the physical object by reconstructing a set of two-dimensional images.

CHAPTER 6
FORMING AN IMAGE RECONSTRUCTION APPROACH

Pursuing a new angle of research once again leaves us with many questions. If we assume the Blind Pepper's Ghost illusion successfully executes, what do the projection images on any given wall tell us about the physical object they represent? In other words, how can we undo the projections on the wall to recreate the object?

6.1 PROJECTION RECONSTRUCTION

Let's consider an example of a box used as the object in the Blind Pepper's Ghost model. If we execute a multi-directional illusion configuration across four walls, we will have four projection shadows. Assuming the object is equidistant from all four walls, we want to know how those four shadows can be puzzled back together to recreate the box by tracing the projections backwards until they intersect as seen in the figures below.

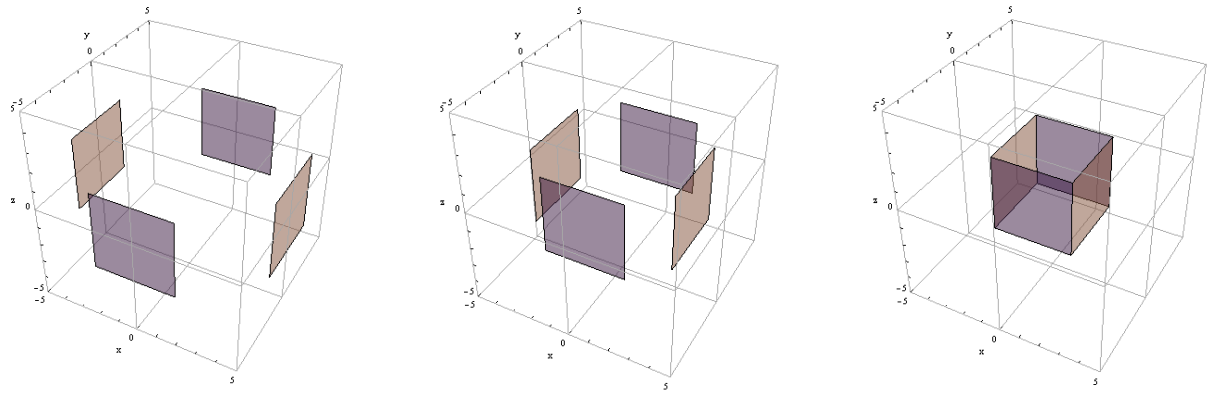

Figure 6: Proposed Image Reconstruction. These images show the image reconstruction we want to attempt by pulling four projections back to meet at corresponding edges. These images are from a program coded in Mathematica.

Given the idea of tracing shadows back to intersect leaves us questioning what further information needs to be known before attempting to reconstruct an object: Do we need to know the distance from the object to a wall? How will the system handle an object with varying thickness throughout, such as a pyramid? In order to answer such questions, it became clear we need to better understand the specifics of turning sound into image by further examining object/sound interaction. If we can understand what object/sound wave interaction occurred within the Blind Pepper's Ghost illusion, then perhaps we can understand how shadows can be traced backwards to reconstruct an image of the object.

6.2 TOMOGRAPHY

Searching for preexisting research about image reconstruction, we discovered a topic of study known as tomography. Tomography is "an X-ray technique that that isolates objects in a particular plane of interest" [6]. Mostly used for medical imaging purposes in CAT scans, tomography gathers data from waves that penetrate an object and uses that data to construct a cross-sectional image of the object in a specific plane [6]. To execute the Blind Pepper's Ghost model, we shift our focus to the study of digital image processing to obtain inspiration for three-dimensional image reconstruction.

In tomography, when waves are sent through an object, an intensity function is produced [6]. The source of the wave can then be moved to produce more intensity functions that can then be stacked upon one another to recreate a three-dimensional image resembling the physical object. The cross-sectional projections are obtained with the Radon transform. The Radon transform is a mathematical transform used to find projections of an object from multiple angles [6]. The inverse of the Radon transform is used in tomography to reconstruct three-dimensional images [2]. The Radon transform is given by

$$d_r(p,\theta) = \iint_{-\infty}^{\infty} d(x,y)\delta(x\cos\theta + y\sin\theta) - s \;\; dy\, dx.$$

where $d_r(p,\theta)$ is a projection image captured from an angle θ on a plane p [6]. Given the intensity functions $d(x,y)$, the Radon transform can find the line integrals of the intensity functions along a

particular line that has a distance s from the origin. With the inclusion of the Dirac delta function δ, a generalized function, we conclude that Radon transforms are a complicated method of reconstructing images [2].

6.3 ABANDONING PROJECTIONS

With the understanding of Radon transforms' ability to reconstruct an image using cross-sections, we abandon the idea of tracing preexisting projections backwards to assemble an object. However, instead of using Radon transforms for image reconstruction, we are inspired by the idea of applying different mathematical transforms to data to produce a three-dimensional image using the Blind Pepper's Ghost model. This once again raises many questions about our configuration: When sound encounters an object versus when it does not, what will differences in the sound waves tell us about the object? What kind of information from the sound is needed to detect such a difference? Essentially, we want to determine what the data obtained from sound waves will tell us about an object in order to reconstruct it. In this study, we will design experiments using the Blind Pepper's Ghost configuration to obtain transformable data to detect differences in sound spectra in MATLAB.

CHAPTER 7
EXPERIMENT DESIGN

In order to determine what information sound waves give us about an object, we must first understand how sound waves behave when encountering an object. In hopes of finding a measurable difference in spectrum when sound encounters an object versus when it does not, we have designed a small-scale configuration of the Blind Pepper's Ghost illusion to conduct sound experiments.

7.1 EXPERIMENTAL BLIND PEPPER'S GHOST CONFIGURATION

As originally proposed, the Blind Pepper's Ghost model requires a device to send out a sound signal and some kind of material to act as a wall to receive the sound. Instead of a wall, we will use a

second device to collect the sound transmitted by the first. For our experiments, such transmitting and recording devices can be found in our back pockets. A smart phone can both record and send sound signals needed for this configuration design. For the purpose of our testing, we will use Apple devices. In an ideal experimental design, we would have used two iPhones. As we only have access to one personal iPhone, we were forced to use an iPad to account for the second device.

The configuration consists of the iPhone and iPad placed flat on a table 31.7 centimeters apart, the length of the ruler used to space them. The speaker end of each device is facing the other. Due to the size difference in the iPad and iPhone, the iPhone is placed in line with the speaker of the iPad to ensure accurate recordings.

Figure 7: Experimental Blind Pepper's Ghost Configuration without Object. This is a view of the configuration from above. The iPhone (left) is spaced 31.7 centimeters from the iPad (right).

When experimenting with objects, the object is then placed halfway between the two devices as in the figure below.

Figure 8: Experimental Blind Pepper's Ghost Configuration with Object. This is a side view of the configuration with simple object placed halfway in between the devices.

For an appropriate source of sound, we use the smart phone application IntervalTimer by Deltaworks. Intended for exercise use, the IntervalTimer app allows the transmitting device to chime at user-specified time intervals. For the purposes of our experiments, we have set the timer to ring a bell every five seconds. Due to the app's slightly inaccurate timer, the bell instead rings every 4.8 seconds in

each sound wave we examine. Each bell chime emitted from the device consists of an initial clang tone that dies away within approximately one second. In each trial, the iPad serves as the sound-transmitting device. It is important to note that the volume of the iPad must remain the same for each experiment as the volume of the bell increases with the iPad controls. Results will be inaccurate if the iPad volume changes at all between trials.

The iPhone is then implemented as the recording device. To record the sound sent from the iPad, we use the preinstalled Voice Memos app on the iPhone. The Voice Memos app allows users to record a sound clip and trim it down to the desired length of time. Each recording can then be emailed to a recipient in the form of an M4A sound file and saved to a computer.

7.2 CLIP EDITING CONVENTIONS

In order to properly compare the sound spectra, the chimes of the bells have to align at the start of every recording. Therefore, each recording has to be trimmed to the appropriate length. Since it is impossible to align the times of the first chime in each recording, milliseconds were trimmed off the front of every sound clip. To keep all trials consistent, the appropriate number of milliseconds was cut from the beginning of each clip to ensure the initial chime rang at the three-second mark. The image below depicts the trimming of the beginning of the recording in the Voice Memos app. Notice that the disturbance of sound in the recording is one chime of a bell from the IntervalTimer app.

Figure 9: Voice Memos Recordings Before and After Trimming. The unedited recording is on the left. The trimmed recording (right) is trimmed so the chime of the bell begins at the three-second mark.

Other conventions were adopted when recording each trial, as well. We allowed the bell to ring four times per recording to give each spectrum a forced periodicity. This periodicity is an important characteristic required to apply mathematical transforms to the model in the coming chapters. The total time length of the sound clips is addressed in the succeeding sections.

7.3 MATLAB IMPLEMENTATION

As previously discussed, each recording is emailed from the iPhone to a recipient. Once the sound recordings are saved to a computer in an M4A file, we use MATLAB to analyze a visual spectrum for each clip. MATLAB uses the `audioread` function to read in a sound file. This function reads each file in as an $n \times 1$ matrix where n is the number of samples taken [16]. The `audioread` function returns the sampling frequency at which the data was recorded. The Voice Memos app records audio at CD sampling rates of 44,100 samples per second. This means the sampling frequency for all of our sound recordings will be 44,100 hertz. To find n, simply multiply the sampling frequency by the time length of the sound

samples. For example, a clip 21.06 seconds long, will read in 928,746 data points. The significance of a 21.06 second sound clip is discussed later.

From here, we know that each data point represents the amplitude of the sound wave recorded at a given time. Plotting the time versus the amplitude will result in the example below.

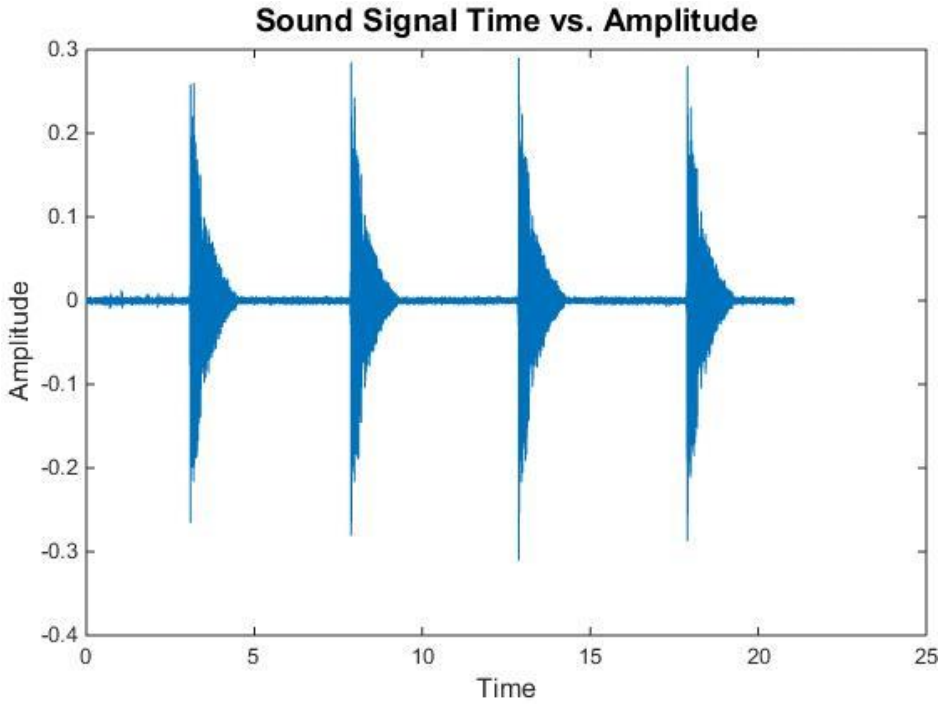

Figure 10: Full Data Spectrum. This graph plots amplitude versus time of 928,746 data points over a 21.06 second recording. Each disturbance in the spectrum represents one ring of the bell chime from the IntervalTimer app.

As we notice in the figure above, there are far too many plotted points to properly analyze the spectrum. Instead of using every point on the plot, we must filter away some of the data to create a more reasonable spectrum. In order to accomplish this filtering, we create a new array in MATLAB and fill it with a sparse sampling of the data, taking one point in every 3,000 to give a total of 310 plotted amplitudes for a 21.06 second recording. We also note that because amplitude is the displacement of a wave from equilibrium, we can take the absolute value of each data point to make future manipulations more manageable. The graph below shows the same signal featured in Figure 10 as a filtered spectrum with amplitudes of positive magnitude.

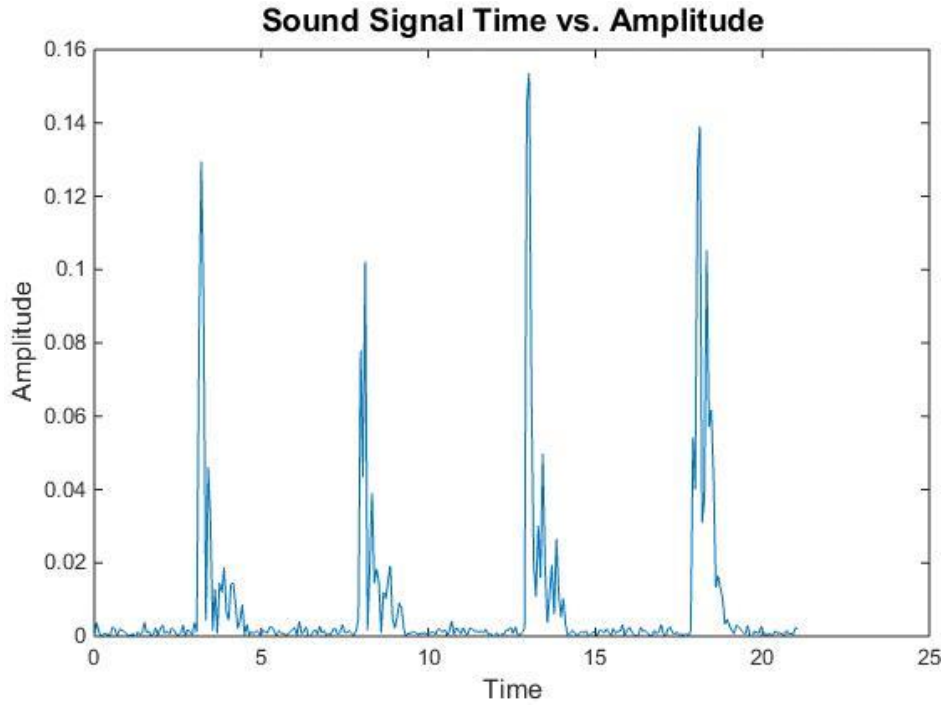

Figure 11: Filtered Data Spectrum. This graph plots 310 points of the spectrum used in Figure 10. This provides a sampling of the data across the spectrum. The absolute value has been taken of each of the amplitudes.

An example of the MATLAB code that we used to generate filtered data plots can be found in the appendix.

7.4 OTHER RECORDING CONVENTIONS

It is important to note that, much like snowflakes, no two sound recordings are the same. Even when measuring a set of control trials with no objects, the spectra are similar, yet different for each recording. Thus, we resolve to take the average of five consecutive filtered sound samples per object to eliminate any extraneous data. The average waveform that results will be the spectrum we use in our analysis. Example graphs of sets of five recordings and their average waveform can be found in the appendix.

As we have mentioned, there is some intricacy involved in determining the total time length of each recording. When using MATLAB to analyze the spectra, it is important that all vectors be the same length. Therefore, we need all recordings to be the exact same time length. Due to the large number of

sound clips recorded, we should note that in order to save us from the time-consuming editing process, only the first sound sample in each group of five recordings was trimmed to a conventional length. The other recordings in the set are deliberately longer than this conventional length and are truncated within the MATLAB code.

To give each spectrum a reasonable length, the first recording in each set of five was trimmed to a length of twenty-one seconds. Because the Voice Memos application tacks an additional few milliseconds to the end of a recording (most likely for purposes ensuring accurate sampling frequency), the total conventional length of the first sound clip in each set is 21.06 seconds. The other recordings are at least twenty-two seconds long and were only read in up until the 21.06-second mark. This ensures each recording is graphed with the same number of data points.

7.5 PROCEDURE

We will adhere to the same procedure for each experiment. As described above, the recording and transmitting devices are placed on a flat surface in a quiet room with as little background noise as possible. Care was taken to ensure the use of the same room and table surface to conduct the major experiments to eliminate possible sources of error and variability unless otherwise noted. To keep the volume of the bell rings consistent, set the iPad volume to level eight. Without an object placed between the devices, press the record button on the Voice Memos app on the iPhone. Wait until at least three seconds have passed, then press the start button on the IntervalTimer app on the iPad. After the bell rings four times, press the stop button on IntervalTimer. Allow the Voice Memo recording to continue until the total time length is at least twenty-two seconds before pressing the stop button. This ensures there will be plenty of time on each end of the sound recording to trim away excess milliseconds. Repeat four additional times for a total of five trials. Trim away the length at the start of each recoding to align the chime with the three-second mark. Next, trim the length at the end of the first recording in the set to twenty-one seconds, resulting in a 21.06 second clip. Email the memos to the desired recipient, and save them to a computer to be read into MATLAB. This set of recordings will be the control group. Repeat the

experiment with various objects placed between the Apple devices. For clarity, only one object at a time is placed between the devices in all object trials unless otherwise specified.

CHAPTER 8
OBJECT DETECTION EXPERIMENT

Unsure if the experimental design would yield any results, we first had to test the configuration for basic object detection. The objective of this experiment is to find a noticeable difference in the sound spectra of the control trials and object trials. Because this experiment was executed in the early stages of the testing process, the trials were run in a different room than the rest of the succeeding experiments. The results of this minor experiment are not used to develop any models, so this should not present any issues.

In this experiment, two objects were tested and compared against control trials without an object. Out of convenience, two textbooks of varying sizes were used as the objects, which we shall label Book X and Book Y. Book X, a small paperback textbook, is 22.7 centimeters long, 15.2 centimeters wide and 2.1 centimeters high. Hardcover and considerably larger than Book X, Book Y is 23.1 centimeters long by 21.9 centimeters wide by 7.8 centimeters high.

Applying the procedure, a book is placed halfway between the recording and transmitting devices for the object trials. Each book is positioned upright with the spine placed flat on the table, the front cover facing the iPhone. The length by width surface faces the recording device with the length by height surface aligned with the table. Three sets of five recordings are taken to account for a control set, a Book X set, and a Book Y set. Each sound file is then read into MATLAB. Using the methods described in Chapter 7, each set of five recordings are averaged into a single spectrum. Comparing the control spectrum to Book X waveforms and Book Y waveforms results in the following graph:

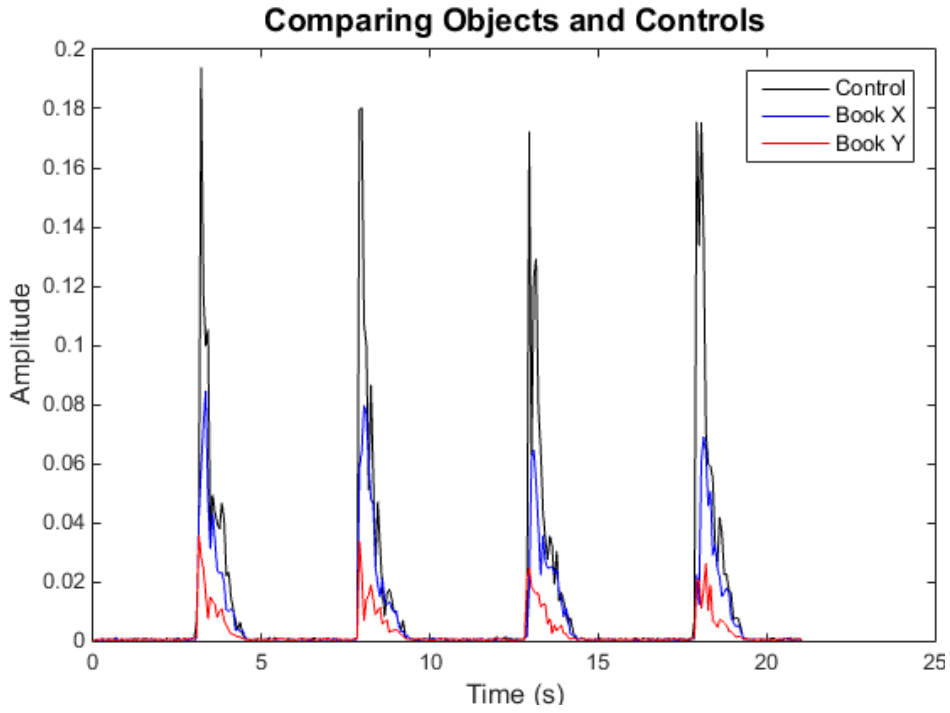

Figure 12: Comparison of Objects and Controls.

We can see that the configuration has detected a significant spectral difference between the recordings of the control, Book X, and Book Y. The amplitude of Book X's waveform is noticeably smaller for each ring of the bell as compared to that of the control while the amplitude of Book Y's waveform is even less than that of Book X. Figure 12 yields promising results, suggesting not only can we detect the presence of an object, but we can also detect a dimensional difference between two objects.

Since we only wanted to detect the presence of an object, this experiment is far too flawed to conclusively prove we are truly measuring a particular dimension of each book. The books each have different dimensions and varying hardness of the covers. The results of this experiment suggest that it may be possible to measure a particular object dimension using sound. We will hereafter refer to this dimension as thickness. As there are too many variables that could have affected this experiment, we will implement a new experiment with more object consistency in an attempt to determine a correlation between differences in sound spectra and object thickness.

CHAPTER 9
DEVELOPING A RAW DATA MODEL

As suggested by the results of the previous tests, the experimental Blind Pepper's Ghost configuration may be capable of measuring an object's thickness. Therefore, we want more consistency in the dimensions and characteristics of the objects we are testing. Ideally, we need objects with the same lengths and widths, varying only in height. By observing the changes in waveform when performing the sound testing with each object, we want to determine a difference in sound spectra caused by object thickness.

9.1 OBJECT DESCRIPTION

Finding objects of the same composition and dimension with varying thickness is not an easy task. We first considered using a 3D printer to build objects to the desired dimensions. In this scenario, we would have printed four objects 10 centimeters long and 15 centimeters wide with respective thicknesses of 1 centimeter, 2 centimeters, 4 centimeters, and 8 centimeters. Unfortunately, this method of printing perfectly proportioned plastic blocks proved to be extremely time consuming.

Remaining consistent with the previous experiment, we chose to continue using books as our test objects. To find multiple books of like length and width dimensions and varying thickness, we searched for book series released with consistent construction. One of the most popular book series of the past twenty years, the *Harry Potter* series matched our criteria perfectly. The series consists of seven books, however, we only had access to five of the seven when performing this experiment: the first, second, fourth, fifth, and seventh books in the series. Each book is the same in length and width, yet varying in thickness from 2.8 to 5.7 centimeters. The exact dimensions of each book are displayed below:

Book Number	Length (cm)	Width (cm)	Height (cm)
1	23.5	15.5	2.8
2	23.5	15.5	3.2
4	23.5	15.5	5.5
5	23.5	15.5	5.7
7	23.5	15.5	5.2

Figure 13: Book Dimensions. Each book has the same length and width with varying height.

Unsure of what factors affected our results in the previous experiment, it is important that we test object positional variations. Therefore, the configuration was tested with each object placed in three different positions which will henceforth be referred to as Side A, Side B and Side C. Side A, like the placement of the books in the previous experiment, features the book with the spine flat on the table, the front cover facing the iPhone. Side B features the book lying flat on the surface between the iPad and iPhone, the length by width surface flat on the table with the width by height surface pointing toward the devices. Side C features the length by height surface flat on the table, the width by height side facing the devices. The images below demonstrate the positions of sides A, B and C for the books.

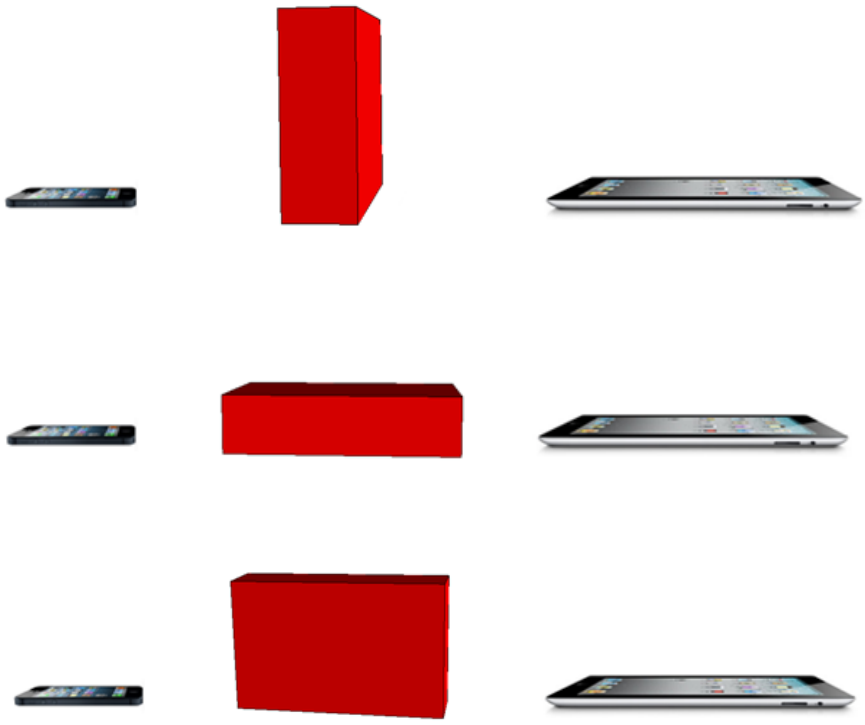

Figure 14: Object Placement Between Devices. These images show the positional placement of each book for sides A (top), B (middle), and C (bottom).

9.2 WAVEFORM LABELING CONVENTIONS

Before we proceed, it is beneficial for the reader to understand the naming conventions used for each recording as we use these abbreviations to label forthcoming graphs. Now that we have established that we will record sound for five out of seven *Harry Potter* book objects from three sides, we will label spectra as HP1A, HP1B, HP1C, HP2A … HP7B, HP7C. Consider the abbreviation HP1A. This label refers to *Harry Potter* book one, Side A.

9.3 SPECTRAL RESULTS

With three angles, five trials per side, and five books, we recorded and edited seventy-five object sound samples to accomplish this experiment. Applying the procedure and manipulating the sound files in MATLAB yielded five average waveforms per side, one for each book. The individual spectra for each recording can be found in the appendix along with the corresponding average waveform. We can compare all of the superimposed average spectra for each side of each book below.

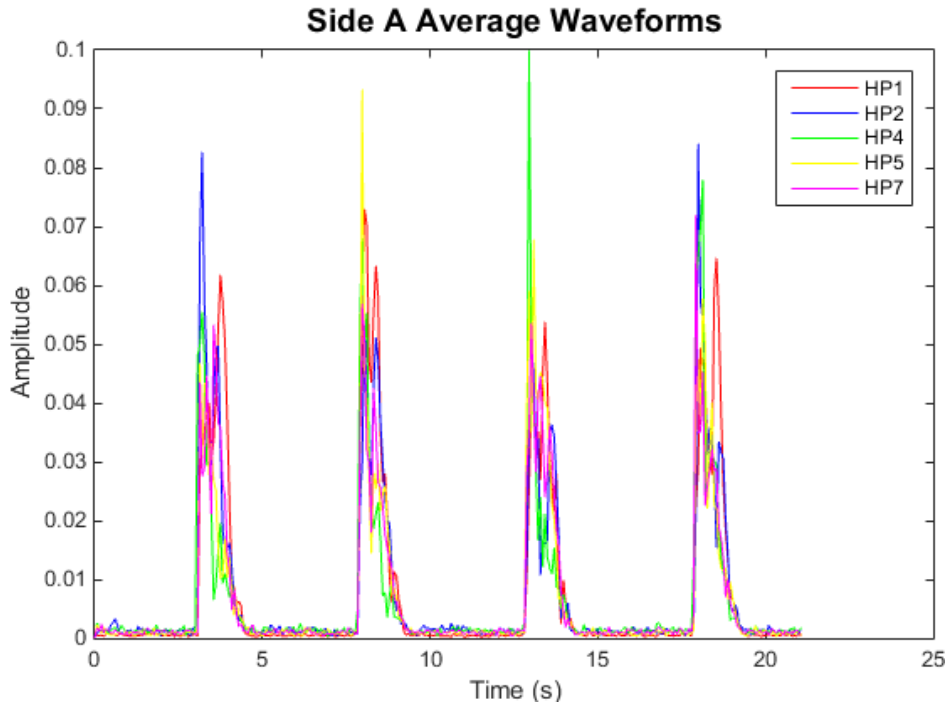

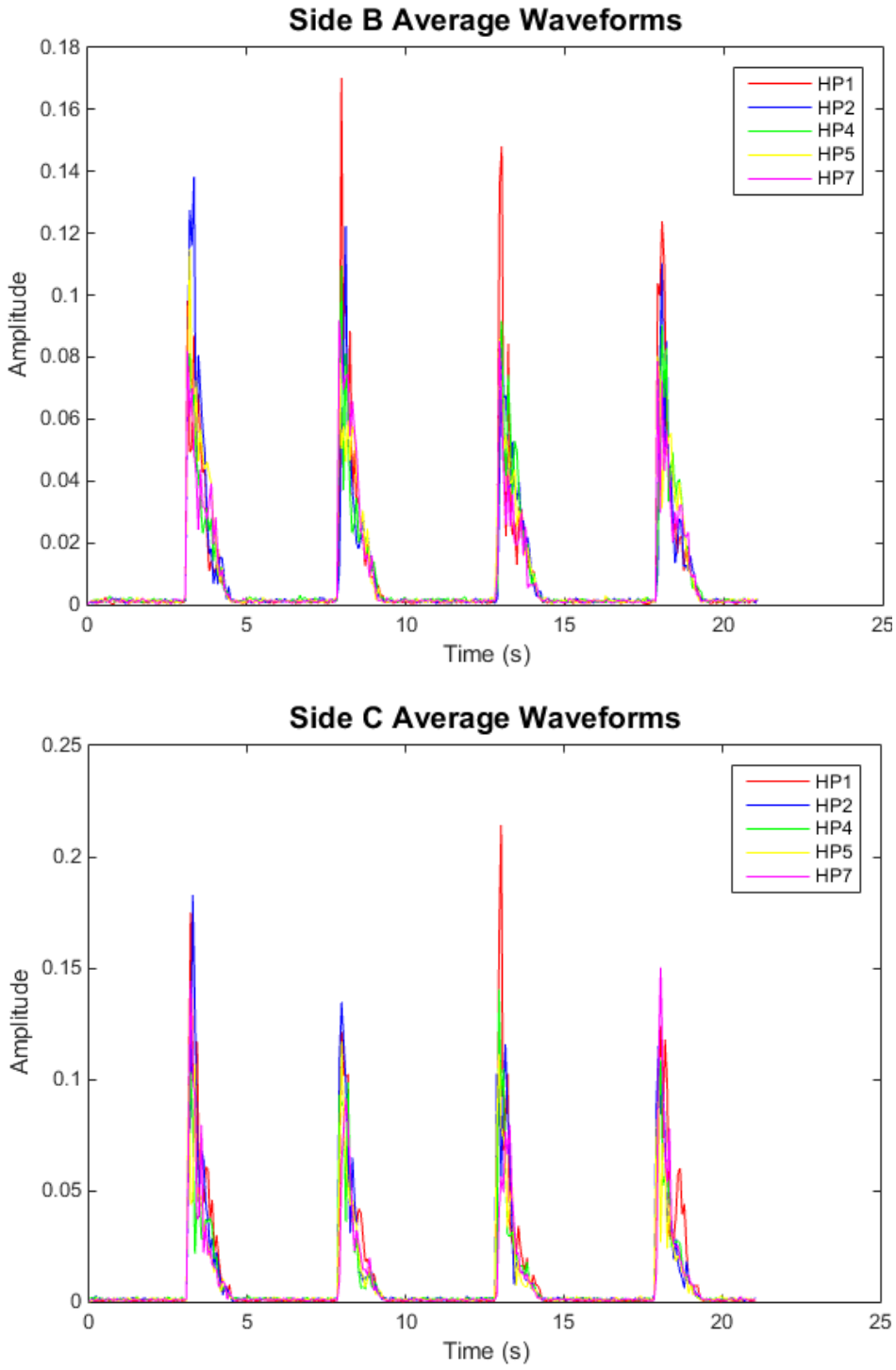

Figure 15: Average Waveforms of Sides A, B, and C.

We can see that there are still differences in the spectrum peaks of each book, though they are not as drastic as the results of the previous experiment due to the smaller difference in thickness between the objects. There are some inconsistently high peaks found throughout the spectra, but we keep in mind that

the recordings do not produce perfectly consistent waves. These fifteen averages can also be viewed individually in the appendix.

Because the length and width of each book are the same, we are now confident that the noticeable difference in each average waveform is somehow indicative of each book's thickness.

In hopes of finding a correlation between each book's thickness and unique waveform, we want to find a numerical difference between the control spectrum and average book spectra. In order to accomplish this, we want to find the area under each object's sound curve and subtract the result from the area of the control curve to obtain a difference.

Thus, we use MATLAB to apply numerical integration to find the area under each waveform. We use the trapezoidal rule to obtain an area approximation for the sixteen waveforms we want to compare. After applying the trapezoidal rule, we obtain areas for each wave shown below. The areas are displayed in respective book number order HP1, HP2, HP4, HP5, and HP7 for sides A, B, and C.

```
areasA =

    0.1669    0.1611    0.1394    0.1416    0.1438

areasB =

    0.2138    0.2066    0.2006    0.2051    0.1874

areasC =

    0.2598    0.2385    0.1959    0.1867    0.1974

areaControl =

    0.2777
```

Now we subtract each book area from the control area to produce three dictionaries of area differences, one for each of Sides A, B, and C. The data from the difference dictionaries is shown below.

```
diffDictionaryA =

    0.1108    0.1166    0.1383    0.1361    0.1338

diffDictionaryB =

    0.0638    0.0711    0.0771    0.0726    0.0903

diffDictionaryC =
```

```
0.0179    0.0392    0.0818    0.0909    0.0803
```

We notice the differences are greater for the sides with the most surface area facing the recording devices. The sides providing less of an obstacle for the sound to diffract around show much smaller differences between the object waveform area and the control area.

To observe the potential correlation between sound spectra and object thickness, we proceed to plot each book's area difference to its thickness to produce the following graphs for each side:

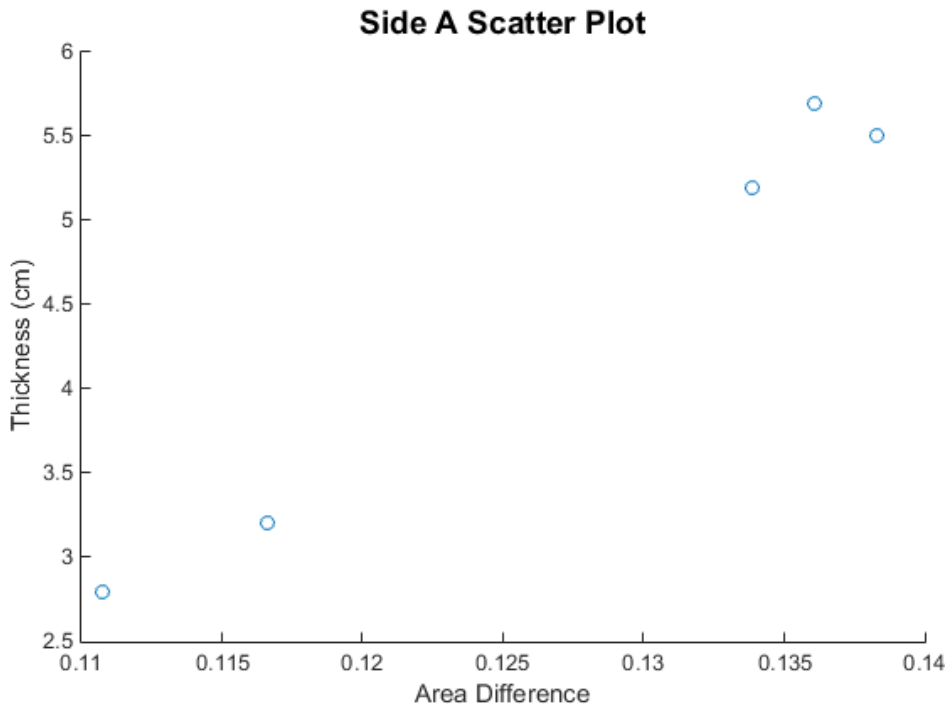

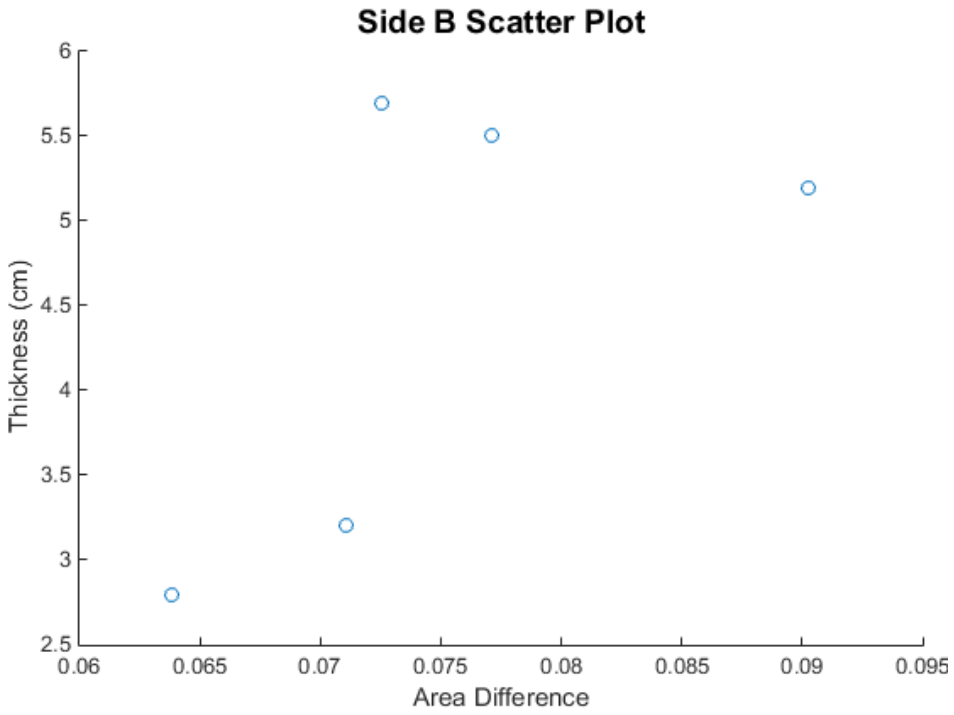

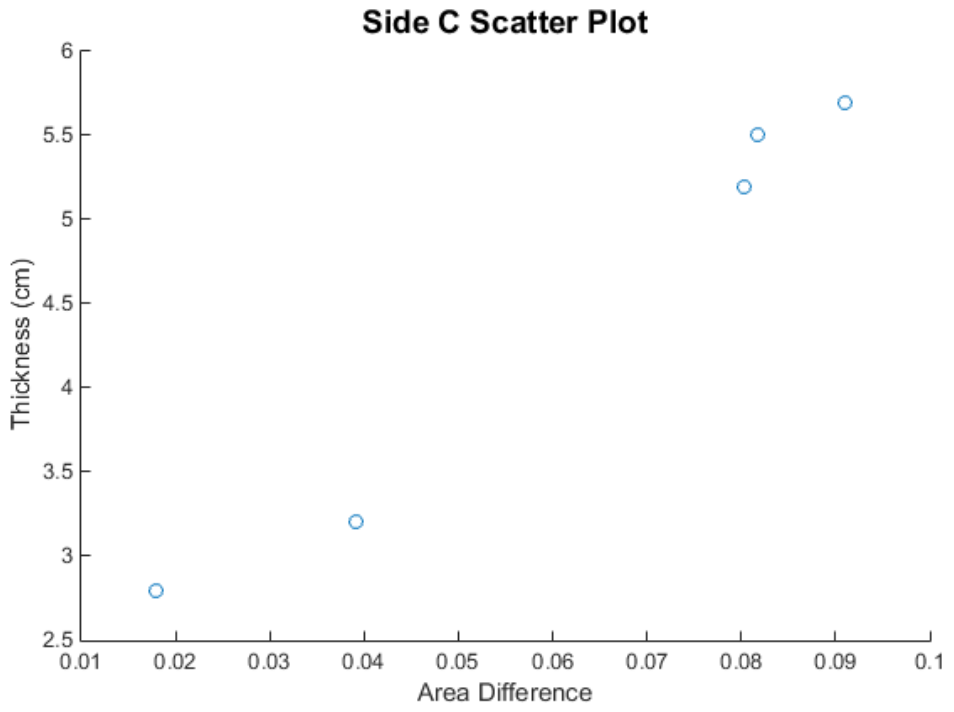

Figure 16: Scatter Plot of Area Difference against Object Thickness for Sides A, B, and C.

Based on the results of the graphs above, we can see sides A and C appear to demonstrate a strong correlation between spectral area difference and object thickness, while Side B produced a comparison graph of seemingly random points. To interpret our results mathematically, we will perform a regression analysis.

9.4 REGRESSION RESULTS

To perform a linear regression, we want to minimize error using the method of least squares [4]. Drawing a line through the data, we want to minimize sum of the squared distance from each data point shown in the graphs above to a best fit line. We will denote the distance from each data point (x_i, y_i) to the line as r_i. Let

$$r_i = y_i - mx_i - b$$

for each data point. Thus, we want to minimize

$$R = \sum_{i=1}^{n} r_i^2 = \sum_{i=1}^{n} (y_i - mx_i - b)^2.$$

In order to do this, we can take the partial derivative of R with respect to m and b and set these equations equal to zero [4]:

$$\frac{\partial R}{\partial m} = 0 = -2\sum_{i=1}^{n} (y_i - mx_i - b),$$

$$\frac{\partial R}{\partial b} = 0 = -2\sum_{i=1}^{n} (y_i - mx_i - b)x_i.$$

From here, we can derive formulas for m and b to minimize each r_i value. However, MATLAB's `polyfit` function will produce the coefficients of the best-fit polynomial we desire to superimpose upon the graphs in Figure 16 for us [15]. Because the points in the graphs of sides A and C appear to show both a linear and quadratic relationship, we perform regression twice per graph with polynomials of degrees one and two. The graphs of the best-fit curves as compared to the original points are shown below.

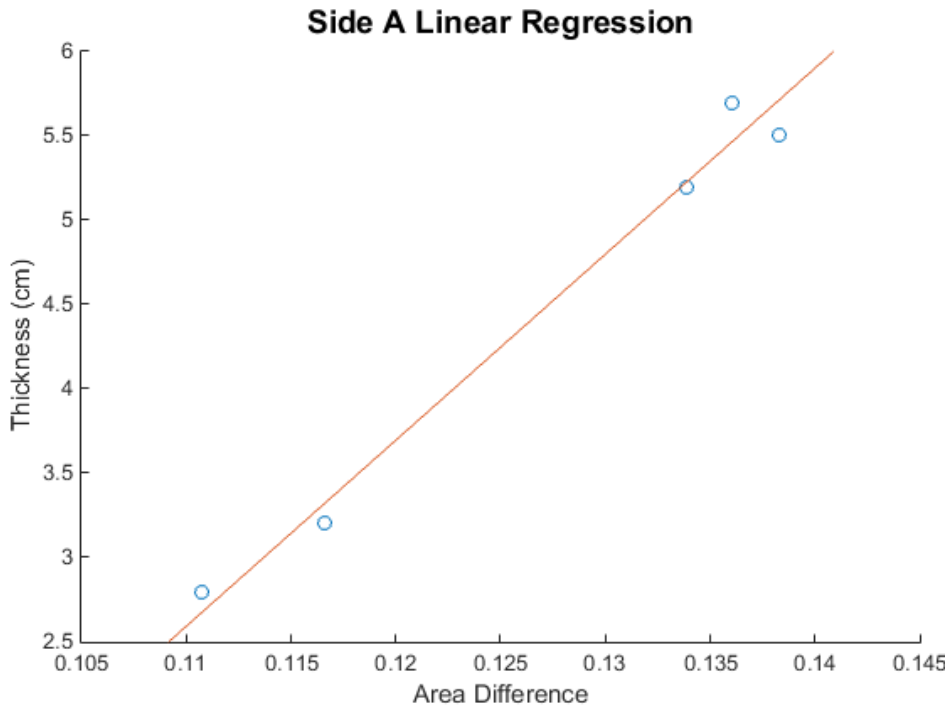
Side A Linear Regression
Thickness (cm)
Area Difference
6
5.5
5
4.5
4
3.5
3
2.5
0.105
0.11
0.115
0.12
0.125
0.13
0.135
0.14
0.145

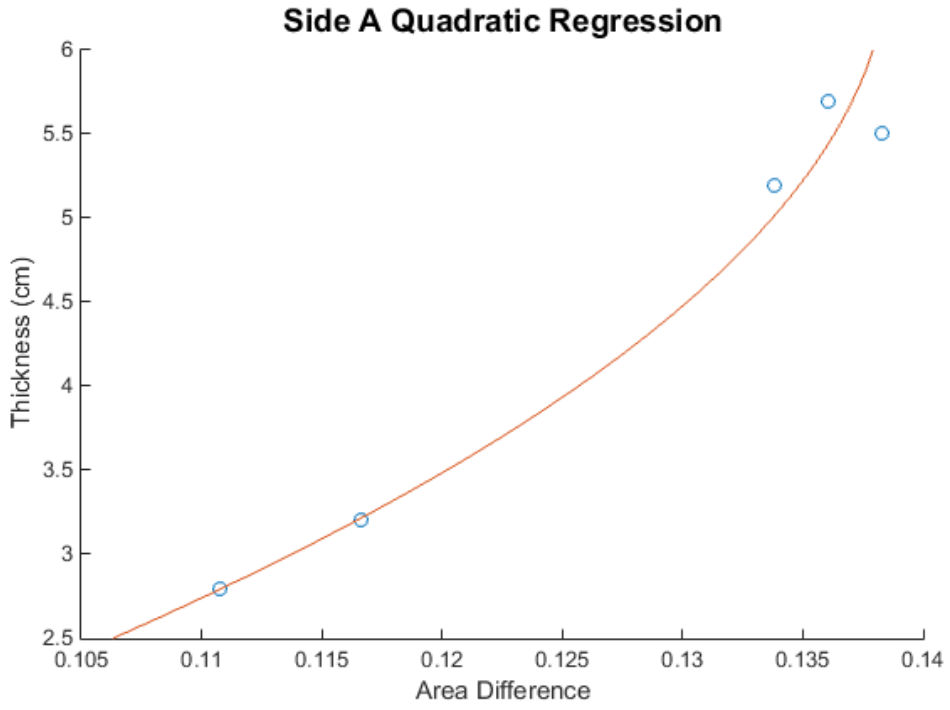
Side A Quadratic Regression
Thickness (cm)
Area Difference
6
5.5
5
4.5
4
3.5
3
2.5
0.105
0.11
0.115
0.12
0.125
0.13
0.135
0.14

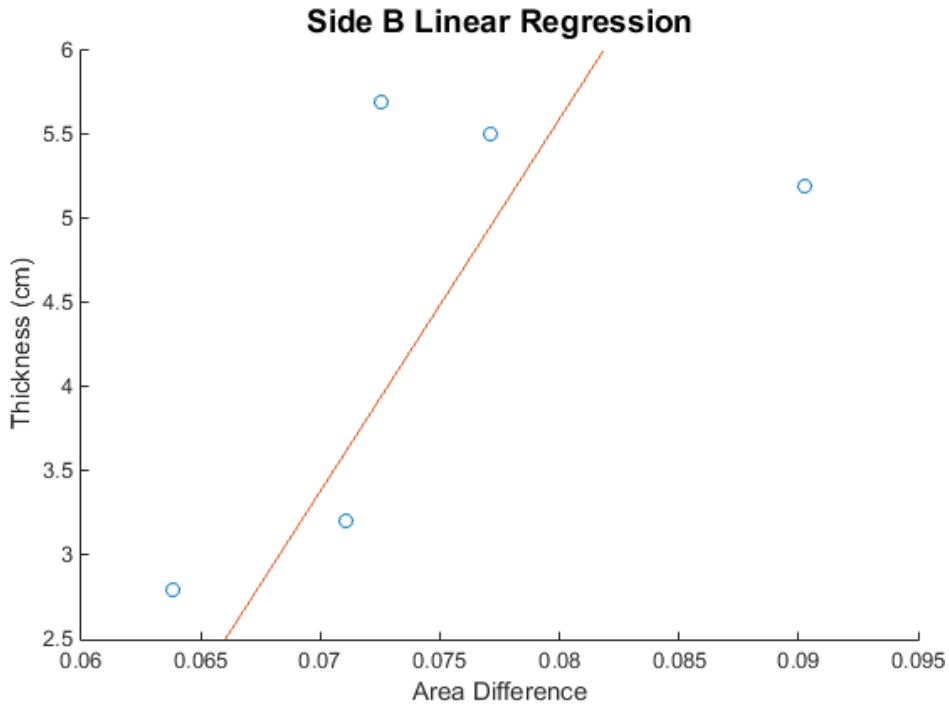
Side B Linear Regression
Thickness (cm)
Area Difference
6
5.5
5
4.5
4
3.5
3
2.5
0.06
0.065
0.07
0.075
0.08
0.085
0.09
0.095

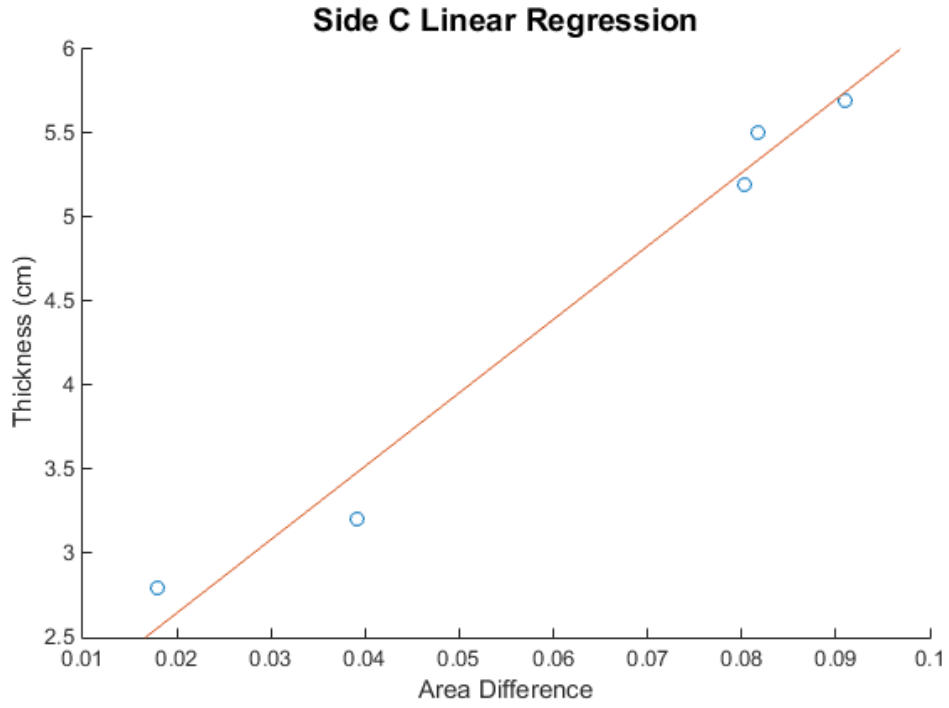
Side C Linear Regression
Thickness (cm)
Area Difference
6
5.5
5
4.5
4
3.5
3
2.5
0.01
0.02
0.03
0.04
0.05
0.06
0.07
0.08
0.09
0.1

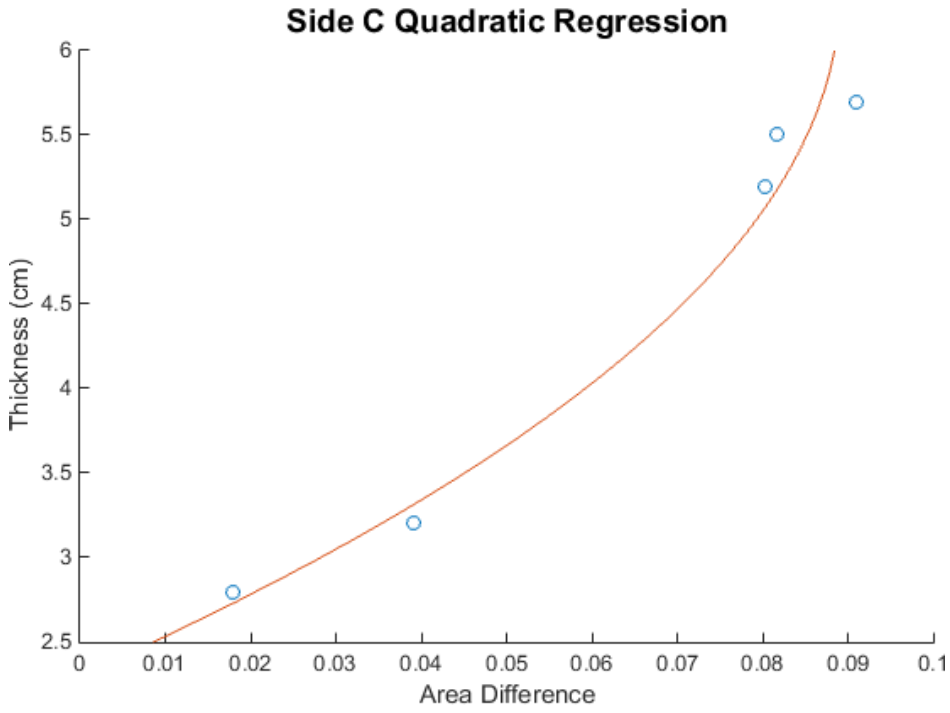

Figure 17: Regression Analysis of Sides A, B, and C. Sides A and C have both linear and quadratic best-fit curves superimposed upon the data. Side B only has linear regression applied because a quadratic curve is irrelevant to the data.

While it is clear the graphs representing the tests of Side A and Side C demonstrate a strong correlation between area difference and object thickness, the graph of the Side B points do not provide an accurate model on which to base any claims. Thus, we will focus mainly on the results of the regression of graphs of sides A and C.

According to the regression results for sides A and C, it is feasible that either a linear or a quadratic relationship exists between average waveform area difference and object thickness. In order to confirm which model is more accurate, more objects would need to be tested. Though both models produce promising results, we use MATLAB to calculate a linear correlation coefficient between area difference and dimension. A correlation coefficient that is approximately equal to one or negative one implies a strong linear relationship between two variables [4]. After implementing the calculations in MATLAB, we determine the correlation coefficients of graph A and graph C to be 0.9916 and 0.9886, respectively. With such a strong implication of a linear relationship, we will assume that the linear model is more reasonably reliable with the bounds of our data.

With a successful regression analysis and an indication of a strong linear relationship between waveform area difference and object thickness in two out of the three sides tested, we claim to have created a model that will predict an unknown object's thickness using the area underneath the waveform produced when sound encounters the object.

9.5 ERROR ANALYSIS OF SIDE B

While the area differences of Side A and Side C waveforms produce clean linear relationships, the results of Side B's area difference and object thickness are far less encouraging. In fact, the correlation coefficient of Side B points is calculated to be 0.6323.

We postulate that the Side B model was inconclusive due to the physical positioning of the books. Because Side B featured a book flat on the table with the front cover juxtaposed to the surface, we believe the sound was able to easily travel over the top of the book to reach the recording device. The height of each book had very little impact on the area difference as compared to the control as seen in the preceding data. The sound did not indicate a significant presence of an object when encountering the Side B position. In hindsight, we should have performed a more thorough experimentation by testing more than three book positions.

Though the results of Side B testing are inconclusive, we are not finished with them as we attempt to develop another model to predict object thickness. Perhaps another approach could prove to be more effective when examining the spectral results of Side B.

CHAPTER 10
DEVELOPING A TRANSFORMED DATA MODEL

10.1 FOURIER TRANSFORMS

Our initial goal was to apply a mathematical transform to analyze the difference in sound waveforms when they encounter various objects. Though the raw data model produced better-than-anticipated results, it relies on a large amount of data over each recording's entire time domain.

Therefore, we want to create a new model with transformed data that can possibly allow us to analyze a spectrum with only a few terms of a series. We hope this model will be simpler in the aspect that we can filter away even more data using a subset of terms that still provide an accurate understanding of each waveform's characteristics. Using the same sound recordings from the raw data experiment, the new model will involve transforming the signal data with Fourier transforms.

10.1.1 DERIVATION OF FOURIER COEFFICIENTS

Fourier transforms are used in digital signal processing to modify a sound signal using mathematical techniques. These transforms allow us to understand new aspects of the signals we have recorded by converting the time domain to a frequency domain [20]. Because we have created a periodic function with each waveform, we can represent our waveform function as series of sines and cosines. The discrete Fourier transform will be used to convert the real, discrete data points we have accumulated from the raw data into a complex quantity consisting of sine and cosine components [20].

The waveform function $f(t)$, a function of time, can be written as a real trigonometric polynomial to represent a sound signal in the time domain as follows [8]:

$$f(t) = a_0 + \sum_{n=1}^{\infty} [a_n \cos(2\pi nt) + b_n \sin(2\pi nt)]. \tag{64}$$

To find the function $f(t)$, we must solve for the unknown coefficients a_0, a_n, and b_n using manipulation of trigonometric identities [8].

In order to calculate these coefficients, we must first understand the results of the following three integrals [23]:

$$\int_0^L \sin(2\pi nt) \sin(2\pi mt)\ dt, \tag{65}$$

$$\int_0^L \cos(2\pi nt) \cos(2\pi mt)\ dt, \tag{66}$$

$$\int_0^L \sin(2\pi nt) \cos(2\pi mt)\ dt. \tag{67}$$

Using trigonometric identities to find the solutions of integrals (65), (66), and (67), we can find a_0, a_n, and b_n. Let us first solve integral (65). Consider the trigonometric identities

$$\cos(2\pi nt + 2\pi mt) = \cos(2\pi nt)\cos(2\pi mt) - \sin(2\pi nt)\sin(2\pi mt) \tag{68}$$

$$\cos(2\pi nt - 2\pi mt) = \cos(2\pi nt)\cos(2\pi mt) + \sin(2\pi nt)\sin(2\pi mt) \tag{69}$$

If we multiply identity (68) through by negative one and add (68) and (69) together, we get

$$2\sin(2\pi nt)\sin(2\pi mt) = \cos(2\pi nt - 2\pi mt) - \cos(2\pi nt + 2\pi mt). \tag{70}$$

Thus, integral (65) becomes

$$\frac{1}{2}\int_0^L [\cos(2\pi nt - 2\pi mt) - \cos(2\pi nt + 2\pi mt)]\ dt. \tag{71}$$

Splitting (71) into two integrals results in

$$\frac{1}{2}\int_0^L \cos(2\pi t(n-m))\ dt - \frac{1}{2}\int_0^L \cos\big(2\pi t(n+m)\big)\ dt. \tag{72}$$

If we perform u-substitution on each integral in (72) and evaluate at the limits of integration from zero to L, we obtain the following solution to integral (65):

$$\frac{\sin\big(2\pi L(n-m)\big)}{4\pi(n-m)} - \frac{\sin\big(2\pi L(n+m)\big)}{4\pi(n+m)}. \tag{73}$$

Now we must consider two cases when interpreting solution (73): $n \neq m$ and $n = m$. If $n \neq m$, we can see that $\sin\big(2\pi L(n-m)\big)$ and $\sin\big(2\pi L(n+m)\big)$ will always be equal to zero. To further explain, let $k = L(n-m)$. It is clear that $\sin(2\pi k) = 0$. A similar case would follow for the term $\sin\big(2\pi L(n+m)\big)$, thus proving (73) is equal to zero when $n \neq m$. If $n = m$, we can rewrite equation (71) to be

$$\frac{1}{2}\int_0^L [\cos(2\pi nt - 2\pi nt) - \cos(2\pi nt + 2\pi nt)]\ dt$$

$$\Rightarrow \frac{1}{2}\int_0^L 1 - \cos(4\pi nt)\ dt. \tag{74}$$

Solving integral (74) gives us the following result:

$$\frac{t}{2} - \frac{\sin(4\pi nt)}{8\pi n} \Bigg|_0^L$$

After we evaluate over the given limits of integration, our solution to (74) is $\frac{L}{2}$ for the case $n = m$ [23].

A similar technique follows to solve integral (66). We once again add identities (68) and (69) together, this time forgoing the multiplication of negative one, to achieve the following result:

$$2\cos(2\pi nt)\cos(2\pi mt) = \cos(2\pi nt - 2\pi mt) + \cos(2\pi nt + 2\pi mt).$$

Thus, integral (66) becomes

$$\frac{1}{2}\int_0^L [\cos(2\pi nt - 2\pi mt) + \cos(2\pi nt + 2\pi mt)]\ dt. \tag{75}$$

The same methods used to solve integral (65) are used to solve integral (75). Applying such methods yields the same results as the previous integral. If $n \neq m$, (75) equals zero. If $n = m$, we conclude

$$\frac{t}{2} + \frac{\sin(4\pi nt)}{8\pi n} \Bigg|_0^L = \frac{L}{2}.$$

To solve the final integral (67), we make use of the trigonometric identity

$$2\cos(2\pi nt)\sin(2\pi mt) = \sin(2\pi nt + 2\pi mt) - \sin(2\pi nt - 2\pi mt). \tag{76}$$

Substituting (76) into integral (67) produces a new integral as shown below:

$$\frac{1}{2}\int_0^L [\sin(2\pi nt + 2\pi mt) + \sin(2\pi nt - 2\pi mt)]\ dt. \tag{77}$$

By splitting (77) into two integrals and using u-substitution on each, the following result occurs:

$$\frac{1}{2}\left(\frac{\cos\big(2\pi t(n+m)\big)}{2\pi(n+m)} - \frac{\cos\big(2\pi t(n-m)\big)}{2\pi(n-m)}\right) \Bigg|_0^L =$$

$$\frac{\cos\big(2\pi L(n+m)\big)}{4\pi(n+m)} - \frac{\cos\big(2\pi L(n-m)\big)}{4\pi(n-m)} - \frac{1}{4\pi(n+m)} + \frac{1}{4\pi(n-m)} \tag{78}$$

When $n \neq m$, notice $\cos(2\pi t(n+m)) = 1$ and $\cos(2\pi t(n-m)) = 1$ due to the angle multiplication factor of 2π. Hence, (78) will equal zero when $n \neq m$ [23].

In the case of $n = m$, reconsider (76). Substituting n for m, this integral becomes

$$\frac{1}{2}\int_0^L \sin(4\pi nt)\ dt.$$

Integrating, we get

$$-\frac{\cos(4\pi tn)}{8\pi n}\Big|_0^L = -\frac{\cos(4\pi nL)}{8\pi n} + \frac{1}{8\pi n} = 0$$

when $n = m$.

The preceding calculations have yielded the following important results we need to calculate the unknown Fourier coefficients a_0, a_n, and b_n in equation (1) [23]:

$$\int_0^L \sin(2\pi nt)\sin(2\pi mt)\ dt = \begin{cases} 0 & \text{if } n \neq m \\ \frac{L}{2} & \text{if } n = m, \end{cases} \tag{79}$$

$$\int_0^L \cos(2\pi nt)\cos(2\pi mt)\ dt = \begin{cases} 0 & \text{if } n \neq m \\ \frac{L}{2} & \text{if } n = m, \end{cases} \tag{80}$$

$$\int_0^L \sin(2\pi nt)\cos(2\pi mt)\ dt = 0. \tag{81}$$

With these results in mind upon returning to equation (1), let us now consider taking the integral of both sides of (1) and multiplying through by a factor of $\sin(2\pi mt)$ to obtain

$$\int_0^L f(t)\sin(2\pi mt)\ dt$$

$$= \int_0^L [a_0 \sin(2\pi mt) + \sum_{n=1}^{\infty} [a_n \sin(2\pi mt)\cos(2\pi nt) + b_n \sin(2\pi mt)\sin(2\pi nt)]]\, dt. \tag{82}$$

Using results (79), (80), and (81) above, if $n \neq m$, we can see that each term of the right hand side of (82) will go to zero, therefore yielding

$$\int_0^L f(t)\sin(2\pi mt)\ dt = 0.$$

However, if $n = m$, it is clear that

$$\int_0^L f(t)\sin(2\pi mt)\ dt = \frac{b_n L}{2}.$$

A similar argument follows to find a_n if we integrate both sides of function (64) and multiply by $\cos(2\pi mt)$. To find a_0, we simply integrate (64) to get

$$\int_0^L f(t)\ dt = \int_0^L [a_0 + \sum_{n=1}^{\infty}[a_n\cos(2\pi nt) + b_n\sin(2\pi nt)]]\ dt = 0$$

Thus, we have obtained the following three important results to determine the Fourier coefficients present in the unknown sound signal function $f(t)$:

$$a_n = \frac{2}{L}\int_0^L f(t)\cos(2\pi nt)\ dt, \tag{83}$$

$$b_n = \frac{2}{L}\int_0^L f(t)\sin(2\pi nt)\ dt, \tag{84}$$

$$a_0 = \frac{1}{L}\int_0^L f(t)\ dt. \tag{85}$$

Notice we can combine the sine and cosine component of each term of $f(t)$ into one complex unit, denoted as c_n:

$$c_n = a_n + ib_n.$$

Using Euler's formula, $e^{i\theta} = \cos\theta + i\sin\theta$, we can write

$$c_n = \frac{2}{L}\int_0^L f(t)e^{2\pi int}\ dt. \tag{86}$$

This equation for c_n is known as the continuous Fourier transform [23].

10.1.2 DISCERTE FOURIER TRANSFORM

Thus far, we have only considered the continuous aspect of Fourier transforms. Because our program reads in 44,100 samples of sound per second, we are reading in a large set of discrete points into MATLAB. Therefore, we must use discrete Fourier transforms (DFTs) to interpret our data. We do not

have a nicely integrating function in $f(t)$, so the integral (86) must be solved numerically [23]. In order to do this, apply the trapezoidal rule

$$\int f(t)\,dt \approx \frac{\Delta t}{2}\,[f(t_0) + 2f(t_1) + 2f(t_2) + \cdots + 2f(t_{n-1}) + f(t_n)] \tag{87}$$

where Δt is $\frac{b-a}{n}$. Recognize that a and b are the endpoints of the domain, and n is the number of equally spaced sub-intervals under $f(t)$ [23]. Condensing the terms $f(t_1), f(t_2), \ldots, f(t_{n-1})$ into a sum and multiplying (87) by $\cos(2\pi nt)$, we obtain

$$\int f(t)\cos(2\pi nt)\;dt \approx \frac{\Delta t}{2}\left[f(t_0)\cos(2\pi nt) + f(t_n)\cos(2\pi nt) + 2\sum_{j=2}^{N-1}[f(t_j)\cos(2\pi nt_j)]\right].$$

Thus, we conclude the discrete Fourier coefficients can be approximated as

$$a_n = \frac{\Delta t}{L}\left[f(t_0)\cos(2\pi nt) + f(t_n)\cos(2\pi nt) + 2\sum_{j=2}^{N-1}[f(t_j)\cos(2\pi nt_j)]\right], \tag{88}$$

$$b_n = \frac{\Delta t}{L}\left[f(t_0)\sin(2\pi nt) + f(t_n)\sin(2\pi nt) + 2\sum_{j=2}^{N-1}[f(t_j)\sin(2\pi nt_j)]\right]. \tag{89}$$

The discrete Fourier transform is expressed as

$$c_n = \frac{\Delta t}{L}\left[f(t_0)(e^{2\pi int}) + f(t_n)(e^{2\pi int}) + 2\sum_{j=2}^{N-1}[f(t_j)(e^{2\pi int})]\right]. \tag{90}$$

10.1.3 FAST FOURIER TRANSFORM FOR MATLAB IMPLEMENTATION

We recognize that there is a great deal of computation involved in solving for the Fourier coefficients using the DFT. So in order to transform our data in MATLAB using discrete Fourier transforms, we will implement a much more efficient algorithm. MATLAB's built-in `fft` function uses a fast Fourier transform (FFT) to transform a set of data points. Before implementing such a powerful tool to analyze the spectra of our sound waves, we must first understand and interpret the output of the `fft` function.

To apply the fast Fourier transform algorithm, we must first ensure the number of data points we are transforming is a power of two. As seen in the MATLAB code in the appendix, we simply change the length of the sound signal by taking the number of data points we have sampled and creating a new length to be the next power of two above the true sample length. Each modified sample we are analyzing consists of 310 data points, so we change the length to be 512 in MATLAB, the next power of 2, to apply the FFT [7].

Applying the fast Fourier transform to our data points in MATLAB will output a list of complex numbers. These complex quantities reveal each c_n, which consists of the Fourier coefficients a_n and b_n. Hence, the FFT provides us with the sine and cosine component of each data point along the sound wave being studied [23]. For analyzing purposes, we have little interest in the sine and cosine contribution of each data point. Instead, we want to take the square of the absolute value of c_n to find the total frequency contribution of each point.

In order to do this, we consider some basic properties of complex numbers. To take the modulus of a complex number, take the square root of the complex number multiplied by its complex conjugate as shown below:

$$|c| = \sqrt{(a + ib)(a - ib)} = \sqrt{a^2 + b^2}. \tag{91}$$

Squaring the results of (91) will give us the power of each data point in the sound signal to produce the power spectrum. This means we are plotting the frequency of each sound signal against the power spectrum of the wave in MATLAB to analyze our data [23].

10.2 MODEL OVERVIEW

Using the same data from the preceding raw data experiment, we can create a new model to predict object thickness by applying the discrete Fourier transform. Our goal is to compare the results from the raw data model to the results of the transformed model to see if either indicates a more precise

prediction. Once again, we want to obtain useable waveforms from different sides of object placement and compare the differences of each object's spectra to the control spectrum by taking the integral under the waveform.

We realize the results of the regression analysis of the first model are difficult to improve upon, but we want to examine the effects of the transformed data to develop another modeling option.

10.2.1 SINGLE WAVEFORM FFT ANALYSIS

In continuation of the book experiment, we apply MATLAB's `fft` function to transform the waveforms we have previously acquired using the *Harry Potter* book series. Initial testing of the FFT on one of the objects resulted in the following graph:

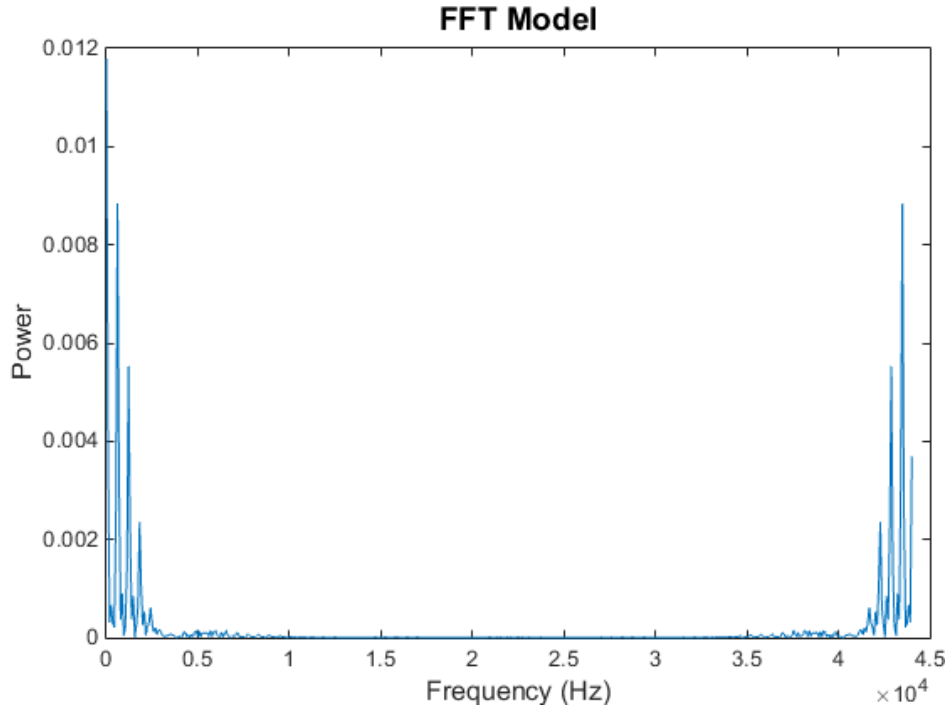

Figure 18: Testing the FFT on a Sound Recording. This is the transformed data of the HP1A average.

Due to the periodicity of the waveform, we recognize that the graph is reflected between frequencies of about [0, 5000] and [40,000, 45,000]. In Fourier analysis, it is widely accepted that the data can be sufficiently analyzed between zero and half of the sampling rate, which is known as the Nyquist frequency [7]. In our case, the Nyquist frequency will be half of 44,100 hertz, or 22,050 hertz. Because

we can obtain all of the necessary information at 22,050 hertz, the graph of the FFT can be centered at zero, providing a symmetric view of the data, as seen in the graph below.

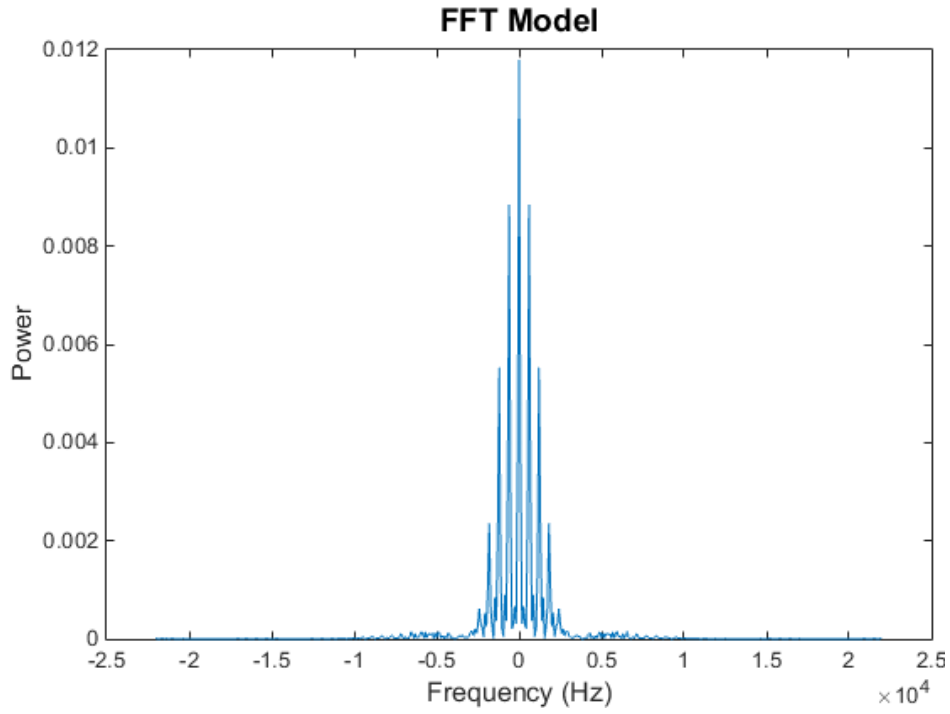

Figure 19: FFT Data Centered at Zero. This graphs the same waveform from Figure 18 centered at zero.

Because it is common practice to center a graph of frequency versus power at zero, we will also adopt this convention to develop our model.

10.2.2 WAVEFORM AVERAGING CONVENTION

So we have determined that the FFT can be successfully implemented given the data of the recordings used in the raw data model. Moving forward with the development of a new model, we are unsure if the fast Fourier transform should be applied to every wave in each set of five recordings and the average recalculated or if the FFT of the average waveforms found in the previous experiment can be used. In other words, we can apply the transform five times per set of recordings and take the average, or we can take a preexisting average used in the previous experiment and apply the FFT once. Testing these two techniques on HP1A waveforms, we obtain the following difference in spectra:

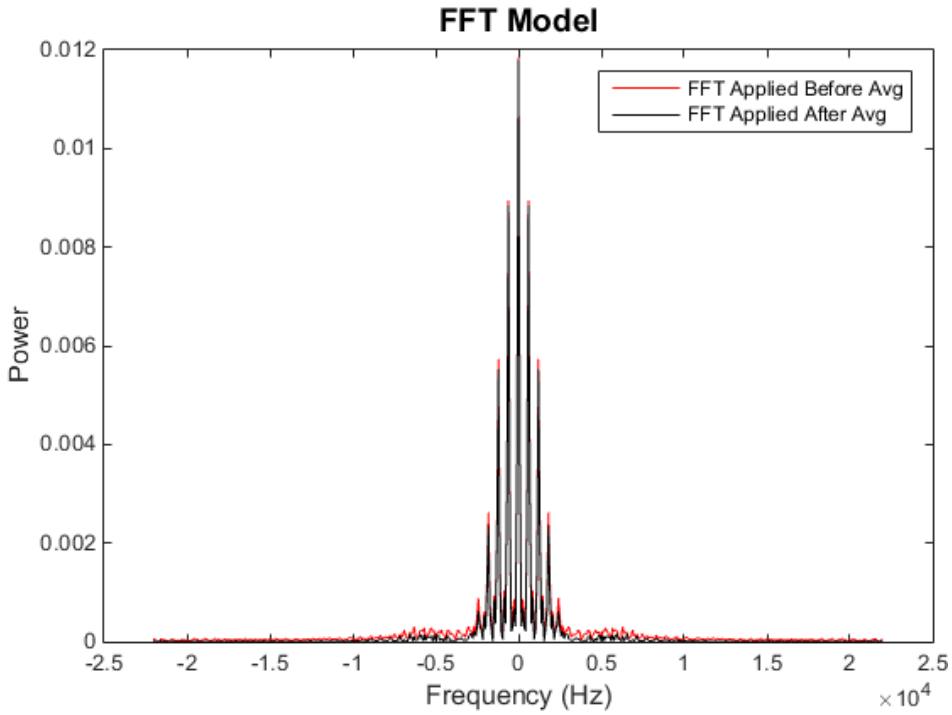

Figure 20: Comparing FFT Data Taken Before and After Averaging Waveforms.

Looking closely, we observe that when the FFT is applied to the data of each of the five waves before averaging, the spectrum has peaks at slightly higher powers. When the FFT is applied once after averaging the data of five waves, the spectrum has slightly smaller peaks. Because the results of this test are so similar, we prefer to apply the transform once per the sixteen preexisting averages of data instead of applying the transform to approximately eighty data sets for the remainder of this model development.

10.3 TRANSFORMED DATA RESULTS

Using MATLAB to transform the data of the controls and each side of each book, we can now compare the waveforms in the following graphs:

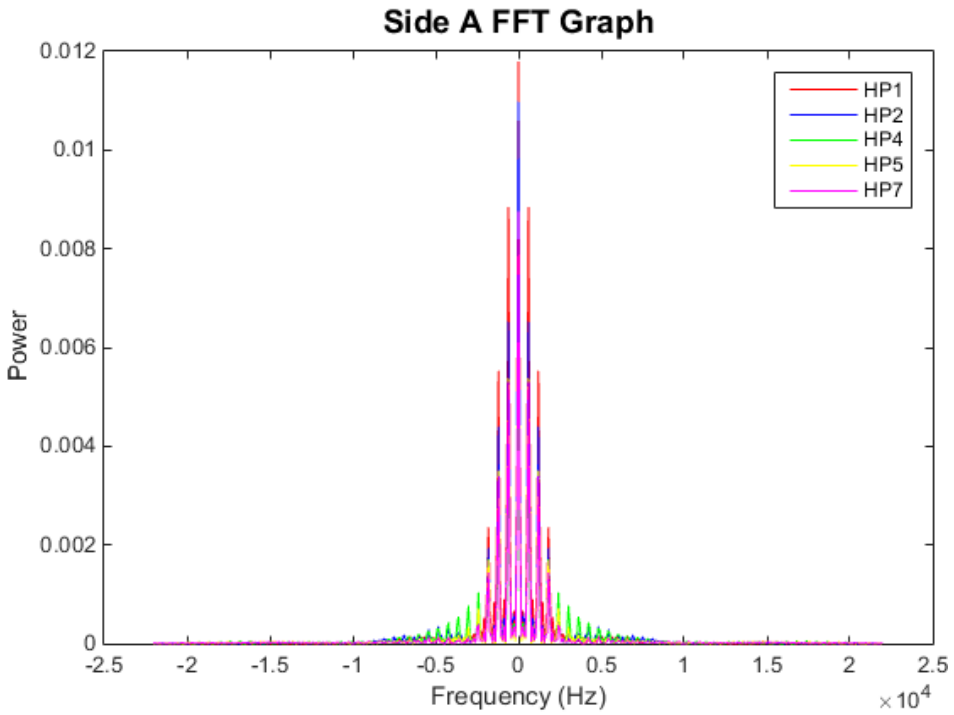
Side A FFT Graph
HP1
HP2
HP4
HP5
HP7
Power
Frequency (Hz)
0.012
0.01
0.008
0.006
0.004
0.002
0
-2.5
-2
-1.5
-1
-0.5
0
0.5
1
1.5
2
2.5
×10^4

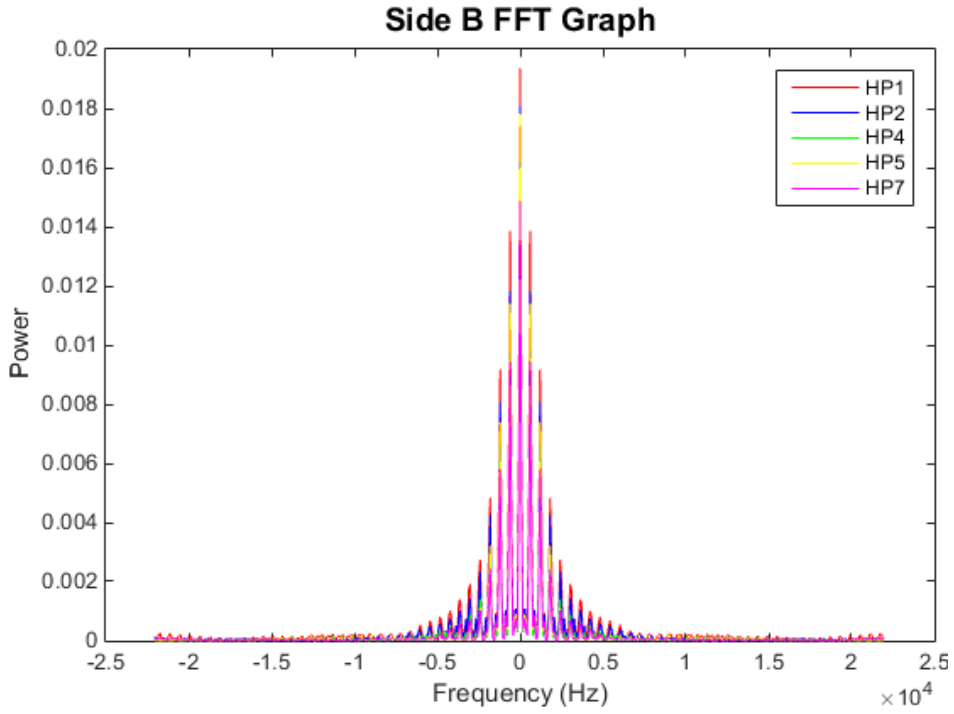
Side B FFT Graph
HP1
HP2
HP4
HP5
HP7
Power
Frequency (Hz)
0.02
0.018
0.016
0.014
0.012
0.01
0.008
0.006
0.004
0.002
0
-2.5
-2
-1.5
-1
-0.5
0
0.5
1
1.5
2
2.5
×10^4

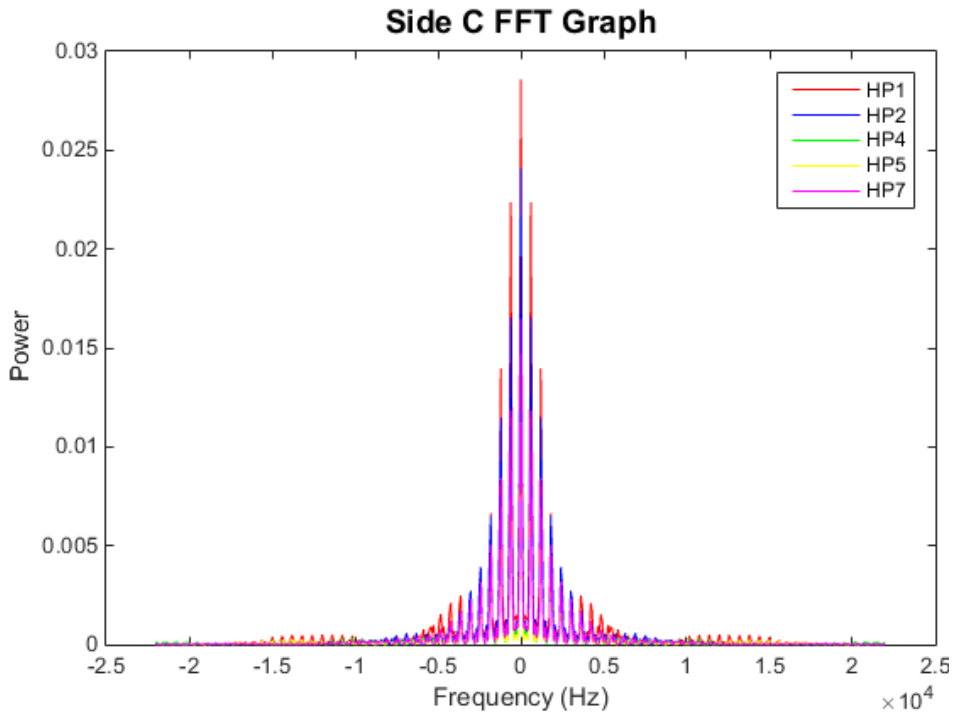

Figure 21: Transformed Average Waveforms of Sides A, B, and C.

Each graph shows the Fourier Transform of each book superimposed into a single image, each graph representing one side of the book. The graphs of the individual averages can be found in the appendix.

Still detecting difference in spectrum between each book, we now use the trapezoidal rule to find the area under each curve and subtract the object trial areas from the control area. Presented in book number order as in the previous experiment, the area differences are shown below.

```
diffDictionaryAfft =

   23.0388   24.4125   25.3511   25.5488   25.9792

diffDictionaryBfft =

   13.9408   17.0233   20.0320   19.8778   21.2622

diffDictionaryCfft =

    5.5747   10.0506   25.3511   19.5518   16.5353
```

Associating each area difference to the corresponding book will give us a scatter plot of the relationship between area and dimension. We once again do a linear regression analysis to get the following graphs:

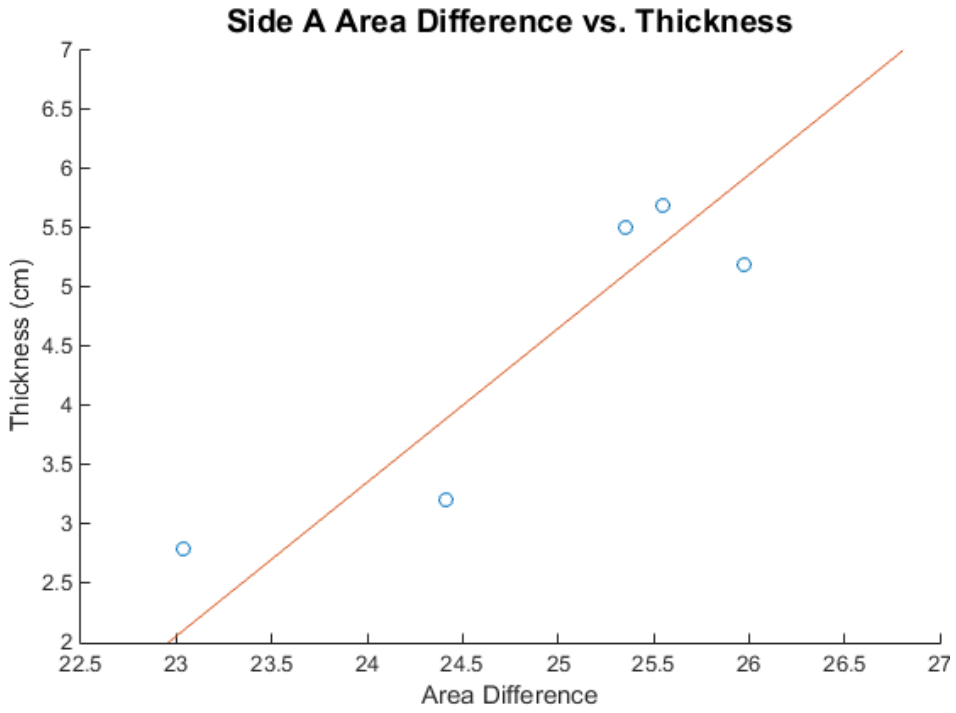
Side A Area Difference vs. Thickness
Thickness (cm)
Area Difference
7
6.5
6
5.5
5
4.5
4
3.5
3
2.5
2
22.5
23
23.5
24
24.5
25
25.5
26
26.5
27

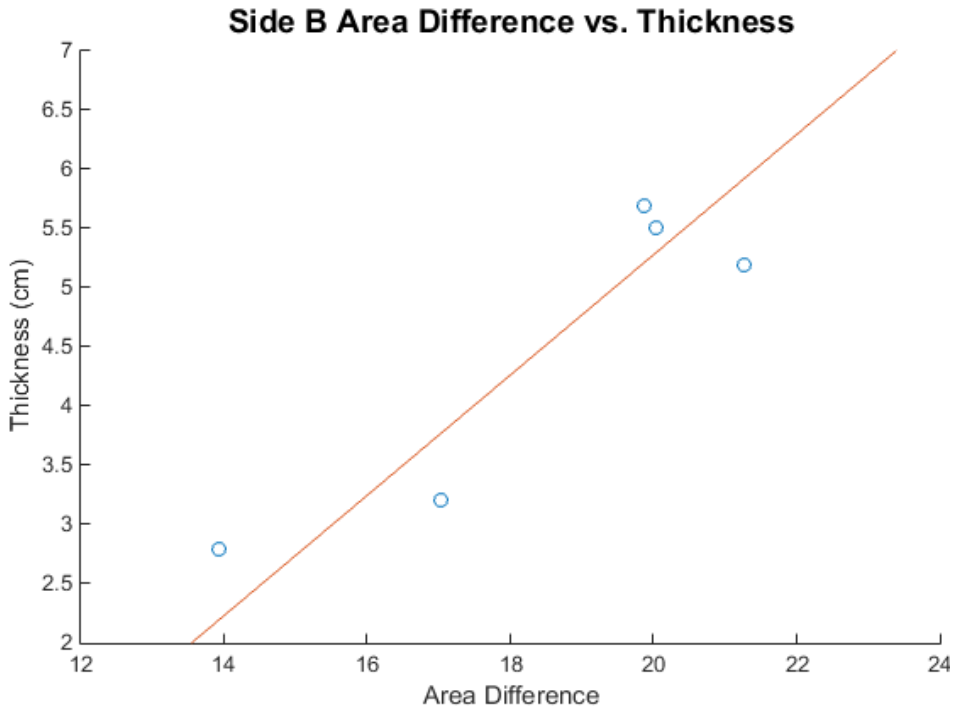
Side B Area Difference vs. Thickness
Thickness (cm)
Area Difference
7
6.5
6
5.5
5
4.5
4
3.5
3
2.5
2
12
14
16
18
20
22
24

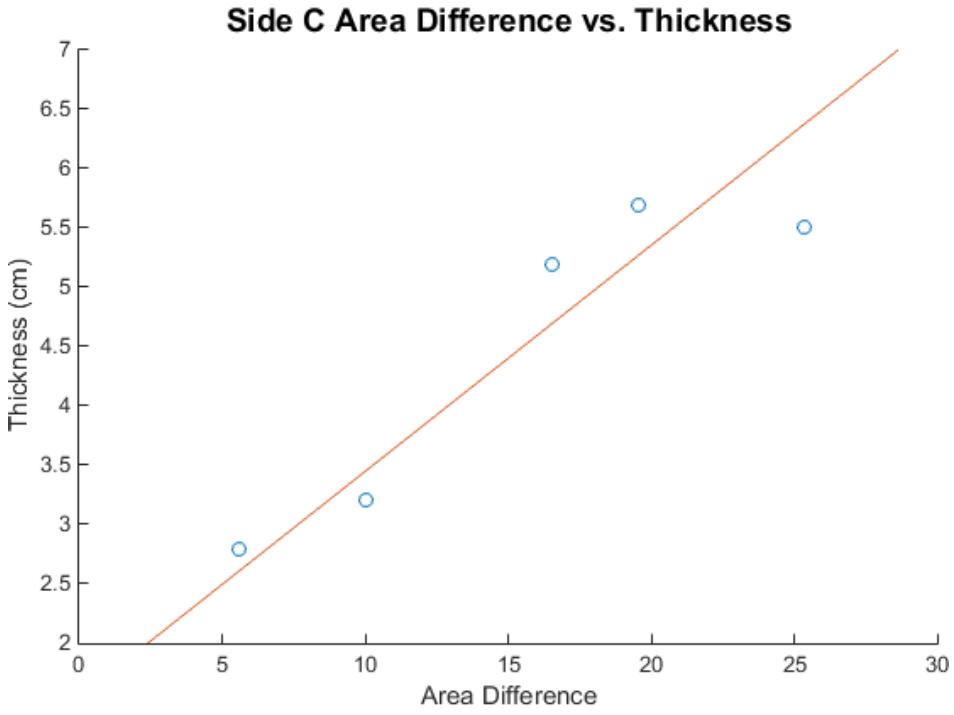

Figure 22: Linear Regression Analysis of Transformed Area Difference versus Thickness.

Sides A, B, and C obtain the following respective correlation coefficients: 0.9006, 0.9143, and 0.9227. In a sense, these results are both an improvement and a diminishment over the results of the raw data experiment. The correlation coefficients for Side A and Side C, while both still fairly close to one, have decreased by 9.2% and 6.7%, respectively. However, the correlation coefficient for Side B has shown a significant improvement with an increase of 43.0%. We speculate that the Side B results have improved with the application of Fourier transforms due to many layers of filtering and averaging data at this point in the experiment. The outlying data has either been averaged out or filtered away. Therefore, we conclude that the FFT model may not be as accurate as the raw data model, but it produces a more linear model for a previously unsuccessful test.

10.4 FILTERING THE TERMS OF THE FOURIER SERIES

As seen in Figure 22, the fast Fourier transform data is concentrated mostly between the frequencies of -5,000 hertz and 5,000 hertz. In an attempt to improve the correlation coefficients obtained

by calculating the area under the entire spectrum, we want to only consider a subset of the calculated Fourier terms c_n to filter away some of the extraneous data. Because we are plotting 512 points in each spectrum across 44,100 hertz as discussed in Section 10.1.3, we know one point is plotted every 86.1328 hertz. Half of the frequency, 22,050 hertz, minus 5,000 hertz yields a frequency difference of 17,050 hertz. This difference represents the frequency range we want to eliminate. Dividing 17,050 hertz by 86.1328 hertz/point gives us about 197.9501 points plotted within that range. Therefore, we want to eliminate the first and last 198 points graphed on the spectrum to achieve a more specific area under each waveform. By narrowing the data to 116 points, we can analyze a more focused area difference. After changing the Δt value for the new subset of data, we implement the trapezoidal rule once more to obtain new areas and thus, new area differences:

```
diffDictionaryAfft =

   20.2190   21.7472   22.7495   22.8234   23.2056

diffDictionaryBfft =

   12.6812   14.8789   17.6626   17.4698   18.8412

diffDictionaryCfft =

    4.8081    8.3984   22.7495   17.4639   14.4772
```

The new FFT Model correlation coefficients are 0.9007, 0.9194, and 0.9231 for sides A, B, and C, respectively. Each correlation coefficient increased with the implementation of this model, but only minutely.

Despite an attempt to create a simpler model by only examining a subset of Fourier coefficients, we see very little improvement in the linearity of the data. We conclude that the transformed data model is not ideal. Some possible reasons for error lie in the initial averaging of the sets of five recordings. While the HP1A graph in Figure 20 displayed little difference between averaging before and after the Fourier transforms were applied, it is possible that the results would not be as similar for different sides of the other books. Future tests could determine which of those techniques results in a more linear relationship between the data.

CHAPTER 11
MODELING OUTCOME

As we have seen, the two models we have developed imply a linear relationship between area difference and object thickness. Both models provide fairly impressive results, but one has clearly proven to produce higher correlation coefficients. Thus, we conclude that the raw data model exhibits a more significant linear relationship between spectral difference and dimensional variation than the transformed data model. We had hoped to create a simpler model by using discrete Fourier transforms to change the domain of the raw data and study a subset of the Fourier terms created. However, the transformed model did not provide the high correlation coefficients as found in the raw data model. Instead, the transformed model can be used as a backup tool if the raw data model does not produce any conclusive results for a given side.

CHAPTER 12
PREDICTING UNKNOWN OBJECT THICKNESS

We have thus shown that it is possible to predict the thickness of an object using the two models we have described. As a small experiment, we test how accurate the raw data model would be given an object of theoretically unknown dimensions.

12.1 PREDICTING BOOK THICKNESS

In order to test our model, we will record another set of sound signals with a different book as our object. In fact, we will use Book Y from the object detection experiment in Chapter 8. As noted in previous chapters, we rerecord five sound trials for this book to maintain room consistency for modeling. Recall the dimensions of Book Y are 23.1 centimeters by 21.9 centimeters by 7.8 centimeters. It is important to note that every dimension of Book Y varies compared to the dimensions of the five books used in the modeling experiments. We hypothesize that the model should still work for predicting height

as long as the dimensional difference in lengths and widths is not too great. For this experiment, we test Side A of Book Y.

Applying the procedure and using MATLAB to find the area under Book Y's average spectrum, we plot the area difference versus the book thickness of 7.8 centimeters against the raw data model. The results of this experiment are shown in the graph below:

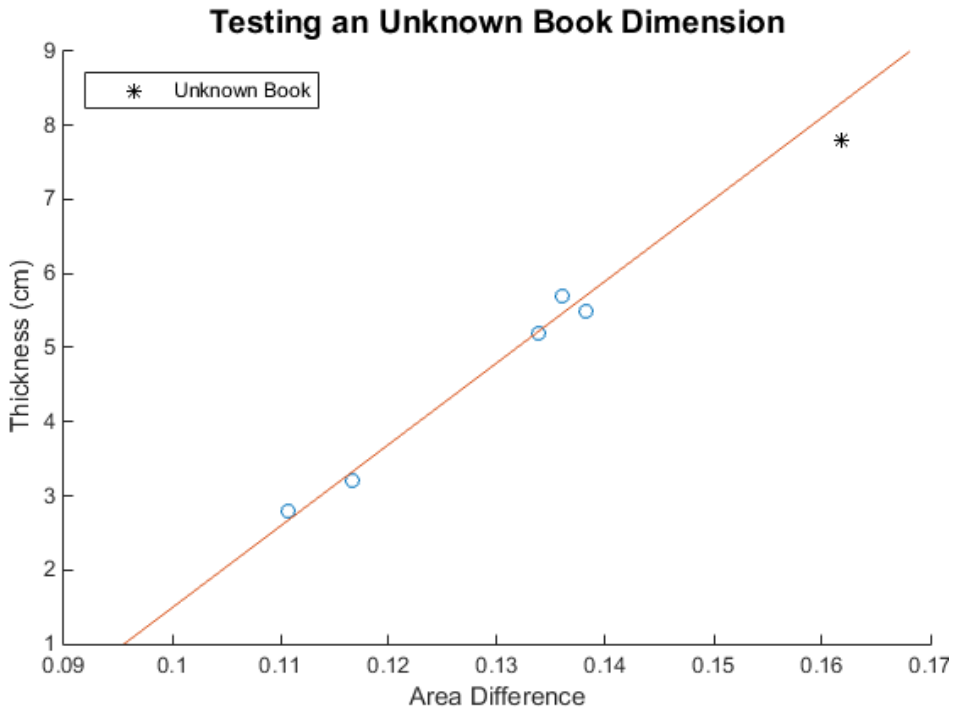

Figure 23: Using the Raw Data Model to Predict Thickness of Unknown Object with Similar Density. We can see the unknown object falls fairly close to the best-fit line used to predict thickness.

Using the raw data model on Side A of Book Y (what we consider to be the unknown object), we can see the model would predict the thickness of the book to be about 8.3 centimeters. Considering the book's actual thickness of 7.8 centimeters, we are only met with a 6.4% error. This result suggests this model can indeed be used to accurately predict the thickness of an unknown object within a few centimeters. Future experimentation would use the raw data model to predict the thickness from Side C. We also would want to see how accurately the transformed data model would predict the thickness of Book Y in future experiments.

12.2 PREDICTING WOODEN BLOCK THICKNESS

In an attempt to predict the thickness dimension of objects other than books, we also examine the average sound spectrum of a block of plywood with dimensions 22 centimeters by 16.5 centimeters by 1.7 centimeters. Once again using the Side A position of the block of wood, the length by width surface facing the iPhone and the length by height surface flat on the surface of the table, we find the average spectral waveform and find the area under it. When comparing the area difference and thickness we obtain from the block of wood to the raw data model, the following graph results:

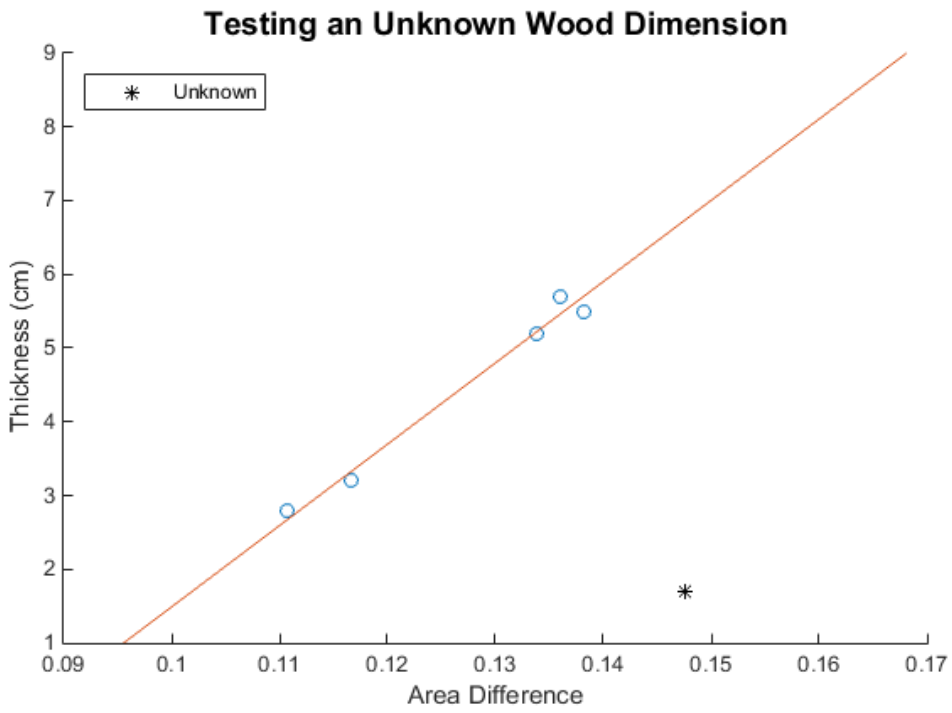

Figure 24: Using the Raw Data Model to Predict Thickness of Unknown Object with Dissimilar Density. This result suggests the material of the object matters.

Unfortunately, the prediction of the thickness of the block of wood would be wildly inaccurate if tested with this model. With an actual thickness of 1.7 centimeters, the wood's calculated area difference would suggest a thickness of about 6.7 centimeters. This five centimeter difference would yield a whopping 294.1% error.

With such a large error produced by the model, we hypothesized that the wooden block was too thin to be analyzed, suggesting the model requires dimensional constraints in order to function properly.

To test the validity of this hypothesis, we test another block of wood with doubled thickness, giving new dimensions of 22 centimeters by 16.5 centimeters by 3.4 centimeters. The graph displaying the new block data point is shown below.

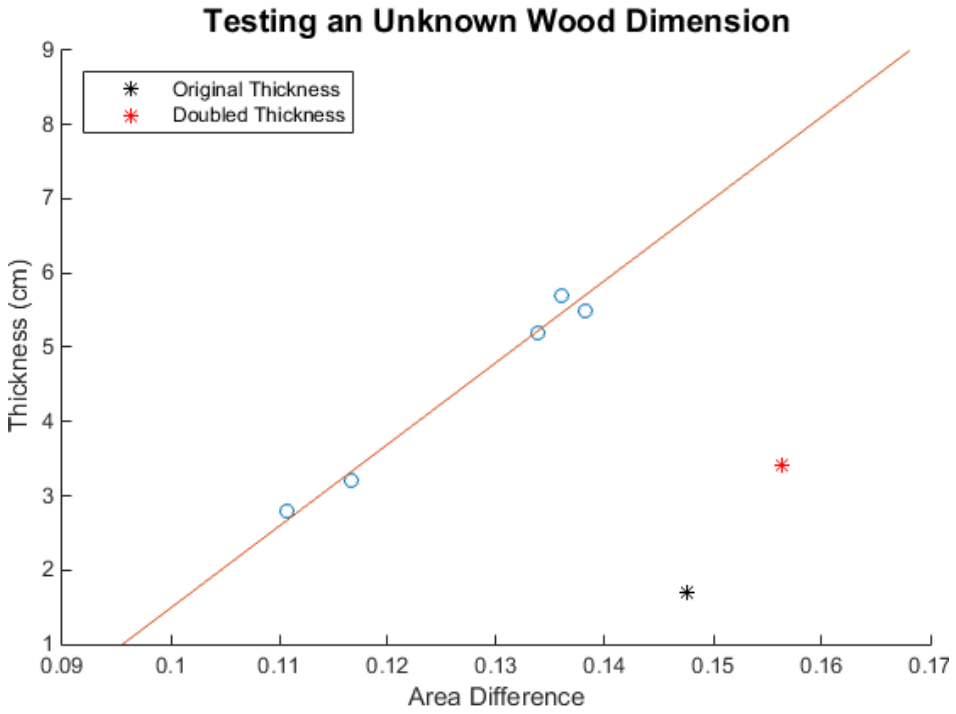

Figure 25: Testing Two Unknown Objects with Dissimilar Density.

Not only was the original block prediction inaccurate, but the doubled-thickness of the second block yields an inaccurate prediction as well. This result seems to suggest the models we have created are dependent on the material of which the object is composed. The compressed paper of the books reacted differently to the sound signals than the lightweight wood of the blocks.

Because the books had more mass than the blocks of plywood, our new hypothesis suggests that the density of the object will affect the area difference we calculate. Therefore, we would need to create new models to predict object thickness based on the density of the object. Before applying a model, we would need to assume we know the density of the object. An interesting study for future research would be to test various materials in the Blind Pepper's Ghost configuration and compare the developed models. Perhaps some materials would not show such a significant discrepancy in area difference when compared.

While the results for unknown object thickness prediction are incomplete, we conclude that the raw data model is capable of predicting thickness of objects that are similar in density and dimension (length and width, specifically) to those of the books we tested to create the model.

CHAPTER 13
CONCLUSION

In conclusion, we have created two models to predict the dimension of height in an object. The first model we developed uses the raw data from each sound signal. Using the amplitudes given by the raw data, we plot the average waveform of the sound signal and numerically integrate to find the area under the curve. Taking the difference between the average control waveform and the various object recording waveforms, we can plot area difference versus thickness for each object. As per our results, there is a linear relationship between area difference and dimensional variation. Using regression, we can create a best-fit line to superimpose upon our data. This best-fit line becomes the model on which we can base our prediction for unknown object thicknesses.

In an attempt to develop a simpler model by filtering away some of the initial signal data, we proceeded to apply the discrete Fourier transform to the average waveforms. Once again, we numerically integrate, plot the area difference versus the thickness, and perform regression analysis to develop a model.

Our results indicate that the raw data model produces a more linear relationship between area difference and object thickness than the transformed data model. Therefore, the raw data model is probably more accurate for predicting object thickness.

Hence, we have shown that it is possible to predict one dimension of an unknown object with only slight error using the Blind Pepper's Ghost configuration. Future research would allow us to develop more models to predict other dimensions of objects with multiple regression analysis. We have provided a framework for predicting the thickness of more complicated objects as well. While our experiments focused on finding the thickness of a rectangular prism on one plane (recall the experimental

configuration was stationed on a flat surface), we see it is possible to move the sound transmitting device and recording device a certain height above the table surface to find the thickness of the object on another plane. This would hopefully allow us to measure thickness throughout an object that does not necessarily have the uniform thickness assumed in the rectangular prisms we studied. For example, we could potentially measure the thickness of a square pyramid on multiple planes. Once the thickness of the object is predicted on multiple planes, we can stack these cross-sections upon one another to eventually reconstruct a three-dimensional image of the physical object without the use of the ubiquitous Radon transform.

Thus, we have created the Blind Pepper's Ghost.

CODE APPENDIX

MATHEMATICA CODE

```
(*********************************************************************
                        Reflection about the y-axis
*********************************************************************
This code shows a basic reflection of an object about the y-axis using
a reflection matrix. This is a simple operation, and we are including
it to demonstrate the simple mathematics of the Pepper's Ghost
illusion.

*********************************************************************)

(* This draws a simple square and puts each point into a matrix. *)
OriginalObject:=Polygon[{{0,1},{1,1},{1,0},{0,0}{0,1}}];
point1 = {0,1};
point2 = {1,1};
point3 = {0,0};
point4 = {1,0};

(* This is the reflection matrix. *)
Reflection = {{-1,0},{0,1}};
Reflection//MatrixForm

Out=
```

$$\begin{pmatrix} -1 & 0 \\ 0 & 1 \end{pmatrix}$$

```
(* We multiply each point by the reflection matrix to get the new
reflected coordinates. *)
point1.Reflection
point2.Reflection
point3.Reflection
point4.Reflection

Out=
```

$$\{0,1\}$$
$$\{-1,1\}$$
$$\{0,0\}$$
$$\{-1,0\}$$

```
ReflectedObject=Polygon[{{0,1},{-1,1},{-1,0},{0,0},{0,1}}];

(* We now draw both figures. The paler figure is the reflected
object.*)
Graphics[{{Opacity[".3"],Purple,ReflectedObject},{Opacity[".8"],
Purple, OriginalObject}},PlotRange→2,Axes→True]
```

Out=

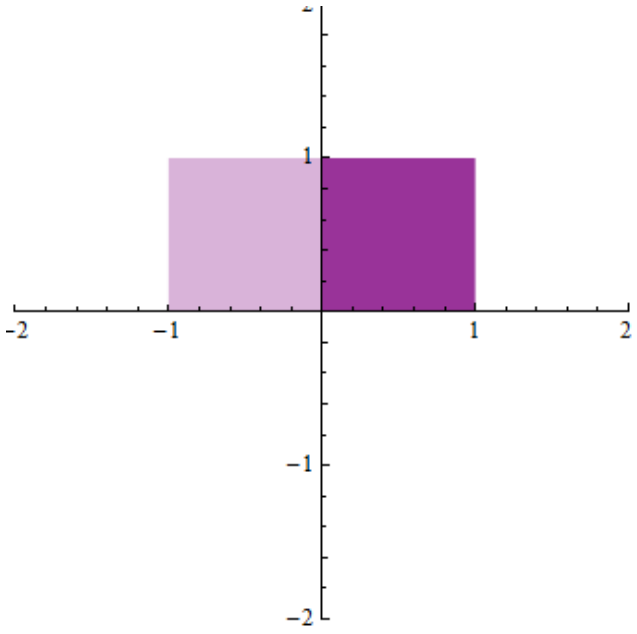

```
(*************************************************************************
                    Reflection about an Arbitrary Line
*************************************************************************
In this code, we find a matrix to reflect an object about any line of
the form ax + by + c = 0. For this example, we are reflecting a triangle
about the line -x + 2y - 4 = 0. The reflection matrix we will use was
found in chapter 2.2 as shown below:
```

$$\begin{pmatrix} \frac{b^2-a^2}{a^2+b^2} & -\frac{2ab}{a^2+b^2} & -\frac{2ac}{a^2+b^2} \\ -\frac{2ab}{a^2+b^2} & \frac{a^2-b^2}{a^2+b^2} & -\frac{2bc}{a^2+b^2} \end{pmatrix}$$

```
The calculations for finding the reflection matrix for this line have
been omitted.
*************************************************************************)


(* Matrix A represents the reflection matrix about the line
-x + 2y - 4 = 0 *)

A={{3/5,4/5,-8/5},{4/5,-3/5,16/5}};


(* Matrix B contains the points of the triangle we wish to reflect
about the line. *)

B={{2,4,2},{4,6,6},{1,1,1}};

(* Multiplying the points by the reflection matrix will result in a
matrix containing the new points of the reflected object. *)

A.B//MatrixForm

Out=
```

$$\begin{pmatrix} \frac{14}{5} & \frac{28}{5} & \frac{22}{5} \\ \frac{12}{5} & \frac{14}{5} & \frac{6}{5} \end{pmatrix}$$

```
(* This draws both objects. The paler triangle is the reflected
object.*)

triangle1=Polygon[{{2,4},{4,6},{2,6}}];
triangle2=Polygon[{{14/5,12/5},{28/5,14/5},{22/5,6/5}}];
Graphics[{{Opacity[.8],Green,triangle1},{Opacity[.3],Green,
triangle2},{Line[{{0,2},{6,5}}]}},PlotRange→7,Axes→True]
```

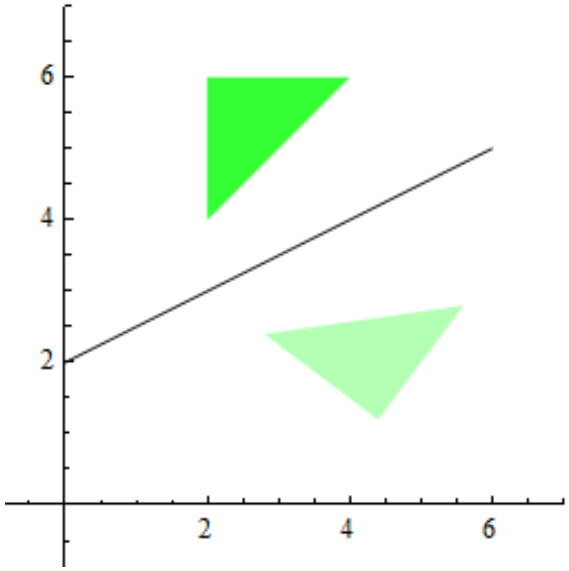
6
4
2
2
4
6

MATLAB CODE

```
%-------------------------------------------------------------------------
%           Modeling the Solution of a Wave over a Finite Boundary
%-------------------------------------------------------------------------
%
% This program draws a vibrating wave across a bounded interval at particular
% time. The wave solution over a finite boundary is found using a Fourier
% sine series. Therefore, in this code we must calculate the A_n and B_n Fourier
% coefficients. The output is an image of the entire wave at a certain time.
%
%-------------------------------------------------------------------------

% We have chosen arbitrary values for L, N, and c. The initial position of
% the wave is set at x = 0.

close all;
clear all;
L = 10;
x = 0;
N = 10;
c = 1;
acoeffs = zeros(N,1);
bcoeffs = acoeffs;
lambdas = bcoeffs;

% Choose functions for f(x) and g(x) in the initial conditions.

f = @(x) (x-5).^2-25;
g = @(x) 0;

% This calculates the Fourier coefficients A_n and B_n and the eigenvalue λ.

for n = 1:N
    if mod(n,100) == 0
        n
    end
    lambda = n*pi/L;
    afun = @(x) f(x).*sin(n*pi.*x/L);
    acoeff = 2/L*integral(afun,0,L);
    acoeffs(n) = acoeff;
    bfun = @(x) g(x).*sin(n*pi*x/L);
    bcoeff = 2/(lambda*c*L)*integral(bfun,0,L);
    bcoeffs(n) = bcoeff;
    lambdas(n) = lambda;
end

% We can now use the coefficients and eigenvalues to determine the wave
% displacement, u, at a particular x and t. We will let t = 0 due to the
% initial conditions.

xtran = linspace(0,L,1000);
x = transpose(xtran);
u = acoeffs;
finaltime = 20;
numsteps = 10;
```

```
stepsize = finaltime/numsteps;
i = 0;
for t = 0:stepsize:finaltime
    i = i+1;
    u = zeros(1000,1);
    for n = 1:N
        u = u + (acoeffs(n)*cos(lambdas(n)*c*t) +
bcoeffs(n)*sin(lambdas(n)*c*t)).*sin(lambdas(n).*x);
    end
    plot(x,u);
    hold on;
end
```

```
% The following image is the output. The endpoints of the wave represent the
% finite boundaries. Each line of the image represents the wave at different
% times t. The shape of each line is determined by the functions f(x) and
% g(x).
```

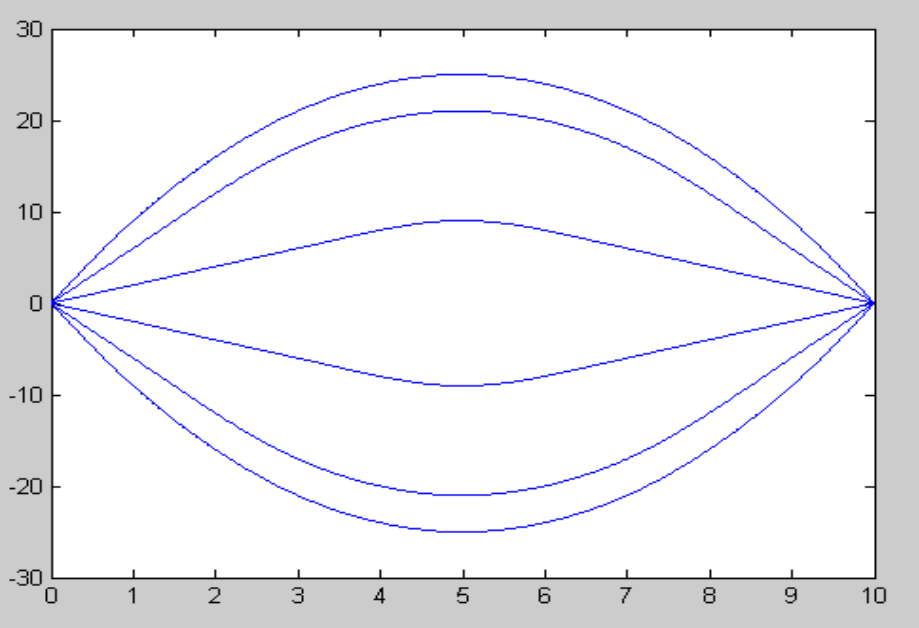

```
%{
--------------------------------------------------------------------------
              Example Class of Sound Clip Filtering and Averaging
--------------------------------------------------------------------------

 This program demonstrates how to read in sound recordings using the
audioread function. The amplitude data received from audioread is then
filtered away to take 1 in every 3000 points. The five recordings are then
averaged to obtain one average waveform for each of sides A, B, and C. Five
classes similar to this are implemented, one for each of the books studied.

--------------------------------------------------------------------------
%}



%Reads in sound clips for Side A
[a1,fs1] = audioread('hp1A1.m4a');
[a2,fs2] = audioread('hp1A2.m4a');
[a3,fs3] = audioread('hp1A3.m4a');
[a4,fs4] = audioread('hp1A4.m4a');
[a5,fs5] = audioread('hp1A5.m4a');

Length = size(a1,1);
sampleTime = Length/44100;
T = linspace(0,sampleTime,Length);
N = 3000;

t = linspace(0,sampleTime,floor(Length/N)+1);

newa1 = zeros(floor(Length/N),1);
newa2 = zeros(floor(Length/N),1);
newa3 = zeros(floor(Length/N),1);
newa4 = zeros(floor(Length/N),1);
newa5 = zeros(floor(Length/N),1);

%Filters amplitude data from each clip by taking one in every N points.
%Takes the absolute value of each amplitude
for i = 1:N:Length
    newa1((i+N-1)/N) = abs(a1(i));
    newa2((i+N-1)/N) = abs(a2(i));
    newa3((i+N-1)/N) = abs(a3(i));
    newa4((i+N-1)/N) = abs(a4(i));
    newa5((i+N-1)/N) = abs(a5(i));
end



avg1A = zeros(floor(Length/N)+1,1);
newLength=floor(Length/N)+1;



%Averages the five sound recordings for Side A
for i=1:newLength
   avg1A(i) = (newa1(i)+newa2(i)+newa3(i)+newa4(i)+newa5(i))/5;
end
```

```
%Repeat for Side B
[b1,fs1] = audioread('hp1B1.m4a');
[b2,fs2] = audioread('hp1B2.m4a');
[b3,fs3] = audioread('hp1B3.m4a');
[b4,fs4] = audioread('hp1B4.m4a');
[b5,fs5] = audioread('hp1B5.m4a');


t = linspace(0,sampleTime,floor(Length/N)+1);
newb1 = zeros(floor(Length/N),1);
newb2 = zeros(floor(Length/N),1);
newb3 = zeros(floor(Length/N),1);
newb4 = zeros(floor(Length/N),1);
newb5 = zeros(floor(Length/N),1);


for i = 1:N:Length
    newb1((i+N-1)/N) = abs(b1(i));
    newb2((i+N-1)/N) = abs(b2(i));
    newb3((i+N-1)/N) = abs(b3(i));
    newb4((i+N-1)/N) = abs(b4(i));
    newb5((i+N-1)/N) = abs(b5(i));
end

avg1B = zeros(floor(Length/N)+1,1);


for i=1:newLength

   avg1B(i) = (newb1(i)+newb2(i)+newb3(i)+newb4(i)+newb5(i))/5;

end


%Repeat for Side C
[c1,fs1] = audioread('hp1C1.m4a');
[c2,fs2] = audioread('hp1C2.m4a');
[c3,fs3] = audioread('hp1C3.m4a');
[c4,fs4] = audioread('hp1C4.m4a');
[c5,fs5] = audioread('hp1C5.m4a');


t = linspace(0,sampleTime,floor(Length/N)+1);
newc1 = zeros(floor(Length/N),1);
newc2 = zeros(floor(Length/N),1);
newc3 = zeros(floor(Length/N),1);
newc4 = zeros(floor(Length/N),1);
newc5 = zeros(floor(Length/N),1);


for i = 1:N:Length
    newc1((i+N-1)/N) = abs(c1(i));
    newc2((i+N-1)/N) = abs(c2(i));
    newc3((i+N-1)/N) = abs(c3(i));
```

```
    newc4((i+N-1)/N) = abs(c4(i));
    newc5((i+N-1)/N) = abs(c5(i));
end


avg1C = zeros(floor(Length/N)+1,1);


for i=1:newLength

   avg1C(i) = (newc1(i)+newc2(i)+newc3(i)+newc4(i)+newc5(i))/5;

end


%Outputs different graphs given all of our data

%plot(T,a2);
%plot(t,newa1,'r',t,newa2,'b',t,newa3,'g',t,newa4,'y',t,newa5,'m');
%plot(t,newb1,'r',t,newb2,'b',t,newb3,'g',t,newb4,'y',t,newb5,'m');
%plot(t,newc1,'r',t,newc2,'b',t,newc3,'g',t,newc4,'y',t,newc5,'m');
%plot(t, avg1A, 'r', t, avg1B,'b',t,avg1C,'y');
%plot(t, avg1C, 'b')


xlabel('Time (s)');
ylabel('Amplitude');
title('Graph','FontSize', 14)
```

```
%{
--------------------------------------------------------------------------------
                Transforming Average Waveform Data Using FFTs
--------------------------------------------------------------------------------

This program applies the Fast Fourier Transform to each average waveform
obtained with raw data. In order to plot the frequencies, this code
calculates the power spectrum.

--------------------------------------------------------------------------------
%}


%Make the number of points being graphed the next power of two.
l = length(avg1A);
w = pow2(nextpow2(l));

%Take fft of each average waveform.
ftCtrl = fft(avgControls,w);
ft1A = fft(avg1A,w);
ft1B = fft(avg1B,w);
ft1C = fft(avg1C,w);
ft2A = fft(avg2A,w);
ft2B = fft(avg2B,w);
ft2C = fft(avg2C,w);
ft4A = fft(avg4A,w);
ft4B = fft(avg4B,w);
ft4C = fft(avg4C,w);
ft5A = fft(avg5A,w);
ft5B = fft(avg5B,w);
ft5C = fft(avg5C,w);
ft7A = fft(avg7A,w);
ft7B = fft(avg7B,w);
ft7C = fft(avg7C,w);


%Find the power spectrum by taking the modulus of the complex values given
%by the FFT
powerCtrl = ftCtrl.*conj(ftCtrl)/w;

power1A = ft1A.*conj(ft1A)/w;
power1B = ft1B.*conj(ft1B)/w;
power1C = ft1C.*conj(ft1C)/w;

power2A = ft2A.*conj(ft2A)/w;
power2B = ft2B.*conj(ft2B)/w;
power2C = ft2C.*conj(ft2C)/w;

power4A = ft4A.*conj(ft4A)/w;
power4B = ft4B.*conj(ft4B)/w;
power4C = ft4C.*conj(ft4C)/w;

power5A = ft5A.*conj(ft5A)/w;
power5B = ft5B.*conj(ft5B)/w;
power5C = ft5C.*conj(ft5C)/w;
```

```
power7A = ft7A.*conj(ft7A)/w;
power7B = ft7B.*conj(ft7B)/w;
power7C = ft7C.*conj(ft7C)/w;

%Shift to center at 0
ftCtrlShift = fftshift(ftCtrl);
ft1AShift = fftshift(ft1A);
ft1BShift = fftshift(ft1B);
ft1CShift = fftshift(ft1C);
ft2AShift = fftshift(ft2A);
ft2BShift = fftshift(ft2B);
ft2CShift = fftshift(ft2C);
ft4AShift = fftshift(ft4A);
ft4BShift = fftshift(ft4B);
ft4CShift = fftshift(ft4C);
ft5AShift = fftshift(ft5A);
ft5BShift = fftshift(ft5B);
ft5CShift = fftshift(ft5C);
ft7AShift = fftshift(ft7A);
ft7BShift = fftshift(ft7B);
ft7CShift = fftshift(ft7C);

%Frequency range when centered at 0
fShift = (-w/2:w/2-1)*(fs1/w);

%Power spectrum when centered at 0
powerCtrlShift = ftCtrlShift.*conj(ftCtrlShift)/w;

power1AShift = ft1AShift.*conj(ft1AShift)/w;
power1BShift = ft1BShift.*conj(ft1BShift)/w;
power1CShift = ft1CShift.*conj(ft1CShift)/w;

power2AShift = ft2AShift.*conj(ft2AShift)/w;
power2BShift = ft2BShift.*conj(ft2BShift)/w;
power2CShift = ft2CShift.*conj(ft2CShift)/w;

power4AShift = ft4AShift.*conj(ft4AShift)/w;
power4BShift = ft4BShift.*conj(ft4BShift)/w;
power4CShift = ft4CShift.*conj(ft4CShift)/w;

power5AShift = ft5AShift.*conj(ft5AShift)/w;
power5BShift = ft5BShift.*conj(ft5BShift)/w;
power5CShift = ft5CShift.*conj(ft5CShift)/w;

power7AShift = ft7AShift.*conj(ft7AShift)/w;
power7BShift = ft7BShift.*conj(ft7BShift)/w;
power7CShift = ft7CShift.*conj(ft7CShift)/w;


%plot(fShift,
power1AShift,'r',fShift,power2AShift,'b',fShift,power4AShift,'g',fShift,power
5AShift,'y',fShift,power7AShift,'m')
```

```
%plot(fShift,
power1BShift,'r',fShift,power2BShift,'b',fShift,power4BShift,'g',fShift,power
5BShift,'y',fShift,power7BShift,'m')
%plot(fShift,
power1CShift,'r',fShift,power2CShift,'b',fShift,power4CShift,'g',fShift,power
5CShift,'y',fShift,power7CShift,'m')


xlabel('Frequency (Hz)')
ylabel('Power')
title('Graph','FontSize', 14)
%legend('HP1', 'HP2', 'HP4', 'HP5', 'HP7','Location', 'northeast')
```

FIGURE APPENDIX

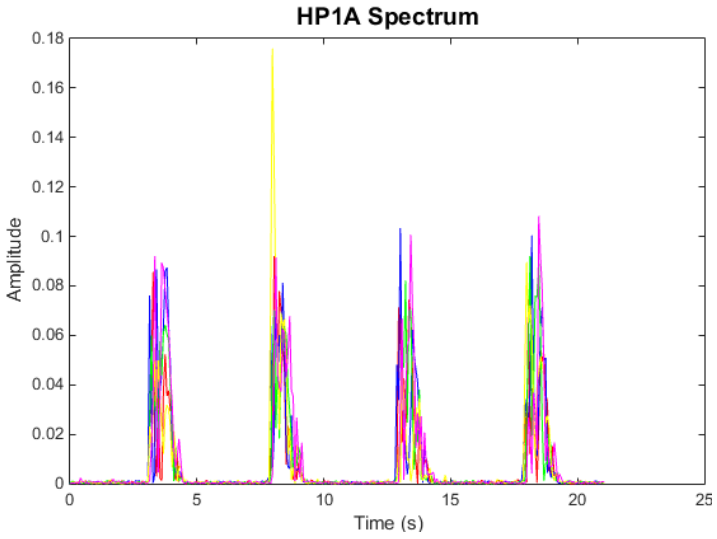
HP1A Spectrum
Amplitude
Time (s)

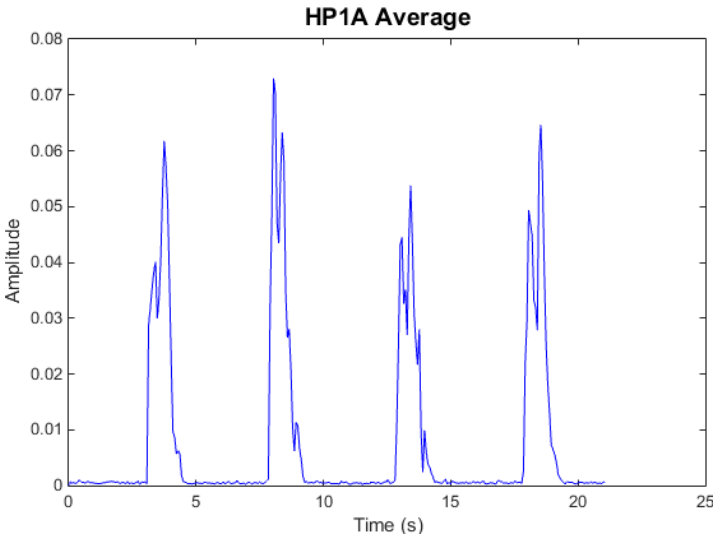
HP1A Average
Amplitude
Time (s)

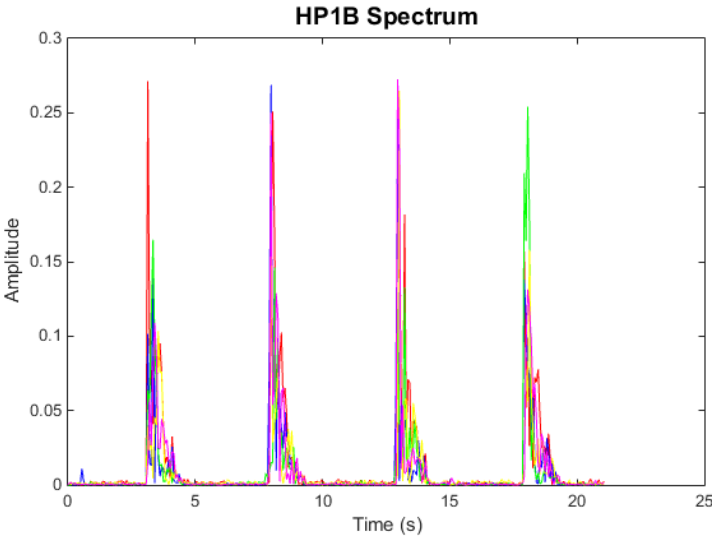
HP1B Spectrum
Amplitude
Time (s)

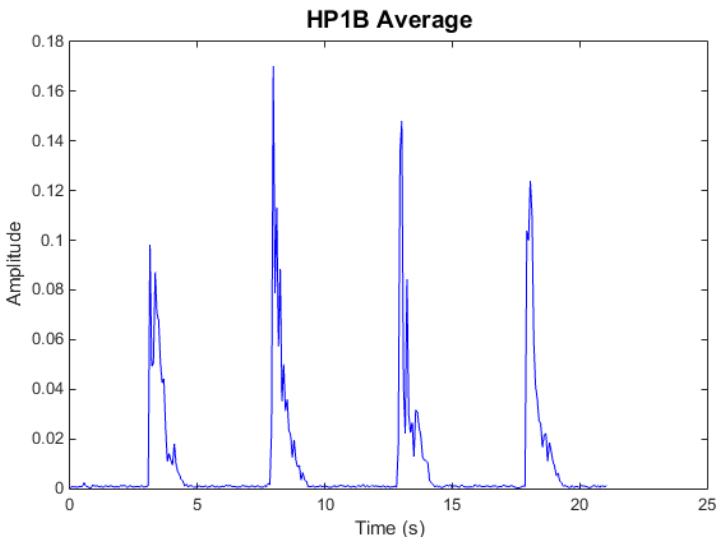
HP1B Average
Amplitude
Time (s)

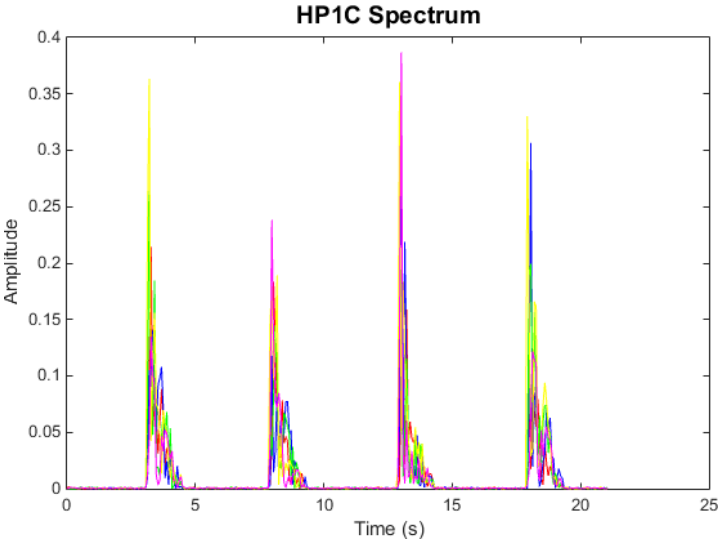
HP1C Spectrum
Amplitude
Time (s)

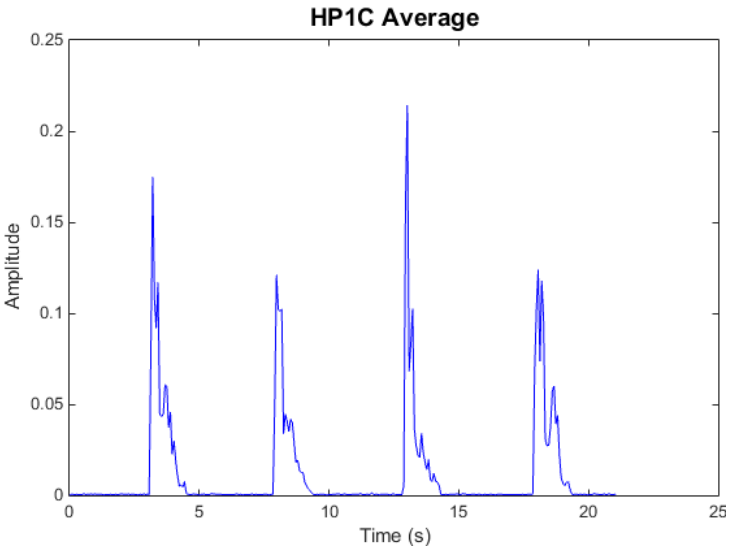
HP1C Average
Amplitude
Time (s)

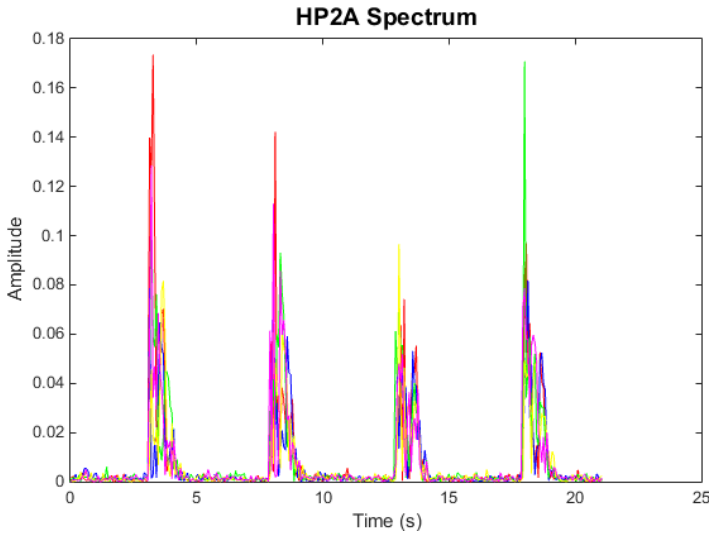
HP2A Spectrum
Amplitude
Time (s)

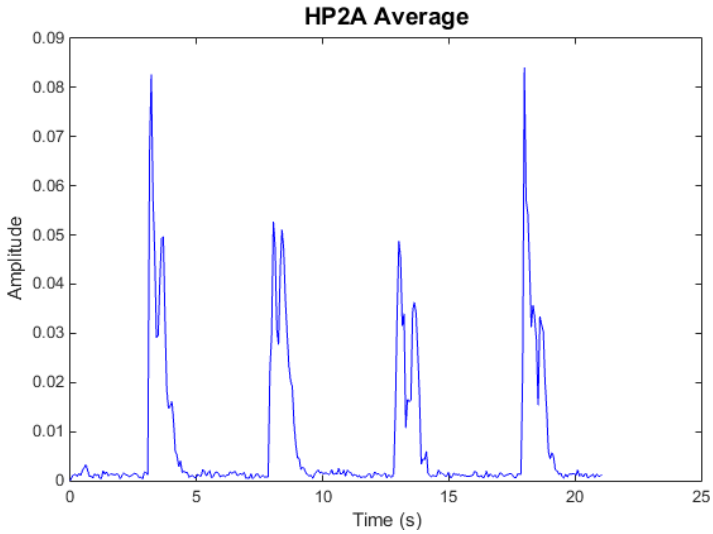
HP2A Average
Amplitude
Time (s)

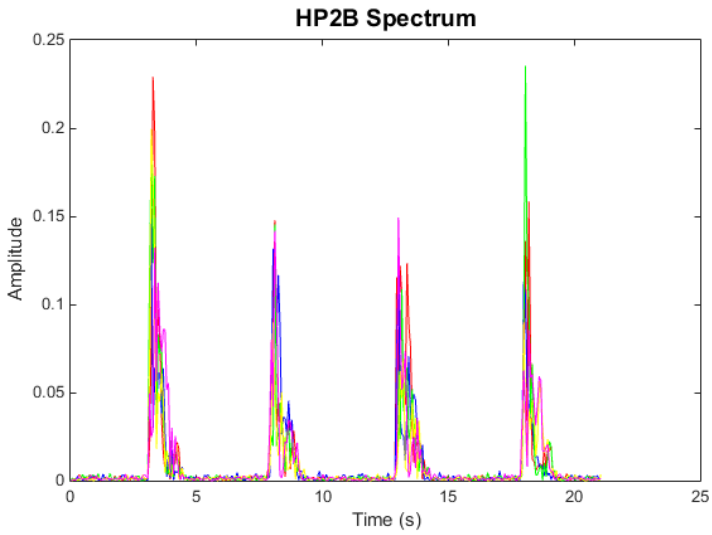
HP2B Spectrum
Amplitude
Time (s)

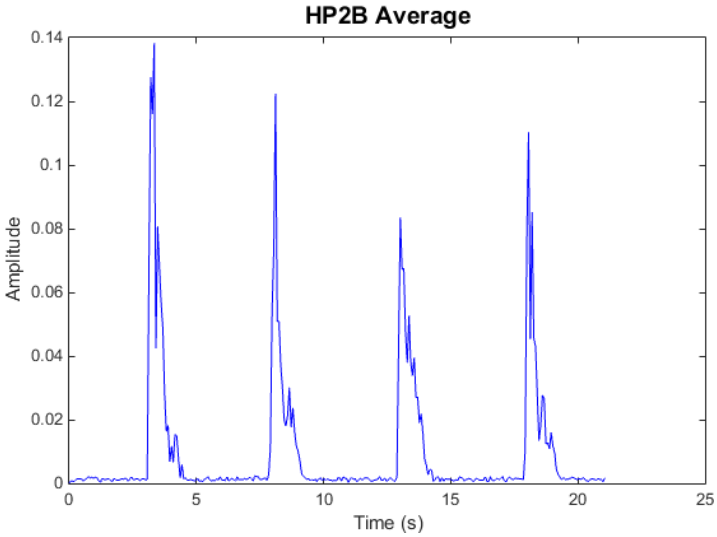
HP2B Average
Amplitude
Time (s)

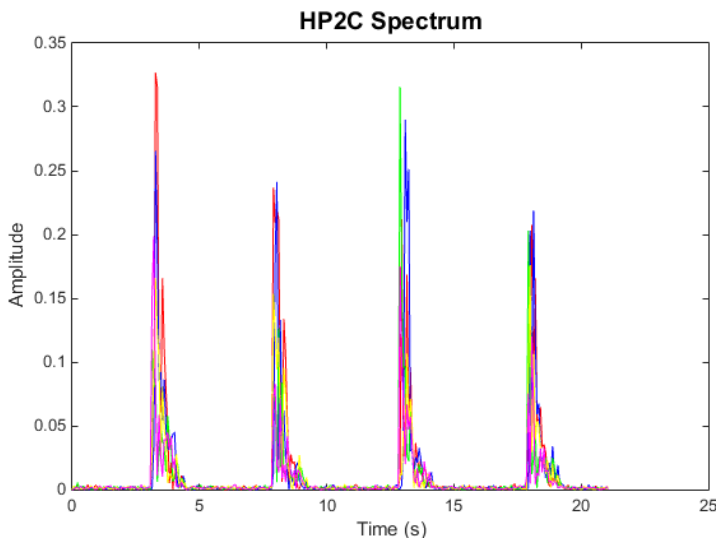
HP2C Spectrum
Amplitude
Time (s)

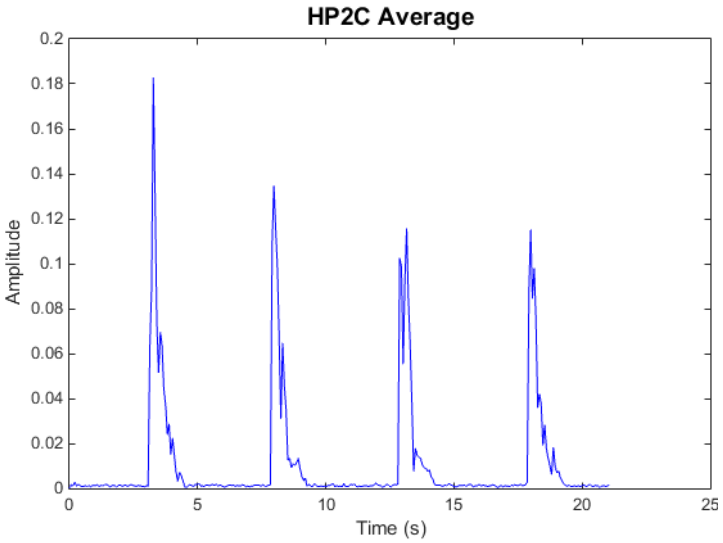
HP2C Average
Amplitude
Time (s)

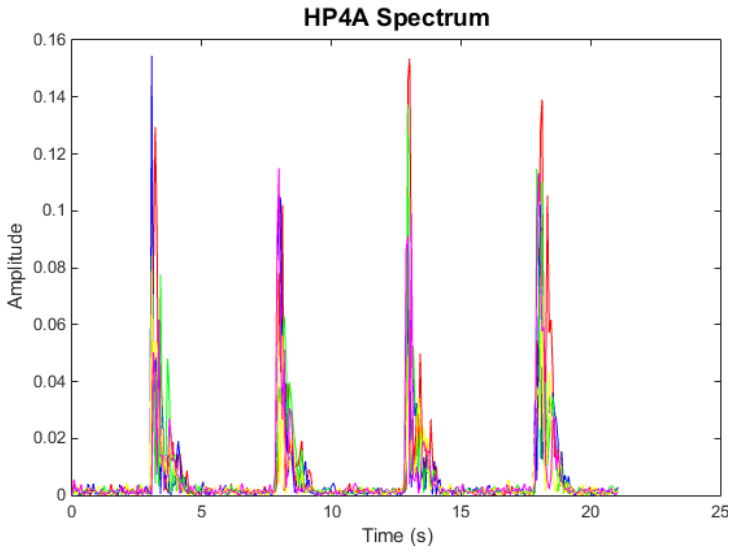
HP4A Spectrum
Amplitude
Time (s)

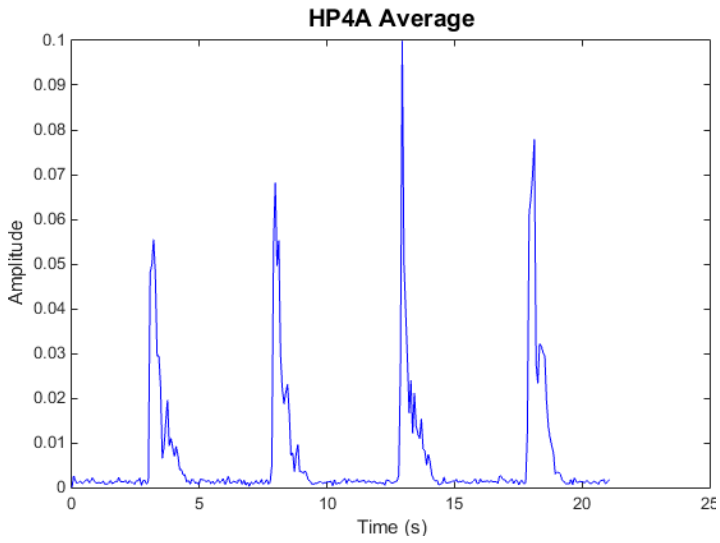
HP4A Average
Amplitude
Time (s)

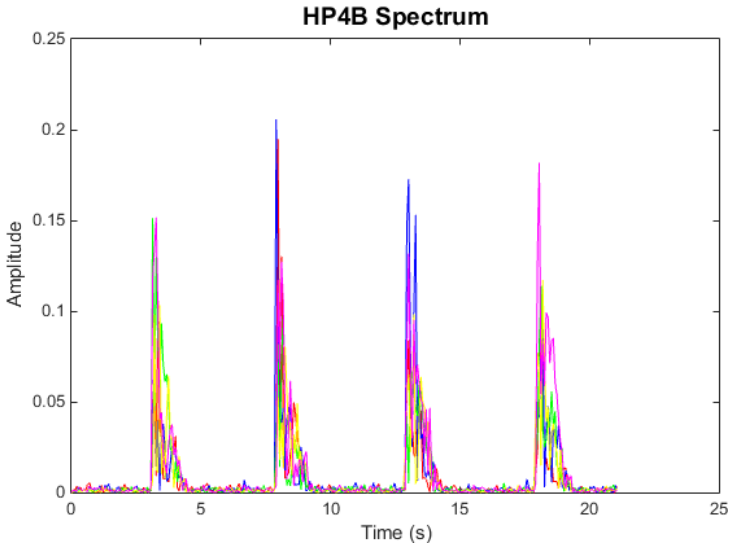
HP4B Spectrum
Amplitude
Time (s)

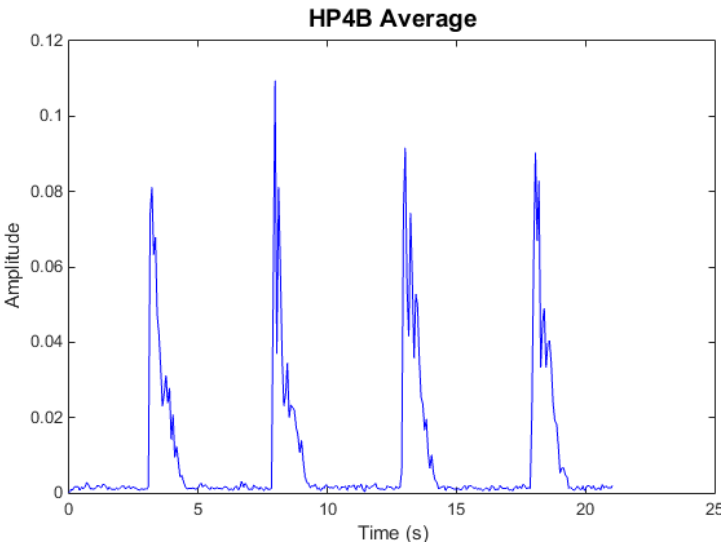
HP4B Average
Amplitude
Time (s)

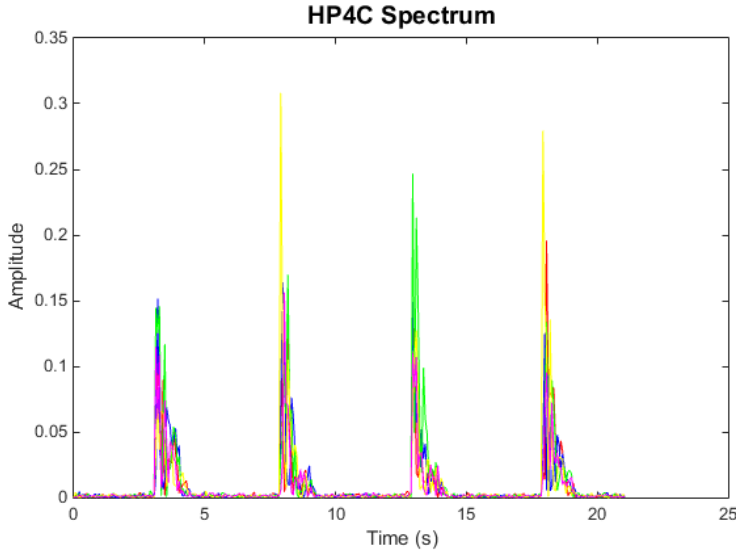
HP4C Spectrum
Amplitude
Time (s)

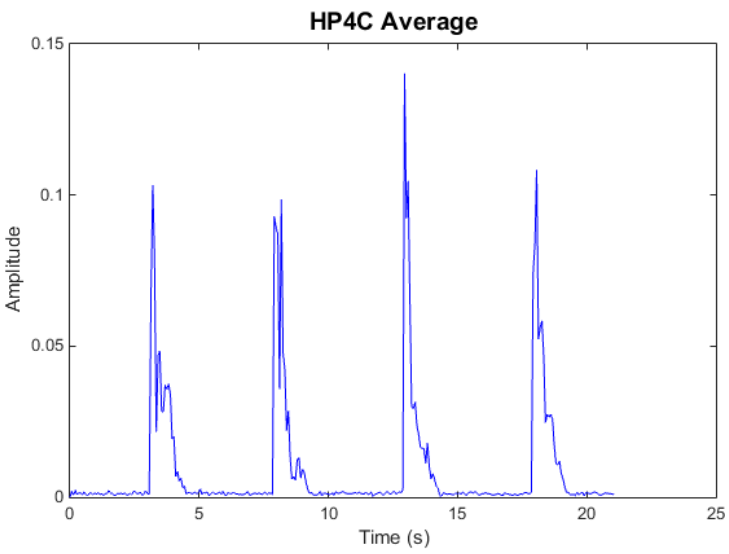
HP4C Average
Amplitude
Time (s)

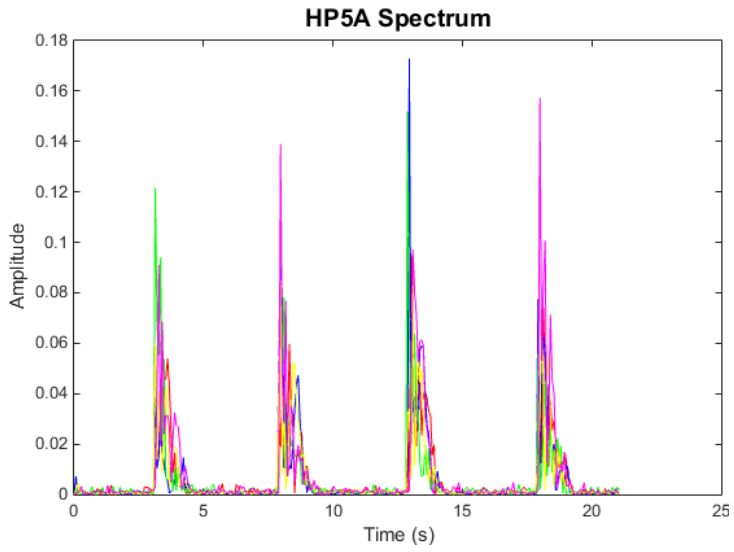
HP5A Spectrum
Amplitude
Time (s)

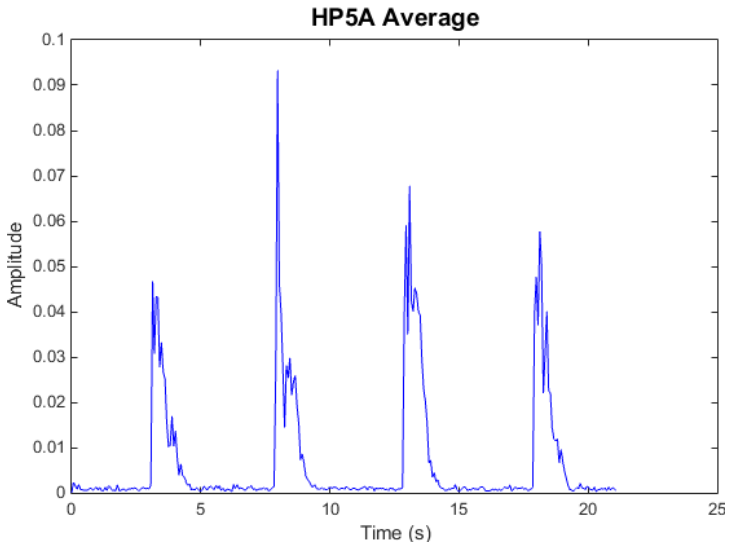
HP5A Average
Amplitude
Time (s)

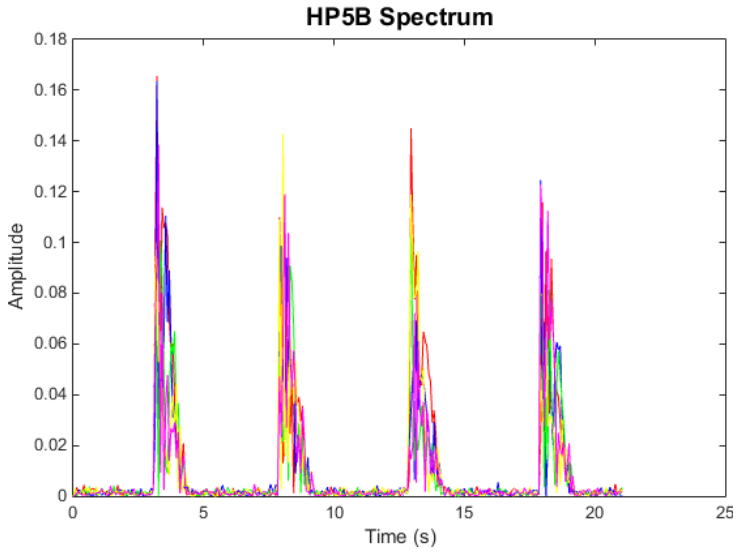
HP5B Spectrum
Amplitude
Time (s)

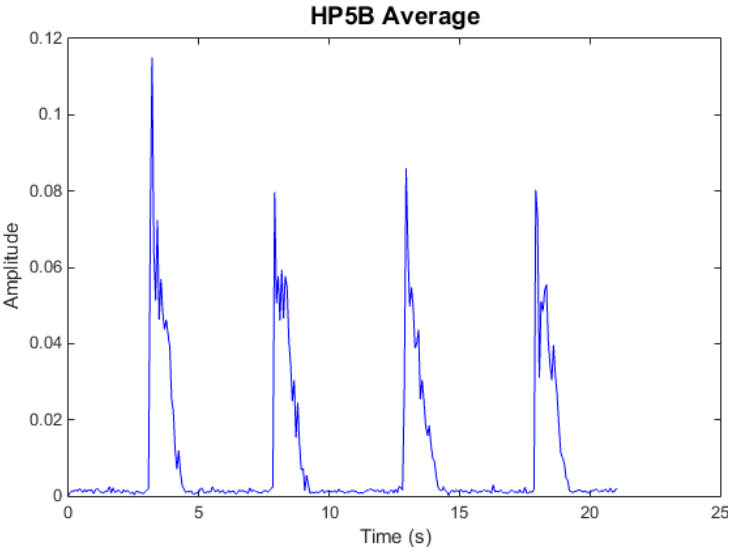
HP5B Average
Amplitude
Time (s)

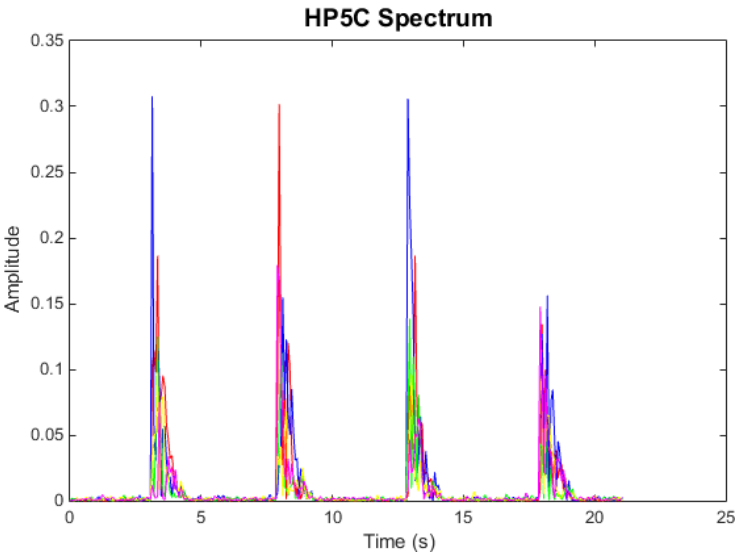
HP5C Spectrum
Amplitude
Time (s)

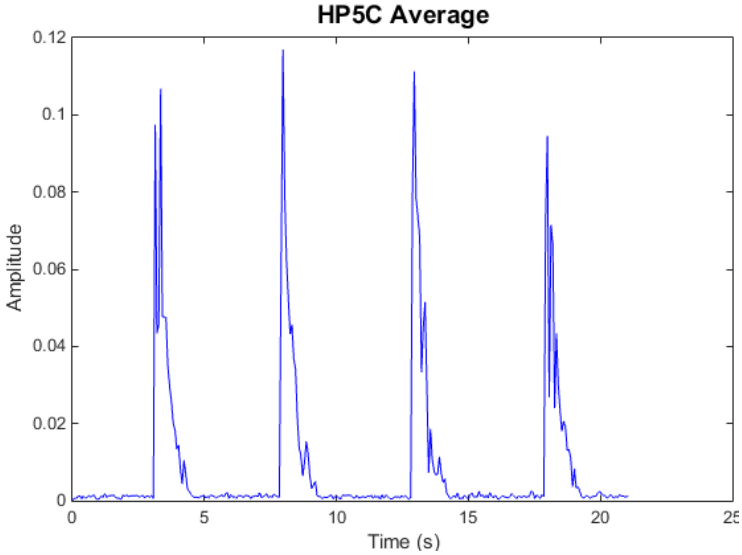
HP5C Average
Amplitude
Time (s)

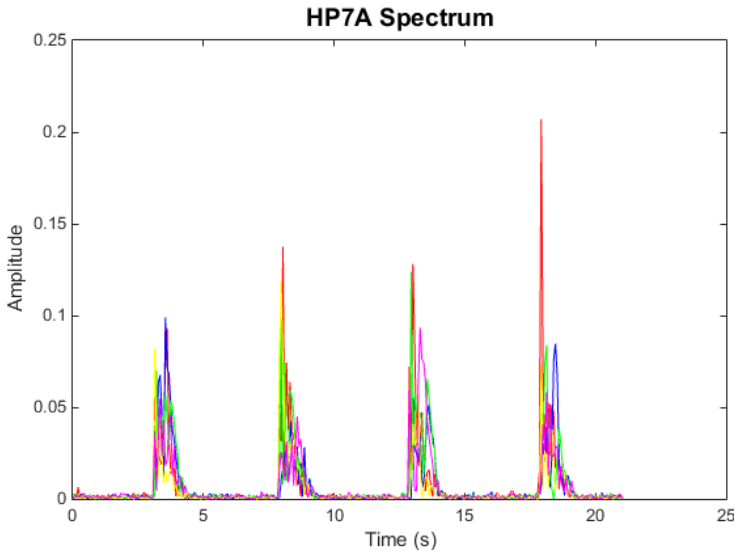
HP7A Spectrum
Amplitude
Time (s)

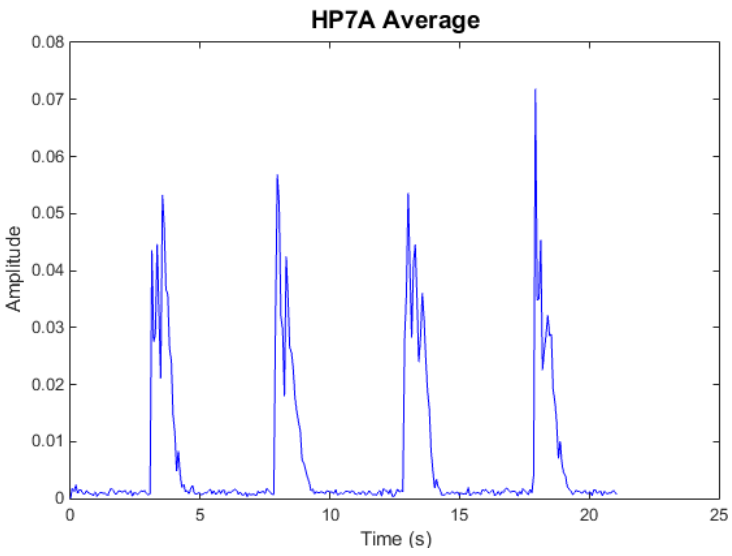
HP7A Average
Amplitude
Time (s)

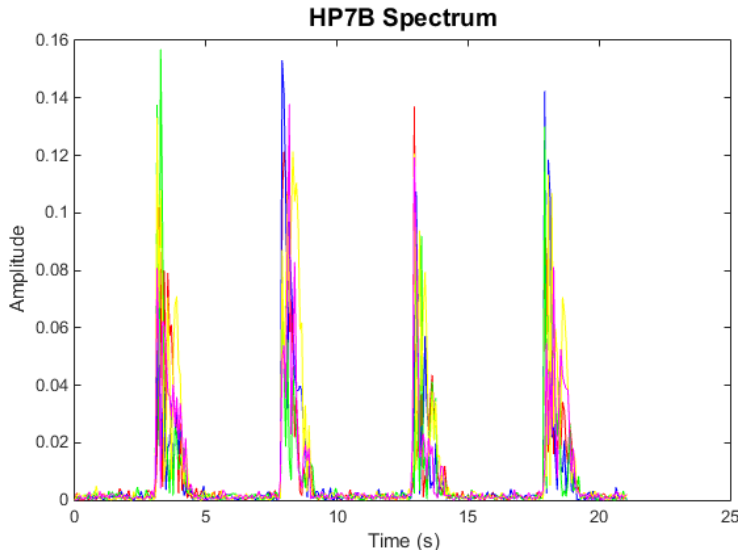
HP7B Spectrum
Amplitude
Time (s)

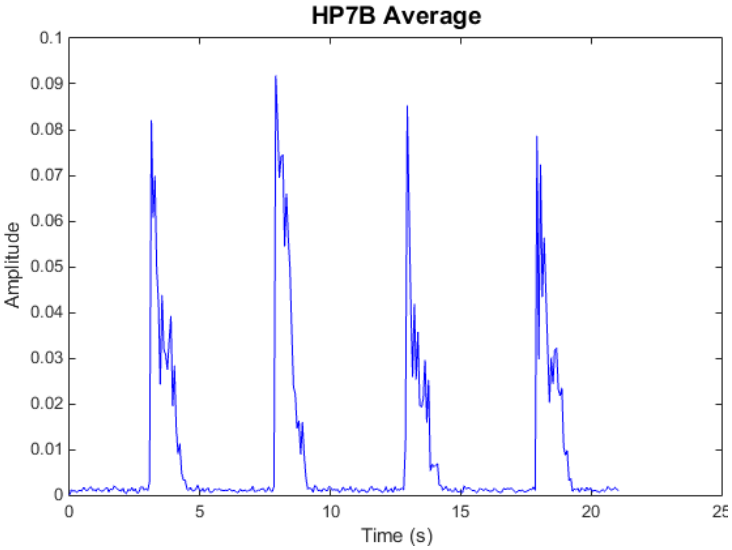
HP7B Average
Amplitude
Time (s)

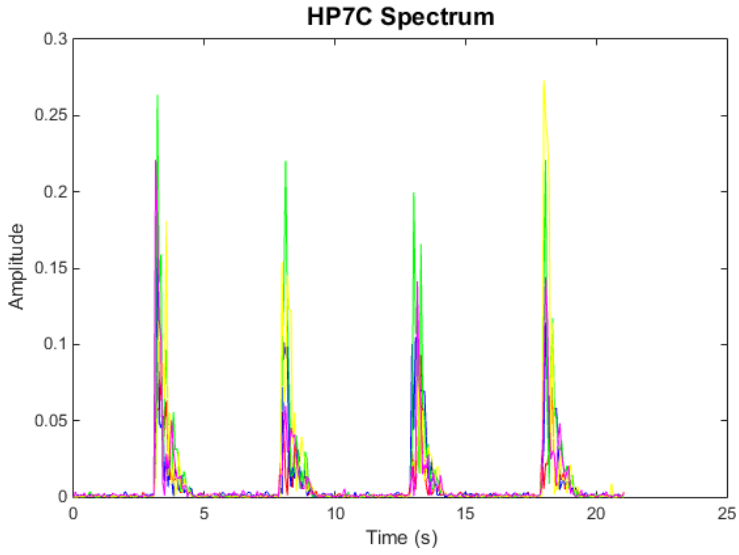
HP7C Spectrum
Amplitude
Time (s)

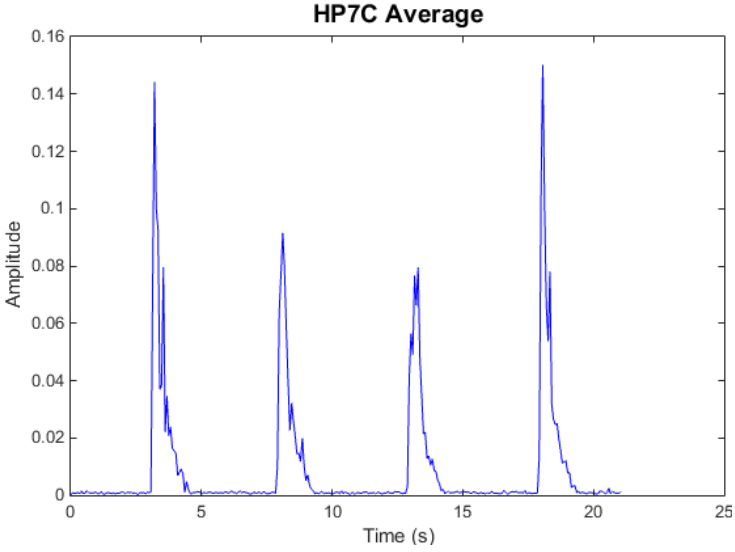
HP7C Average
Amplitude
Time (s)

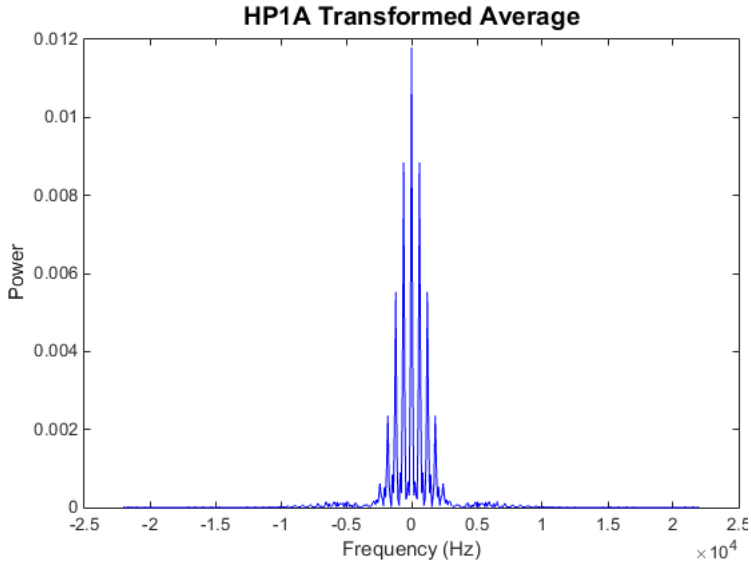
HP1A Transformed Average
Power
Frequency (Hz)
×10^4

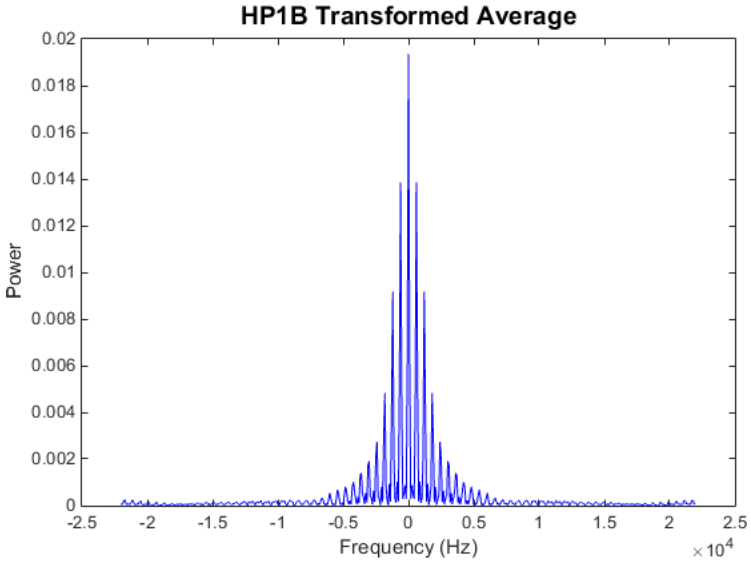
HP1B Transformed Average
Power
Frequency (Hz)
×10^4

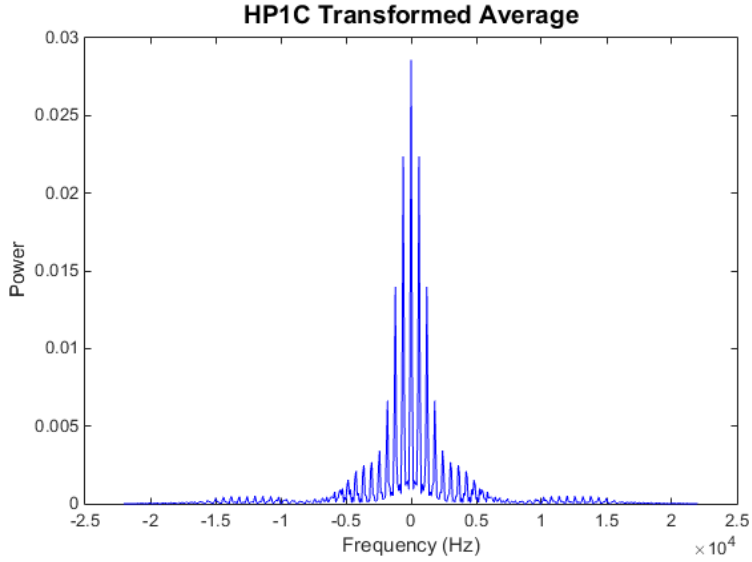
HP1C Transformed Average
Power
Frequency (Hz)
×10^4

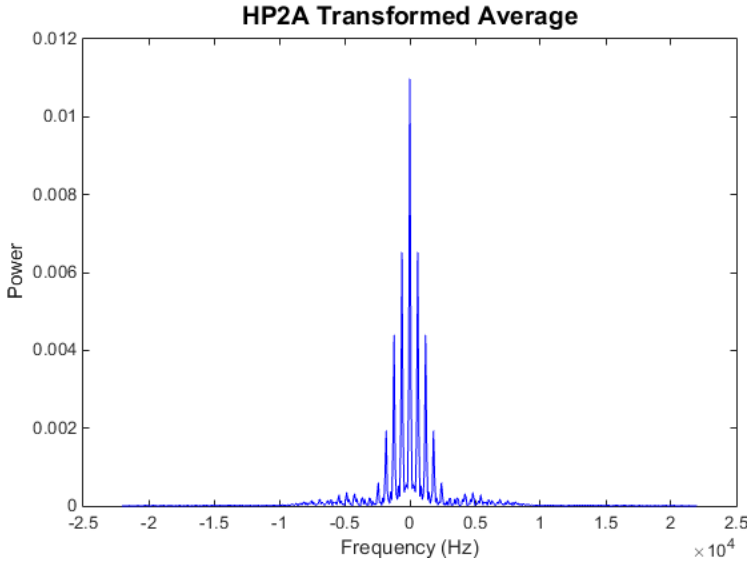
HP2A Transformed Average
Power
Frequency (Hz)
×10^4

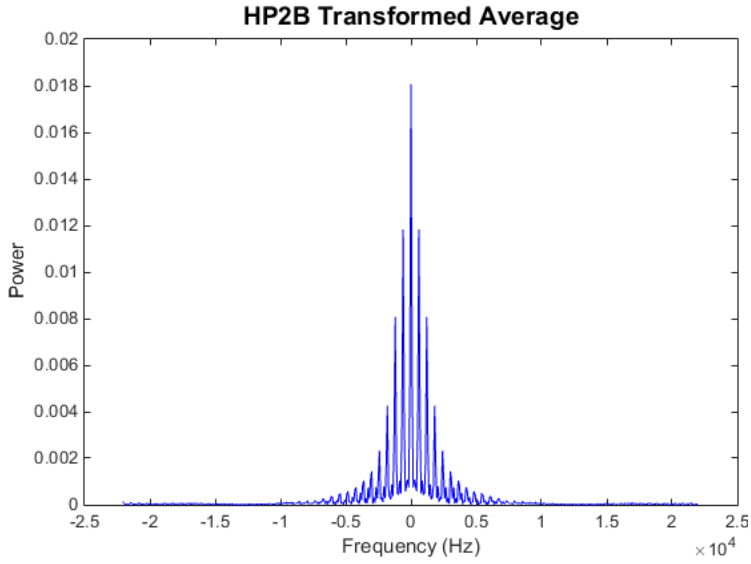
HP2B Transformed Average
Power
Frequency (Hz)
×10^4

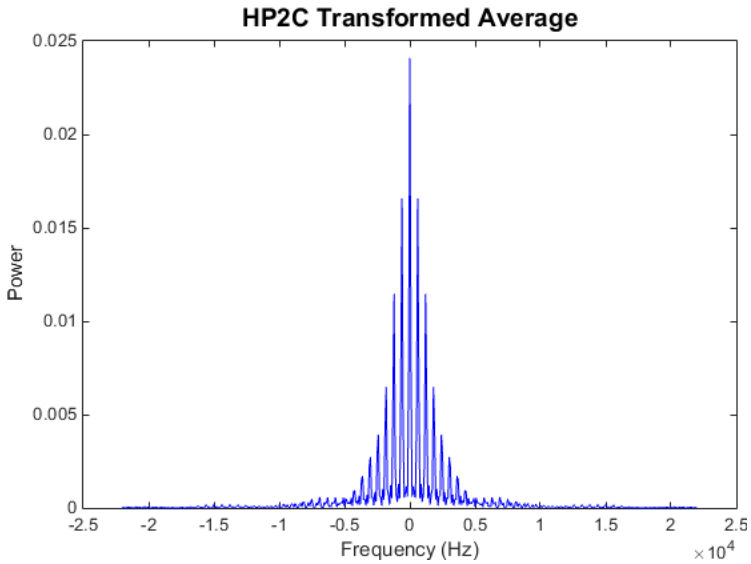
HP2C Transformed Average
Power
Frequency (Hz)
×10^4

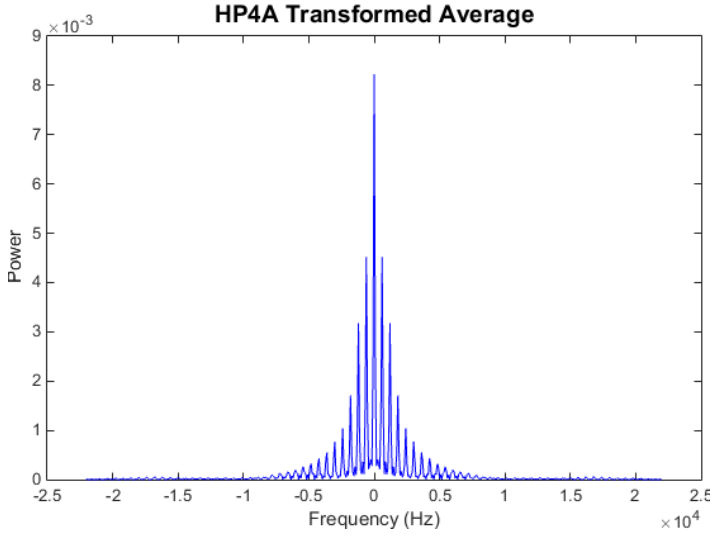
HP4A Transformed Average
Power
Frequency (Hz)
×10^-3
×10^4

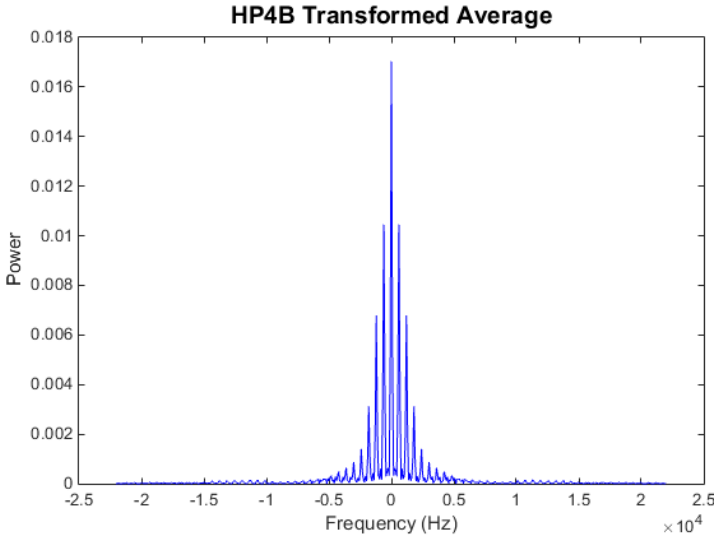
HP4B Transformed Average
Power
Frequency (Hz)
×10^4

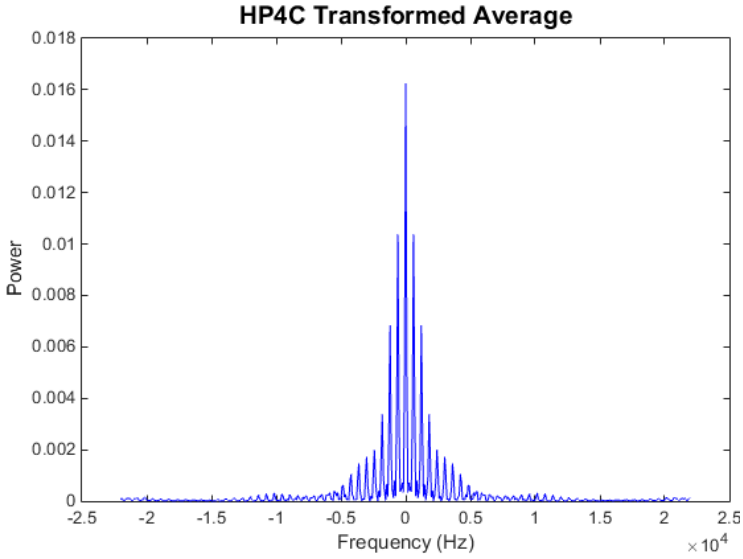
HP4C Transformed Average
Power
Frequency (Hz)
×10^4

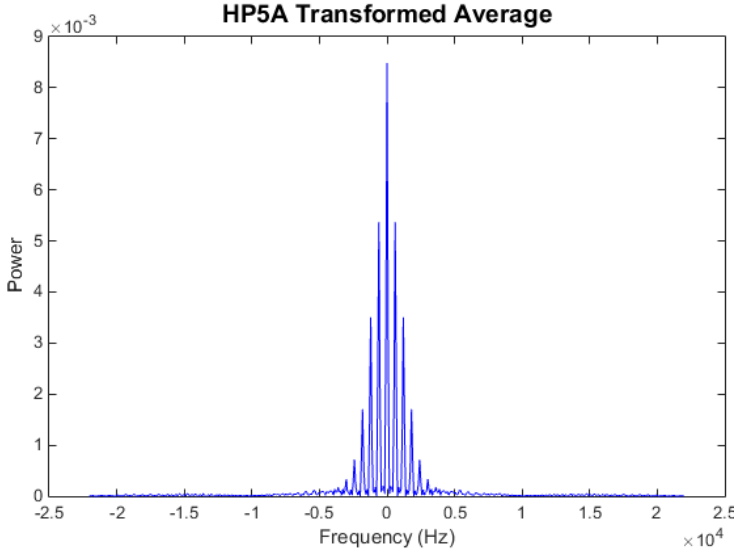
HP5A Transformed Average
Power
Frequency (Hz)
×10^-3
×10^4

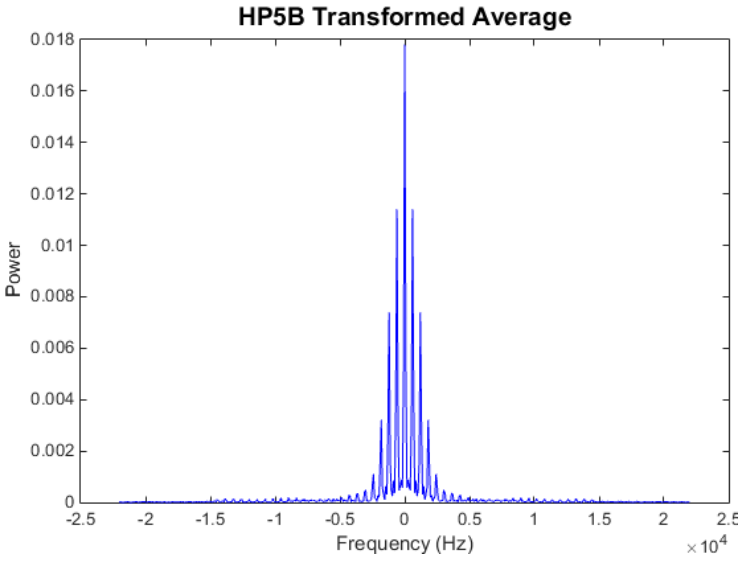
HP5B Transformed Average
Power
Frequency (Hz)
×10^4

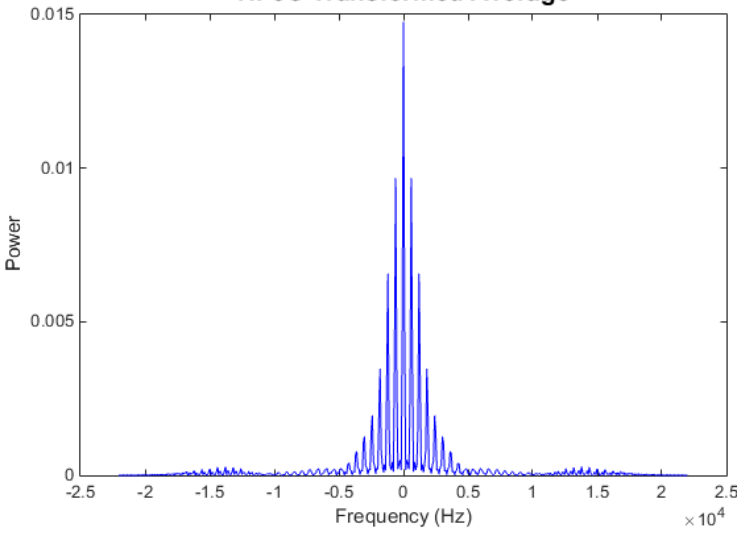
HP5C Transformed Average
Power
Frequency (Hz)
×10^4

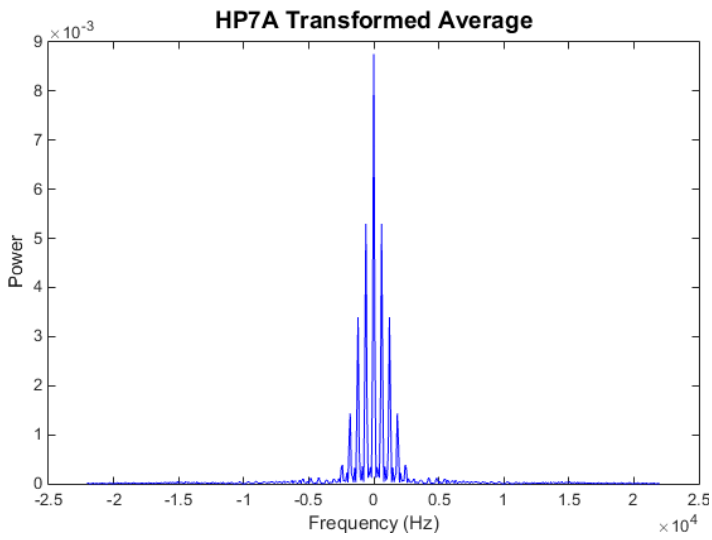
HP7A Transformed Average
×10^-3
Power
Frequency (Hz)
×10^4

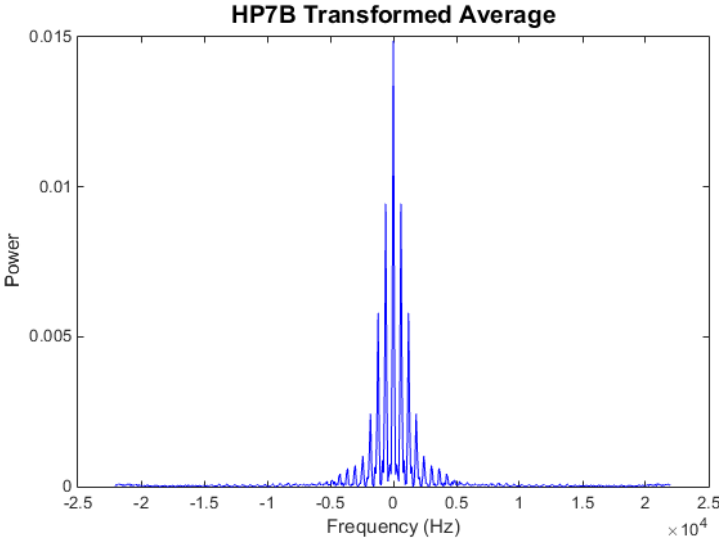
HP7B Transformed Average
Power
Frequency (Hz)
×10^4

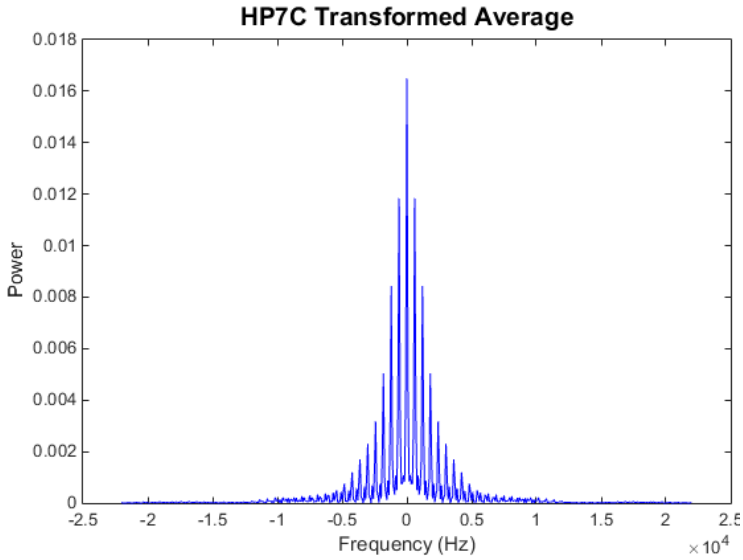
HP7C Transformed Average
Power
Frequency (Hz)
×10^4

REFERENCES

[1] Atencio, Xavier, and Buddy Baker. *Grim Grinning Ghosts* recording. Haunted Mansion Attraction Soundtrack.

[2] Averbuch, A., R. R. Coifman, D. L. Donoho, M. Israeli, Y. Shkolnisky, and I. Sedelnikov. "A Framework for Discrete Integral Transformations II—The 2D Discrete Radon Transform." *SIAM Journal on Scientific Computing* 30.2 (2008): 785-803. Web.

[3] Bimber, Oliver. "Interactive Rendering for Projection-Based Augmented Reality Displays." Diss. U of Technology Darmstadt, 2002. < https://diglib.eg.org/EG/DL/dissonline/doc/bimber.pdf>

[4] Bingham, N. H., and John M. Fry. *Regression: Linear Models in Statistics*. New York: Springer, 2010. Print.

[5] "Boundary Behavior." *The Physics Classroom*. Web. <http://www.physicsclassroom.com/class/sound/Lesson-3/Boundary-Behavior>.

[6] Castleman, Kenneth R. "Three-Dimensional Image Processing." *Digital Image Processing*. Upper Saddle River, NJ: Prentice-Hall, 1996. Print.

[7] "Fast Fourier Transform (FFT)." *MathWorks*. Web.

[8] Fausett, Laurene V. "Fourier Methods." *Applied Numerical Analysis Using MATLAB*. 2nd ed. Upper Saddle River, NJ: Pearson Prentice Hall, 2008. Print.

[9] Groth, Helen. "Reading Victorian Illusions: Dickens's Haunted Man and Dr. Pepper's "Ghost"" *Victorian Studies* 50.1 (2007): 43-65.

[10] Haberman, Richard. *Elementary Applied Partial Differential Equations*. Englewood Ciffs, NJ: Prentice-Hall, 1987.

[11] "The Haunted Mansion: Disney's Magic Show." *Magic: An Independent Magazine for Magicians* Oct. 1991: 24-27.

[12] "Image Characteristics." *The Physics Classroom*. <http://www.physicsclassroom.com/class/refln/Lesson-2/Image-Characteristics>.

[13] Jia, Yan-Bin. "Transformations in Homogeneous Coordinates," 2014. < https://www.cs.iastate.edu/~cs577/handouts/homogeneous-transform.pdf>

[14] Luckhurst, Mary, and Emilie Morin. *Theatre and Ghosts: Materiality, Performance and Modernity*. Basingstoke, Hampshire: Palgrave Macmillan, 2014.

[15] "Polynomial Curve Fitting." *MathWorks*. Web

[16] "Read Audio File." *MathWorks*. Web.

[17] Reilly, Kara. "Spectres and Spectators: The Poly-Technologies of the Pepper's Ghost Illusion." *Theatre, Performance and Analogue Technology: Historical Interfaces and Intermedialities*. Basingstoke, Hampshire: Palgrave Macmillan, 2013.

[18] Ross, Shepley L. "Chapter 4 Explicit Methods of Solving Higher-Order Linear Differential Equations." *Differential Equations*. 3rd ed. Hoboken, New Jersey: John Wiley & Sons, 1984.

[19] Sharma, K. K. *Optics: Principles and Applications*. Amsterdam: Academic, 2006.

[20] Stade, Eric. *Fourier Analysis*. Hoboken, NJ: John Wiley & Sons, 2005. Print.

[21] Stanek, Billy. "The Birds, Beasts, and Beauty of Disney's Audio-Animatronics Characters." *D23.com*. < https://d23.com/audio-animatronics-disneyland-magic-kingdom-walt-disney-world/>

[22] Steinmeyer, Jim H. *The Science Behind the Ghost*. Burbank, California: Hahne, 1999.

[23] Storey, Brian D. "Computing Fourier Series and Power Spectrum with MATLAB." Web.

[24] Surrell, Jason. *The Haunted Mansion: From the Magic Kingdom to the Movies*. Disney Editions, 2009.

[25] Taylor, Angus E., with W. Robert Mann. "Chapter 20 Uniform Convergence." *Advanced Calculus*. Boston: John Wiley & Sons, 1983. 621-22.